

STUDY OF INTERFACIAL INTERACTION DURING CHEMICAL MECHANICAL  
POLISHING (CMP) OF DIELECTRIC SILICON DIOXIDE

By

WONSEOP CHOI

A DISSERTATION PRESENTED TO THE GRADUATE SCHOOL  
OF THE UNIVERSITY OF FLORIDA IN PARTIAL FULFILLMENT  
OF THE REQUIREMENTS FOR THE DEGREE OF  
DOCTOR OF PHILOSOPHY

UNIVERSITY OF FLORIDA

2003

Copyright 2003

by

Wonseop Choi

To my family

## ACKNOWLEDGMENTS

My sincere and deepest appreciation goes to Dr. Rajiv K. Singh, my advisor, for his professional guidance, support, and encouragement. The enthusiasm for research that he has shown is strongly impressed on my memory. I would also like to thank Dr. Brij M. Moudgil, Dr. Hassan El-Shall, Dr. David P. Norton, and Dr. Chang-Won Park for their advice and support.

I wish to acknowledge the Particle Engineering Research Center (PERC) at the University of Florida, which gave me the financial support and excellent opportunities to develop and enhance my knowledge of particle and surface science by providing many informative seminars and meetings.

Many thanks are due and sincerely given to all the friends and coworkers for their friendship and helpful scientific discussion. Kyu-Gong, Uday, Zhan, Mike, Nabil, Josh, Srini, Chad, Jeremiah, Karthik, Vishal, Kuide-Qin, Bahar, Scott, Suresh, Kyoung-Ho, Joo-Han Seung-Mahn, Sang-Hyun, Jaeyoung, Kyo-Se, Jin-Ki, SanghYup, Won-Seok, Joodong, Hyuk-Soo, Han Ho, Su-Ho, Byung-Seong, and others are gratefully acknowledged for their love and friendship. In addition, I would like to thank my friends, who are in Korea, Jang-Han, Jang-Hyun, Hong-Ki, Young-Seok, Kyoung-Wan, Tae-Ho, Sang-Yup, Young-Choel, and Jae-Hyun, for their friendship and encouragement thru the years.

I am grateful to Margaret for her kind support and loving heart. I also thank PERC staff Gary, Gill, John, and Sophie for their sincerity and dedication.

I would like to give my love to my Siloam family, Wonsuk Lee, Inok Kim, Hun Ju Lee, Inoak Jeon, Keechan Kim, Kathy Noe, Heesun Yang, Jaeock Kim, Jiwon Jeong, Seong-Hee Han, Huyn Jong Park, Cathy Jung, Jawoo Koo, Soonho Kim, Tae Joong Yu, Ji Young Kim, for their faithful love.

I would like to express my gratitude to my parents, Kyoung-Tae Choi and Jeoung-Hee Kim, my sisters, So-Young and Mi-Young, parents-in-law, Jin Baik and Cheon-Kang Oh, brother-in-law, Eun-Ki, sister-in-law, Seung-Ok, and the rest of my family for their love and encouragement. They were geographically very far from me but so close in my heart.

Most of all, I would like to express my love to my wife, Lanhee Baik. With the love of my wife, I was able to persevere through the long and hard years of study away from my hometown. My son and daughter, Jaehyung and Jaeyoon, added happiness, joy, and love to my life. I especially thank all of them.

## TABLE OF CONTENTS

|   | <u>Page</u> |
|---|-------------|
| ACKNOWLEDGMENTS .....   | iv          |
| LIST OF TABLES .....  | ix          |
| LIST OF FIGURES .....   | x           |
| ABSTRACT .....  | xv          |
| <br>CHAPTER   |             |
| 1. INTRODUCTION .....   | 1           |
| Background .....  | 1           |
| Research Outline .....  | 5           |
| 2. LITERATURE REVIEW OF CHEMICAL MECHANICAL POLISHING .....   | 7           |
| Interconnects on Integrated Circuits (ICs) .....  | 7           |
| Power Consumption .....   | 11          |
| Circuit Reliability .....   | 11          |
| Multilevel Interconnection (MLI) .....  | 12          |
| Planarization for MLI Fabrications .....  | 15          |
| Chemical Mechanical Polishing (CMP) Processes .....   | 17          |
| Abrasive Polishing Slurry .....   | 19          |
| Polishing Pad .....   | 21          |
| Materials to Be Polished .....  | 26          |
| Polishing Mechanism in Metal CMP .....  | 31          |
| Tungsten CMP .....  | 31          |
| Copper CMP .....  | 33          |
| Polishing Mechanism in Oxide CMP .....  | 34          |
| Friction in CMP .....   | 39          |
| Principles and Causes of Friction .....   | 39          |
| Friction during Chemical Mechanical Polishing .....   | 43          |
| Modeling of Chemical Mechanical Polishing .....   | 46          |
| 3. STUDY OF FRACTIONAL SURFACE COVERAGE OF ABRASIVE PARTICLES<br>DURING CHEMICAL MECHANICAL POLISHING ..... | 50          |
| Introduction .....  | 50          |

|   |            |
|---|------------|
| Experimental.....   | 52         |
| Results and Discussion .....  | 54         |
| Particle Size and Size Distribution in CMP Slurries.....  | 54         |
| Effect of Down Pressure, Particle Size, and Solids Loading on Friction Force.....               | 56         |
| Comparison of Friction Force for a Fixed Number of Particles.....                               | 58         |
| Fractional Surface Coverage of Particles in Contact with Wafer to be Polished.....              | 60         |
| Summary.....  | 63         |
| <b>4. STUDY OF INTERFACIAL CONTACT VARIATION DURING CHEMICAL MECHANICAL POLISHING.....</b>      | <b>65</b>  |
| Introduction.....   | 65         |
| Experimental .....  | 66         |
| Modeling of Contact Area .....  | 67         |
| Contact between a Rigid Flat Surface and Single Particle .....                                  | 67         |
| Number of Particles Participating in Contact at the Interface .....                             | 69         |
| Friction Force Based on the Interfacial Contact.....  | 71         |
| Results and Discussion .....  | 72         |
| Summary.....  | 77         |
| <b>5. DYNAMIC CONTACT CHARACTERISTICS DURING CHEMICAL MECHANICAL POLISHING.....</b>             | <b>78</b>  |
| Introduction.....   | 78         |
| Experimental .....  | 79         |
| Results and Discussion .....  | 80         |
| Summary.....  | 86         |
| <b>6. STUDY OF PH EFFECTS ON SILICON DIOXIDE DIELECTRIC CHEMICAL MECHANICAL POLISHING .....</b> | <b>88</b>  |
| Introduction.....   | 88         |
| Experimental .....  | 90         |
| Characterization of Slurry.....   | 92         |
| Chemical Analysis.....  | 92         |
| Particle Size Analysis .....  | 93         |
| Solubility of Silica.....   | 95         |
| Results and Discussion .....  | 96         |
| Effects of pH on Polishing Rate .....   | 96         |
| Effect of pH and pressure on friction force .....   | 100        |
| Surface Analysis by AFM .....   | 102        |
| Summary.....  | 105        |
| <b>7. EFFECTS OF SLURRY PARTICLES ON SILICA CHEMICAL MECHANICAL POLISHING .....</b>             | <b>106</b> |
| Introduction.....   | 106        |
| Experimental.....   | 109        |

|  |         |
|--|---------|
| Results and Discussion .....   | 110     |
| Analysis of Shape and Size of Silica Particles .....   | 110     |
| Analysis of <i>In Situ</i> Friction Force .....  | 112     |
| Surface Finish Analysis .....  | 121     |
| Analysis of Polishing Rate .....   | 128     |
| Summary .....  | 130     |
| <br>8. EFFECTS OF COLLOIDAL SILICON DIOXIDE PARTICLES ON CHEMICAL<br>MECHANICAL POLISHING OF DIELECTRIC SILICON DIOXIDE..... | <br>132 |
| Introduction.....  | 132     |
| Experimental .....   | 134     |
| Characterization .....   | 135     |
| The Size Characterization of Colloidal Silica Particles.....   | 135     |
| Fundamentals of Characterization of Polished Surfaces .....  | 136     |
| Results and Discussion .....   | 137     |
| Effects of Particle Size and Solids Loading on Polishing Rate.....   | 137     |
| Surface Characterization (Solids Loading and Particle Size Effects) .....  | 139     |
| The <i>In Situ</i> Friction Force Measurements (Particle Size and Solids Loading<br>Effects).....                            | 141     |
| Effects of Down Pressure on Polishing Rate.....  | 143     |
| Surface Characterization (Down Pressure Effects) .....   | 144     |
| Proposed Interfacial Contact Model .....   | 146     |
| Particle Size and Solids Loading Effects on Interfacial Contact .....  | 146     |
| Down Pressure Effects on Interfacial Contact .....   | 147     |
| Summary .....  | 148     |
| <br>9. SUMMARY .....   | 150     |
| <br>LIST OF REFERENCES .....   | 154     |
| <br>BIOGRAPHICAL SKETCH .....  | 162     |



## LIST OF TABLES

| <u>Table</u>   | <u>page</u> |
|--|-------------|
| 1-1. Correlation of system-level variations with micro- and nanoscale effects and output parameters in chemical mechanical polishing ..... | 2           |
| 2-1. Pad properties. ....  | 22          |
| 2-2. Low resistivity materials for interconnect conductor materials. ....  | 27          |
| 2-3. The most promising candidates for low-k ILD materials. ....   | 30          |
| 3-1. <i>In situ</i> lateral friction force with down pressure and particle sizes for 35wt. % solids loading. ....                          | 62          |
| 4-1. Variation in size of particles by light scattering techniques .....   | 73          |
| 6-1. Variation in size of supplied abrasive particles. ....  | 94          |

## LIST OF FIGURES

| <u>Figure</u>   | <u>page</u> |
|---|-------------|
| 1-1. The images of chemical mechanical polishing tool: (a) the Strasbaugh 6EC chemical mechanical polishing tool, (b) a close-up of the tool. ....  | 3           |
| 1-2. Number of transistors per chip as a function of year .....   | 4           |
| 2-1 Total delay time caused by interconnection and gate at different feature sizes .....  | 8           |
| 2-2. Schematic of the closed-packed ICs interconnect and capacitance associated with metal interconnect lines as a function of feature size.....  | 9           |
| 2-3. Cross section of multilevel interconnects with silica dielectric and aluminum metallization. ....  | 13          |
| 2-4. A cumulative increase in topography by multi-level interconnection without using a planarization method. ....  | 14          |
| 2-5. Cross section of multilevel metallization scheme with silica dielectric and aluminum metallization: (a) unplanarized, (b) surface smoothing, (c) local planarization, and (d) global planarization. .... | 15          |
| 2-6. Schematic illustration of a typical CMP tool.....  | 18          |
| 2-7. Schematic illustration of CMP pads manufactured by Rodel.....  | 21          |
| 2-8. SEM cross-section of IC 1000/Suba IV stacked polishing pad (40 ×). ....  | 23          |
| 2-9. IC1000 polishing pad; (a) optical microscopy, (b) SEM micrograph, and (c) profilometer scan of cross-section of pad surface. ....  | 23          |
| 2-10. SEM images of Suba IV pad surface (150×). (a) Before polishing (new pad) (b) After polishing (glazed). ....   | 25          |
| 2-11. The effect of pad glazing and conditioning on polishing rate. ....  | 25          |
| 2-12. Process flow of dual damascene process for copper interconnection. ....   | 29          |
| 2-13. Current recorded for one stroke during the tribological experiments for anodic applied potential (+2V) in 0.5M H <sub>2</sub> SO <sub>4</sub> for a sphere motion cycle of 0.2 second ...               | 32          |

|   |    |
|---|----|
| 2-14. Anodic current as a function of time for tungsten measured in 0.5M H <sub>2</sub> SO <sub>4</sub> at various potentials.....  | 32 |
| 2-15. Penetration of different liquids into a glass surface during indentation. ....  | 35 |
| 2-16. Solubility of amorphous silica particles. ....  | 35 |
| 2-17. Schematic of interlocking in two different surfaces. ....   | 40 |
| 2-18. Schematic of macro-displacement.....  | 41 |
| 2-19. Relation between tensile strength and surface energy decrease of fused silica in various atmospheres. ....  | 42 |
| 2-20. Lubrication in Journal bearing & the Stribeck curve. ....   | 44 |
| 2-21. Characteristic of slurry film thickness.....  | 45 |
| 3-1. Schematic presentation of <i>in situ</i> lateral friction force instrument.....  | 53 |
| 3-2. Size distributions of particles measured by dynamic light scattering (a) mean diameter (0.204μm), standard deviation (0.0444μm), (b) mean diameter (1.087μm), standard deviation (0.899μm). .... | 54 |
| 3-3. <i>In situ</i> lateral friction force as a function of time for different down pressure, particle size, and solids loading.....  | 55 |
| 3-4. <i>In situ</i> lateral friction force as a function of solids loading for different down pressure and particle size.....   | 57 |
| 3-5. <i>In situ</i> lateral friction force as a function of the number of particles per unit volume (cm <sup>3</sup> ) for different down pressure and particle size. ....                            | 59 |
| 3-6. The normalized fractional surface coverage (f) of particles in contact with wafer....  | 63 |
| 4-1. Two-dimensional interfacial contact of a single particle with a rigid wafer and a pad. ....  | 68 |
| 4-2. Particle size distribution for different lots of silica particles diluted in DI water at pH 10.5.....  | 72 |
| 4-3. SEM images of abrasive particles: (a) 100K, (b) 50CK-V1, and (c) 50CK.....   | 74 |
| 4-4. Friction force as a function of time for various particle sizes. Solids loading is varied every 30 sec.....  | 75 |
| 4-5. Friction force as a function of solids loading for different particle sizes. ....  | 76 |

|   |     |
|---|-----|
| 5-1. Size distribution of abrasive particles measured by dynamic light scattering technique. ....   | 80  |
| 5-2. Friction force as a function of time for different platen velocity and solids loading. ....  | 81  |
| 5-3. (a) Friction force as a function of platen velocity for different solids loading, (b) slope in friction force vs. platen velocity as a function of solids loading. ....                            | 82  |
| 5-4. Effects of solids loading on slurry viscosity. ....  | 84  |
| 5-5. Friction force as a function of down pressure for different solids loading. ....   | 85  |
| 6-1. Friction force as a function of time at down pressure of 2.5 psi. ....   | 91  |
| 6-2. The FTIR spectrum of as received colloidal silica slurry. ....   | 92  |
| 6-3. Particle size and size distribution of colloidal silica as a function of pH. ....  | 93  |
| 6-4. SEM image of colloidal silica particle dispersed at pH 10.5. ....  | 94  |
| 6-5. Solubility of amorphous silica particle and silica wafer as function of pH. ....   | 95  |
| 6-6. Polishing rate as function of pH for various down forces. ....   | 96  |
| 6-7. Log plot of silica polishing rate vs. pH for different down force. ....  | 97  |
| 6-8. Zeta potential of silica slurry as a function of pH. ....  | 99  |
| 6-9. The interaction force between a silica particle 25 $\mu\text{m}$ in radius and a silica plate in 0.001 M sodium chloride solution as a function of pH. ....  | 99  |
| 6-10. Friction force as a function of pH under the down pressure of 3.5 psi. ....   | 101 |
| 6-11. Friction force as a function of down pressure for different pH conditions. ....   | 101 |
| 6-12. Surface roughness (RMS) of silica wafer polished with colloidal silica as a function of pH at down pressure of 10.5 psi. ....   | 103 |
| 6-13 Overview and cross-section for the silica wafer polished with colloidal silica slurry of (a, top) pH 9 and (b, bottom) pH 10.5. ....   | 104 |
| 7-1. Wear patterns for (a) fused silica and (b) 1018 steel using two-body abrasion (top) and three-body abrasion (bottom) . ....  | 108 |
| 7-2. Scanning Electron Microscopy (SEM) images of silica particles with different particle size: (a) 0.2 $\mu\text{m}$ , (b) 0.5 $\mu\text{m}$ , (c) 1.0 $\mu\text{m}$ and (d) 1.5 $\mu\text{m}$ . .... | 111 |
| 7-3. Size distribution of silica particles measured by dynamic light scattering. ....   | 112 |

|   |     |
|---|-----|
| 7-4. Friction force as a function of time for various solids loading of 0.2 $\mu\text{m}$ silica particles. ....  | 113 |
| 7-5. Friction force as a function of time for 0.5 $\mu\text{m}$ silica particles: (a) Low solids loading (less than 7 wt.%), (b) High solids loading (more than 8 wt.%). ....   | 114 |
| 7-6. Friction force as a function of time for 1.0 $\mu\text{m}$ silica particles: (a) Low solids loading (less than 4 wt.%), (b) High solids loading (more than 5 wt.%). ....   | 116 |
| 7-7. Friction force as a function of time for 1.5 $\mu\text{m}$ silica particles: (a) Low solids loading (less than 3 wt.%), (b) High solids loading (more than 5 wt.%). ....   | 118 |
| 7-8. Friction force as a function of solids loading for different particle sizes. ....  | 120 |
| 7-9. AFM over-view images for the wafer polished with 0.2 $\mu\text{m}$ Geltech silica particles of different solids loading: (a) 0.5 wt.%, (b) 5 wt.%, (c) 15 wt.%, and (d) 30 wt.%. ....  | 122 |
| 7-10. AFM over-view images for the wafer polished with 0.5 $\mu\text{m}$ Geltech silica particles of different solids loading: (a) 0.5 wt.%, (b) 5 wt.%, (c) 15 wt.%, and (d) 30 wt.%. ....   | 123 |
| 7-11. AFM over-view images for the wafer polished with 1.0 $\mu\text{m}$ Geltech silica particles of different solids loading: (a) 0.5 wt.%, (b) 2 wt.%, (c) 15 wt.%, and (d) 30 wt.%. ....   | 125 |
| 7-12. AFM over-view images for the wafer polished with 1.5 $\mu\text{m}$ Geltech silica particles of different solids loading: (a) 0.5 wt.%, (b) 2 wt.%, (c) 15 wt.%, and (d) 30 wt.%. ....   | 126 |
| 7-13. Surface roughness (Root Mean Square) as a function of solids loading for various particle sizes: (a) 0.2 $\mu\text{m}$ , (b) 0.5 $\mu\text{m}$ , (c) 1.0 $\mu\text{m}$ , and (d) 1.5 $\mu\text{m}$ . ....                                 | 127 |
| 7-14. Polishing rate as a function of solids loading for different particle size. ....  | 129 |
| 8-1. Surface profile of cross-sectional area of top surface. ....   | 136 |
| 8-2. Polishing rate as a function of solids loading for various particle sizes under the condition of down pressure of 7.5 psi. ....  | 137 |
| 8-3. The over-view images and cross-section of silica wafer surface polished with colloidal silica particle having particle diameter of 88 nm for various solids loading: (a) 2 wt.%, (b) 5 wt.%, and (c) 15 wt.%. ....                         | 139 |
| 8-4. The over-view images and cross-section of silica wafer surface polished with colloidal silica particles for two solids loading conditions: (a) 10 wt. % (48 nm), (b) 10 wt.% (110 nm), (c) 30 wt.% (48 nm), and (d) 30 wt.% (110 nm). .... | 141 |

|   |     |
|---|-----|
| 8-5. Friction force as a function of solids loading for various particle size at down pressure of 3.5 psi .....   | 142 |
| 8-6. Polishing rate as a function of down pressure for various particle size. ....  | 143 |
| 8-7. The over-view images and cross-section of silica wafer surface polished with 30 wt.% colloidal silica particles for two different particle sizes and solids loading conditions: (a) 4.5 psi (48 nm), (b) 15 psi (48 nm), (c) 4.5 psi (110 nm), and (d) 15 psi (110 nm). .... | 145 |
| 8-8. A schematic diagram of the interfacial contact at the pad-particles-wafer interface with the change of particle size and solids loading .....  | 147 |
| 8-9. A schematic diagram of the interfacial contact at the pad-particles-wafer interface with the change of down pressure. ....   | 148 |

Abstract of Dissertation Presented to the Graduate School  
of the University of Florida in Partial Fulfillment of the  
Requirements for the Degree of Doctor of Philosophy

STUDY OF INTERFACIAL INTERACTION DURING CHEMICAL MECHANICAL  
POLISHING (CMP) OF DIELECTRIC SILICON DIOXIDE

By

Wonseop Choi

December 2003

Chair: Rajiv K. Singh

Major Department: Materials Science and Engineering

Chemical mechanical polishing (CMP) is an advanced technology utilized to achieve local and global planarization through synergistic interactions of both mechanical abrasion by abrasive particles and chemical reaction via chemical additives. The CMP process has played an important role in the microelectronic device fabrication industry. The introduction of CMP to microelectronic fabrication processes enables multilevel interconnections, yielding high packing densities, the density of transistors per square millimeter of silicon. The high packing density is responsible for the high-speeds achieved by semiconductor devices.

As interconnection dimensions shrink and the number of metal layers grows in multilevel interconnects, the need for CMP increases. In spite of the growth in the role of the CMP process in microelectronic device fabrication, the principles and mechanisms of polishing have not been clearly understood. The clear delineation of polishing phenomena assist in further optimization of the CMP process.

The CMP is the result of interfacial interactions at the pad-particles-wafer interface. Real-time observations of the interfacial interaction are essential in understanding polishing principles and mechanisms. This study details observations and gives analysis of interfacial interactions in order to delineate polishing mechanisms.

The variation in friction force has been investigated via *in situ* friction force measurement. Based on the friction force arising from the pad-wafer interface or pad-particles-wafer interface, the contact variation at the interface was delineated. The contact variation was analyzed using a contact model developed from the principles of friction force and micro-contact mechanics.

Slurry properties such as pH, particle size, and solids loading are important factors in determining polishing rate. The effect of pH, particle size, and solids loading of colloidal silica slurry on polishing performance such as polishing rate, surface finish was investigated to validate polishing mechanism performed by colloidal silica slurry; we verified that the polishing rate and surface finish were significantly dependent on the dynamic motions such as rolling or sliding of particles, interaction force between two surfaces, contact area, and indentation depth of particles into the wafer surface.



## CHAPTER 1 INTRODUCTION

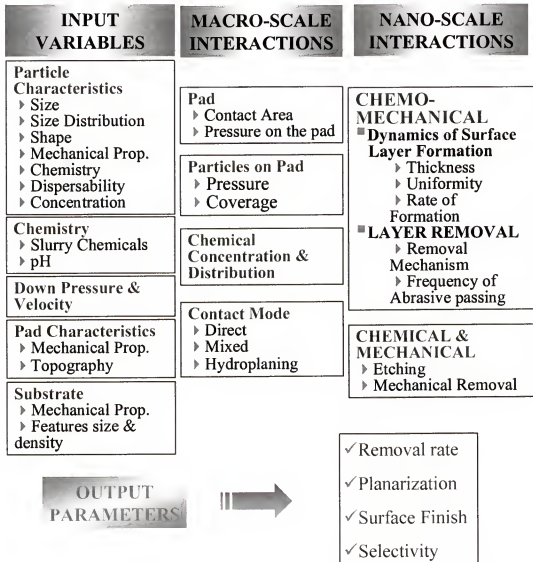
### **Background**

Chemical mechanical polishing (CMP) is the process of smoothing and planarization via chemical and mechanical interactions. The CMP has been used to polish a variety of materials for thousands of years. Recently optically flat and damage-free glass and semiconductor surfaces have been prepared utilizing the CMP process [Ste97]. Additionally, The CMP has been successfully introduced as the planarization technique of choice for the interlayer dielectric (ILD) materials and metals used to form interconnects. The effectiveness of the CMP process has led to the widespread use of this process at various stages of integrated circuit (IC) fabrication, for a variety of high performance and application-specific ICs, and for a variety of materials.

Continued miniaturization of the device dimensions and the related need to interconnect an increasing number of devices on a chip have led to building multilevel interconnections on planarized levels [Rya95]. The difference between the historical uses of CMP and those in Si IC fabrication lies in the amount of material that can be removed prior to achieving the desired planarity. Non-planar surfaces develop as a result of the fabrication process due to non-uniform deposition of the metal or dielectric film on a previously patterned surface. A complicating factor for any planarization scheme is the low thickness (less than  $0.5\mu\text{m}$ ) of the layer to be polished [Ste97]. Maintaining precise control on the remaining thickness, which is very small to within  $0.01 - 0.05\mu\text{m}$ , while maintaining the integrity of underlying structures is required for obtaining the desired

performance of CMP. Understanding the CMP process, which consists of a large number of variables, which is seen in Table 1-1, has become essential in developing a reliable high-performance and cost-effective CMP process [Sin02a]. Most of the variables will be discussed in the next chapters.

Table 1-1. Correlation of system-level variations with micro- and nanoscale effects and output parameters in chemical mechanical polishing [Sin02a].



As seen in Figure 1-1 [Str03], the CMP process simply consists of moving the sample surfaces to be polished against a polymer pad that is used to provide support

against the sample surface (the pad thus experiences the pressure exerted on the sample). The slurry, which contains abrasive particles, is carried between the sample surface and pad to affect the polishing leading to planarization. Abrasive particles in the slurry cause mechanical damage on the sample surface, loosening the material for enhanced chemical attack or fracturing off the pieces of surface into slurry where they dissolve or are swept away.

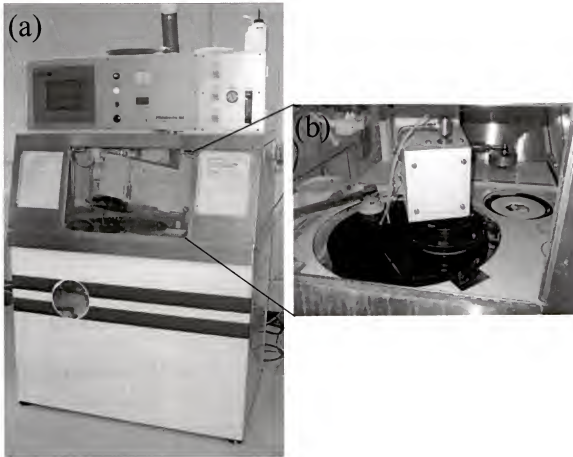


Figure 1-1. The images of chemical mechanical polishing tool: (a) the Strasbaugh 6EC chemical mechanical polishing tool, (b) a closed-up of the tool [Str03].

The process is tailored to provide an enhanced material removal rate from high points on surfaces (compared to low areas), thus affecting the planarization rate. Note chemistry alone will not achieve planarization because most chemical actions are isotropic.

Mechanical grinding alone, theoretically, may achieve the desired planarization but is not desirable because of extensive associated damage of material surfaces [Ste97]. Details of the process are discussed in subsequent chapters.

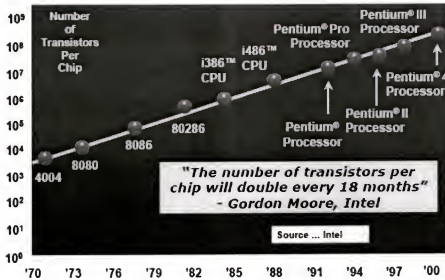


Figure 1-2. Number of transistors per chip as a function of year [Moo65].

Modern integrated circuits (ICs) contain tens to hundreds of millions of logic devices to achieve complex functions. As seen in Figure 1-2, Moor's law [Moo65] suggests that the number of transistor per chip (packing density) be doubled every 18 months. The increasing packing density demands an ever increasing number of interconnection levels in high performance circuits and memories, leading to the increased planarity requirements. Successful application of the CMP process in silicon integrated circuits (ICs) was started with building multilevel (greater than 2) interconnection structures employing deposited  $\text{SiO}_2$  as the ILD and the chemical vapor deposited (CVD) tungsten as the via fill metal with sputtered aluminum as the planar interconnection metal [Moy89]. In this application CMP achieved two results: (1) planarization of the  $\text{SiO}_2$  surface and (2) removal of CVD tungsten from the horizontal

surface, thus allowing the excellent via fill metal to be then connected to horizontal aluminum interconnections formed by sputter deposition and the subsequent reactive ion etching. Thus initial process developments focused on the CMP of  $\text{SiO}_2$  and tungsten layers. Since these developments, the use of CMP has expanded to (1) a large variety of materials including metals (Al, Cu, Ta, Ti, TiN, W, and their alloy, insulator ( $\text{SiO}_2$  and doped  $\text{SiO}_2$  glasses,  $\text{Si}_3\text{N}_4$ , and polymer) (2) a variety of applications requiring much larger planarized area such as those used in multichip modules and in other IC packaging and in flat panel displays, (3) planarizing materials at different levels of silicon device and integrated front-end circuit processing [Ste97].

### **Research Outline**

In spite of the increase in the role of CMP in microelectronic device fabrication, the fundamental principles of CMP are not clearly understood. Understanding of CMP principles is required for obtaining desired CMP performance. The performance of CMP is determined by the interfacial interactions between polishing pad, slurry containing abrasive particles and chemical additives, and materials to be polished. Therefore, the delineation of the interfacial interactions is critical when seeking to understand the fundamental principles in the CMP process. The objective of this study is to validate polishing mechanisms by investigating the interfacial interactions altered by the change of a variety of variables such as platen velocity, down force, chemical conditions in slurry, particle size, and solids loading. A synopsis of the efforts constituting this study is organized as follows.

Chapter 1 gives the general introduction for this study. Chapter 2 describes the literature review of chemical mechanical polishing (CMP) starting with the motivation of CMP in the microelectronic device fabrication industry. The CMP process is briefly

explained with a schematic of a typical CMP tool containing polishing slurry, polishing pad, and material to be polished. The friction force in CMP is reviewed from the basic principles. The models of material removal rate in CMP are also discussed. Chapter 3 presents the contact variation of particles during CMP. Fractional surface coverage of particles is determined by both the variation of friction force obtained via *in situ* friction force measurements and a model developed from the principles of friction force. Chapter 4 focuses on the interfacial contact variation as a function of solids loading and particles size. An interfacial micro contact model is developed to determine the contact variation of particles during CMP. Chapter 5 concentrates on the dynamic contact at the pad-particles-wafer interface as a function of platen velocity and down pressure for different solids loading. Chapter 6 discusses the effect of pH and down load on polishing rate. It is found that both electrostatic repulsion force and the formation of gel layer play an important role in determining polishing rate. Chapter 7 presents the effects of slurry particles on silica CMP. The dynamic motion (sliding or rolling motion) of silica particles, which is detected by *in situ* friction force measurements, plays a critical role in determining polishing rate and surface topography. Chapter 8 discusses the effects of colloidal silica particles on chemical mechanical polishing of dielectric silicon dioxide. The interfacial contact of colloidal silica particles between the pad and the wafer are investigated to validate polishing mechanism by colloidal silica particles during polishing. Finally, Chapter 9 presents a summary of this study.

## CHAPTER 2

### LITERATURE REVIEW OF CHEMICAL MECHANICAL POLISHING

This chapter briefly gives an overview of chemical mechanical polishing (CMP) starting with the reasons that CMP is utilized in the microelectronic device industry. The main CMP components: abrasive containing polishing slurry, polishing pad, and materials to be polished are not only discussed, but polishing mechanisms in metal and oxide CMP have also been reviewed. In addition, friction in CMP will be reviewed in order to delineate the polishing behavior occurring at the pad-particles-wafer interface during CMP. Finally, modeling in CMP is analyzed to identify specific research needed for developing reliable predictive methodologies for CMP applications.

#### **Interconnects on Integrated Circuits (ICs)**

As the integrated circuits (ICs) increase in complexity and density and become increasingly miniaturized, the role of CMP in microelectronic device fabrication has increased [Ste97]. The continuous demand in the semiconductor industry for faster and more functional integrated circuits (ICs) has driven the scaling down of microelectronic devices. Reduction in semiconductor device dimensions provides higher densities and improved performance for integrated circuits. Most high performance systems must accommodate increased current density, decreased wire width, increased amount of devices on a chip, increased tolerance to noise, and minimized power variations across the chip, and reduced (R) and capacitance (C) interconnection schemes to maintain chip performance [Rya95]. A reduction in the total delay time is necessary to improve the performance of integrated circuits with high device densities. According to scaling

theory, the small dimension of MOS (metal-oxide semiconductor) transistors enhances its switching speed by lowering gate delay [Liu99]. A reduced scale of interconnect increases the parasitic resistance (R) and capacitance (C) associated with the interconnect delay. Therefore, today, the interconnect delay is found to be the main contribution to increase the total delay times (Figure 2-1).

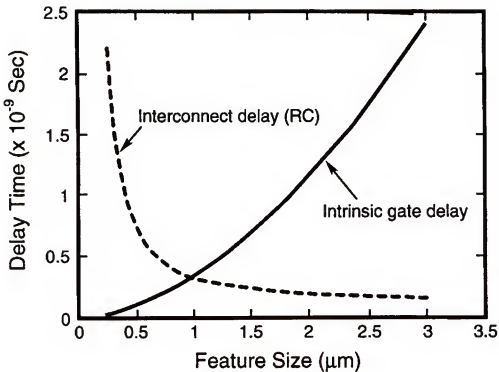


Figure 2-1 Total delay time caused by interconnection and gate at different feature sizes [Jen94].

The interconnect delay is characterized by RC (resistance  $\times$  capacitance) time constant. The most commonly used measure of the interconnect delay is the RC time delay, which is the time it takes for the voltage at one end of a metal line to reach 63% of its value at the other end of the metal line when a step input is present [Ste97]. High speed of the interconnects can be achieved by reducing the RC time constant. Figure 2-1



shows that the role of RC time delay becomes more significant in the total delay time as the size of the device becomes smaller [Liu99].

The resistance in the interconnect line is expressed by

$$R = \rho \cdot \frac{l}{w \cdot t_{metal}} = \frac{l}{A} \quad (2.1)$$

where  $\rho$  is the resistivity of the interconnect metal and  $l$ ,  $w$ ,  $t_{metal}$ , and  $A$  are the length, width, thickness, and cross sectional area of the interconnect metal line, respectively.

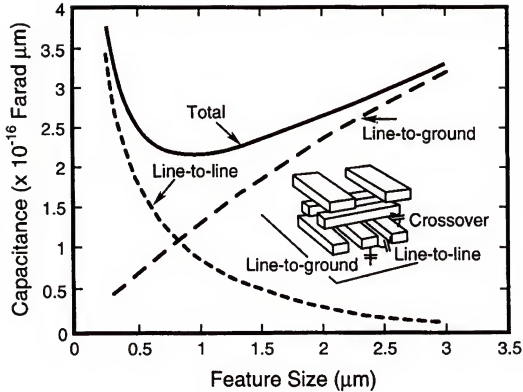


Figure 2-2. Schematic of the closed-packed ICs interconnect and capacitance associated with metal interconnect lines as a function of feature size [Jen94].

The total line capacitance is composed of line-to-line capacitance ( $C_{ln-ln}$ ) and line-to-substrate capacitance ( $C_{ln-sub}$ ). The schematic of the closed-packed IC interconnect and capacitance associated with interconnect metal line is presented in Figure 2-2. Line-to-

line capacitance ( $C_{\text{ln-ln}}$ ) between two adjacent interconnect lines separated by a distance,  $d$ , is given by

$$C_{\text{ln-ln}} \propto \varepsilon \cdot \frac{t_{\text{metal}} \cdot l}{d} \quad (2.2)$$

where  $\varepsilon$  is the permittivity and  $d$  is the spacing between two adjacent metal interconnect lines. Note that permittivity,  $\varepsilon$ , is equal to the insulator dielectric constant,  $\varepsilon_r$ , times the permittivity of free space,  $\varepsilon_0$ . Line-to-substrate capacitance ( $C_{\text{ln-sub}}$ ) between an interconnect line and the silicon substrate is

$$C_{\text{ln-sub}} \propto \varepsilon \cdot \frac{w \cdot l}{t_{\text{dielectric}}} \quad (2.3)$$

where  $t_{\text{dielectric}}$  is the thickness of the dielectric insulator. Therefore, the total line capacitance can be given by [Dan81]

$$C_{\text{total}} = K_1 \cdot (C_{\text{ln-ln}} + C_{\text{ln-sub}}) \quad (2.4)$$

where  $K_1$  is a factor that takes into account the fringing field. The interconnect RC time delay is given by combining Equation 2.1 and 2.4 as follows:

$$RC \propto \rho \cdot \varepsilon \cdot l^2 \cdot \left( \frac{1}{w \cdot d} + \frac{1}{t_{\text{metal}} t_{\text{dielectric}}} \right) \quad (2.5)$$

The first term is dominant for the device dimension  $\leq 0.25 \mu\text{m}$ , whereas the second term is the dominant factor in the device dimension of more than  $1.0 \mu\text{m}$ . From this relationship, it is apparent that the interconnect RC time delay does not depend on either the metal line thickness or the oxide thickness in the device whose size is less than  $0.25 \mu\text{m}$ . This expression suggests that a decrease in the interconnect RC time delay is achieved by reducing  $\rho, \varepsilon$ , or  $l$ , or an increase in  $w$  or  $d$ . As the device dimensions are

scaled down, the metal line width and the space between two adjacent metal lines decreases, leading to an increase in RC time delay. As seen in Equation 2.5, the decrease in line length has a major impact on the RC time delay since the delay increases with the square of the length. Thus, it is advantageous to avoid long metal lines in device circuit designs. In addition, the adoption of the low resistivity metals and low dielectric materials in integrated circuit designs assists in reducing the RC time delay. Multilevel interconnection (MLI) is adapted to the ICs technology because forming MLI decreases  $L$ . The new interconnect metal also needs to be a better conductor than Al or its alloys, and an interlayer dielectric (ILD) with lower dielectric constant (commonly referred as low- $k$  materials) than  $\text{SiO}_2$  is needed.

### **Power Consumption**

The scaling of the device size has negative impacts on both the interconnect RC time delay and the power consumption of the interconnect system. The power consumption by interconnects ( $P_{\text{interconnect}}$ ) at a certain operation condition is described by [Wes85]

$$P_{\text{interconnect}} = C_{\text{total}} \cdot V^2 \cdot f \quad (2.6)$$

where  $V$  is the voltage and  $f$  is the frequency. Equation 2.6 shows that the power consumed by the interconnect system is proportional to the total capacitance ( $C_{\text{total}}$ ). Thus, reduction in the power consumption can be achieved by reducing the line-to-line capacitance in a small device.

### **Circuit Reliability**

The current density through the interconnect line is increased with the thinning of the interconnect line. This increased current density may cause failure in the metal

interconnect due to the electromigration [Sze81]. The mean-time-to-failure (MTTF) of an interconnect line due to the electromigration is derived from an empirical relation, which is known as Black's law [Bla69]:

$$MTTF^{-1} = B \cdot j_e^n \cdot \exp\left(-\frac{E_e}{k \cdot T}\right) \quad (2.7)$$

where  $B$  is a constant,  $J_e$  is the current density,  $n$  depends on the interconnect material, and  $E_e$  is the activation energy for electromigration. According to Equation 2.7, it is clear that MTTF is inversely proportional to the current density. The thinning of the interconnect metal line causes higher current density at a given current. Thus, if the resistance to electromigration is not high enough, a shorter lifetime of the interconnect metal line is expected.

### **Multilevel Interconnection (MLI)**

In the last decades, interconnects have evolved from a single layer to multilevel interconnects (MLI). Forming metal interconnections in a multilevel scheme, where different levels of interconnections are isolated by the dielectric and are contacted by vertical vias through the dielectric, reduces interconnect delay by several means [Mur91]. Figure 2-3 illustrates the cross-sectional scheme of multilevel metallization [Sti97]. The MLI technique is usually accompanied by increasing the capacity and reducing RC time delay for small dimensions.

The use of multilevel interconnect technology has a positive impact on both circuit performance and reliability. First, the use of the MLI reduces the total length of the interconnect metal lines due to the direct routing of metal lines. Second, the multilevel scheme enables the uses of the wider interconnect metal lines with a reduced packing density. Consequently, as seen from equation 2.1 to 2.5, the resistance and the

capacitance of the interconnect technology are significantly reduced, leading to a decrease in the interconnect RC time delay. The power consumption is also minimized due to a reduction in the total capacitance. Finally, the use of wider interconnect metal lines decreases the current density of the lines, leading to an improved current reliability.

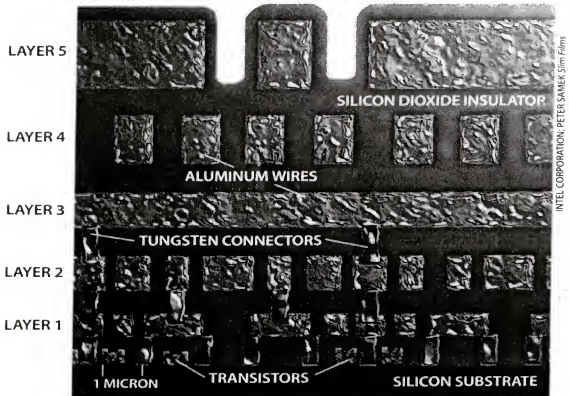


Figure 2-3. Cross section of multilevel interconnects with silica dielectric and aluminum metallization [Sti97].

To achieve MLI, several steps are required, including deposition, lithography, etching, and planarization. Initially, the dielectric surface is planarized and high aspect ratio via holes are etched into it. Then these holes are filled with metal and the excessive metal is removed by polishing. Finally, the next layer of dielectric is deposited and planarized to build the subsequent level. The decreasing device dimensions and the increasing number of metal layers necessitate improved planarization of the surface for

MLI, since non-planarity of the surface becomes cumulative as the layers are built one on top of another. Figure 2-4 shows the cumulative increase in topography by multi-level interconnection without using a planarization method. High topographic variations result in poor step coverage and electromigration problems [Ols93]. Especially, below the 0.5  $\mu\text{m}$  regime, the lithography tools require high numerical aperture lenses to print fine line dimensions. The depth of field of these lenses is about 270 nm across a 27 by 27 mm stepper field [Mog92].

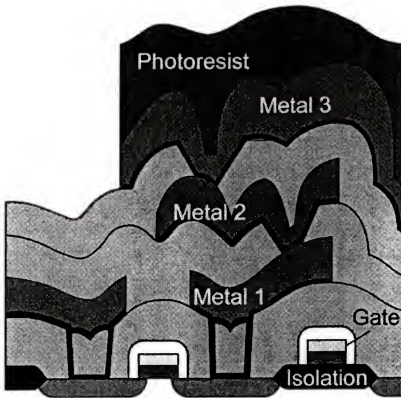


Figure 2-4. A cumulative increase in topography by multi-level interconnection without using a planarization method [Vic01].

Due to this finite depth, the optical steppers require less than 150 nm variations in topography across the stepper field [Mur93]. As seen in Figure 2-4, the uneven surface

topography also causes uneven photoresist thickness, resulting in overexposure of the thinner resist layers. Therefore, MLI requires effective planarization of the wafer surface.

### Planarization for MLI Fabrications

A solution to achieve submicrometer miniaturization of device dimensions and to increase the number of devices on a chip is the use of multilevel interconnection schemes where interconnections are made through vias in the dielectric layers isolating various levels of interconnections.

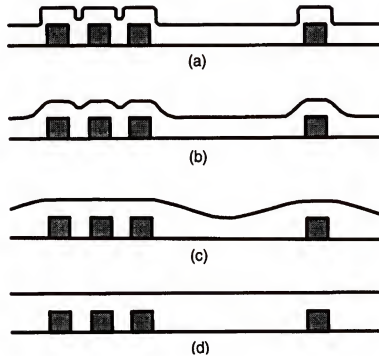


Figure 2-5. Cross section of multilevel metallization scheme with silica dielectric and aluminum metallization: (a) unplanarized, (b) surface smoothing, (c) local planarization, and (d) global planarization [Sti97].

There are three degrees of planarity, as shown in Figure 2.5: (1) surface smoothing, where feature corners are smoothed and high aspect ratio holes are filled, (2) local planarity where surface are flat locally but the surface height may vary across the die, and (3) global planarity where the surface is flat across an entire stepper field [Ols93]. For

such a scheme to work it is important that each level is flat so that lithography and patterning can be precise to allow vertical interconnections to be made. Three different approaches have been taken to achieve planarization at each level: (1) bias-sputtering, (2) dry-etching or reactive ion etching, and (3) chemical mechanical polishing (CMP).

In bias-sputtering, the substrate is biased so that back-sputtering is facilitated on the surface. Thus, sputter deposition and back-sputter occur simultaneously. Back-sputtering is asymmetric and is favored at sharp corners and edges so that when optimally used it results in excellent step coverage of the deposit, leading to a flat surface. Fujii *et al.* [Fuj88] reported the selective planarization of SiO<sub>2</sub> ILD to fine aluminum line using bias-sputtering. Bias-sputter deposition rates are, however, low. Also, ion damage occurs in these depositions. Considerable research and development work is necessary to make this process practical. The disadvantage is that the process does not provide the required large area planarization. The second alternative for planarization is dry etching or reactive ion etching (RIE). After the deposition of the oxide layer, a thick layer of photoresist is deposited on the surface, covering the steps. Photoresist is usually so thick that it covers all the steps well and the top surface is flat. Now a plasma or reactive etch process is chosen to etch the resist and the deposit at the same rate. The surface is etched until all resist and some glass is etched off, leaving the surface flat. The role of the sacrificial photoresist layer is to make the top surface flat prior to etching. The flatness can easily be achieved with spin-on applications of the viscous photoresist. During the subsequent isotropic etching of the surface, the flatness is retained because of the underlying deposit etches at the rate equal to the sacrificial photoresist layer. This technique is disadvantageous, since this process is lengthy and time consuming, and several repeats



are required and the plasma used is composed of hazardous gases [Mur93, Ste 97]. The third alternative is chemical mechanical polishing (CMP), which is described in the following sections.

### **Chemical Mechanical Polishing (CMP) Processes**

Chemical mechanical polishing (CMP) is a long-established technique, which is applied to many industrial areas. Before CMP was applied to ICs fabrication industry, polishing processes had been utilized to polish glass pieces in the fabrication of lenses [Hol64, Izu79]. Much of the understanding of glass polishing may be applied to oxide CMP. In the fabrication of ICs, silicon polishing as a final step in the preparation of starting wafers has been in use for several decades. However, CMP used for planarization of thin films differs from lens fabrication and wafer preparation in one important respect. In all three applications, a high degree of planarity or flatness is required; however, in CMP, the same degree of flatness must be achieved with far less material removal. In addition, the tolerances for material removal are much tighter for CMP. Wafer thickness, for example, may vary by several mils while ILD thickness must vary less than  $\sim 100\text{nm}$  from wafer to wafer. Thus, CMP used for planarization demands much tighter process control [Ste97].

The CMP has been received increased interest in microelectronic device fabrication industries since Beyer applied the concept of CMP to semiconductor processes at IBM [Bey99]. The main advantage of CMP arises from its ability to achieve global planarization, which reduces planarity related defects such as material stringers and poor step coverage. CMP can be applied to various materials and it is a simple technique. Thus, CMP creates an alternative for materials like copper, which are not amenable to dry

etch [Ste97]. In spite of its advantages, CMP has its own challenges leading to planarization including, (1) the process immaturity: an entire new tool set is needed for its integration into the IC manufacturing, (2) several potential defect modes: scratches, pitting, stress cracking of the films, corrosive attack of the slurry chemicals, delamination of film interfaces and residual particles on the film surfaces [Lan92]. The integration of CMP into IC processes offers many promising advantages in terms of performance and cost. However, there remain many uncertainties to CMP. Therefore, to increase CMP performance, it is vital to understand the fundamental of CMP.

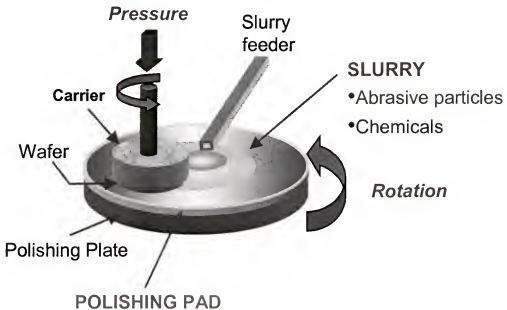


Figure 2-6. Schematic illustration of a typical CMP tool.

As the name suggests, CMP is a polishing process in which the surface topography on a wafer is planarized through chemical reactions and mechanical abrasion at the pad-slurry particles-wafer interface. Figure 2-6 illustrates the schematic representation of polishing tools. The rotating wafer to be polished is pressed down against a rotating polishing pad that is used to provide support against the sample surface and to carry the

polishing slurry. The polishing slurry consists of submicron size particles suspended in an aqueous medium containing chemical reagents. The polishing slurry is distributed across the pad by centrifugal force, forming a thin sheet of liquid on the pad. The combination of mechanical action from the down force and relative velocity applied to the abrasive particles and chemical reaction from the water and chemical reagents results in material removal from the surface of the wafer. In CMP, planarization is achieved by maintaining high removal rates at the high surface features, while low surface features are removed relatively slowly [Car90]. To understand polishing and planarization, the main components of CMP, polishing pad, slurry, and the surface to be polished are described here.

### **Abrasive Polishing Slurry**

The polishing slurry utilizes both chemical and mechanical reactions to remove and subsequently planarize the wafer surface. Typically used slurries are water-based and contain both abrasives and chemical additives. The polishing slurry affects the various CMP output variables such as polishing rate, selectivity, planarity, surface quality, surface damage, and post CMP cleaning.

The slurry abrasive particles provide the mechanical abrasion. Size and concentration of slurry abrasive particles, and stability of the abrasive suspension have a direct effect on mechanical abrasion. Sub-micron or nano sized  $\text{SiO}_2$ ,  $\text{Al}_2\text{O}_3$ , or  $\text{CeO}_2$  particles are commonly used as abrasive particles in slurries [Sin02a]. Silica ( $\text{SiO}_2$ ) is most often used for oxide polishing while alumina ( $\text{Al}_2\text{O}_3$ ) and silica are used for metal polishing. Ceria ( $\text{CeO}_2$ ) is also a candidate polishing compound due to characteristics of high removal rate and high selectivity [Zha01]. In addition, the distribution of abrasive size has a dramatic effect on surface damage. Cook suggests that monodispersion in

abrasive size leads to super polishing or extremely smooth surfaces [Coo90]. Poor control of abrasive size distribution results in increased scratching. The concentration of abrasive particles affects the number of “cutting tools” at the surface. Generally, higher abrasive concentration leads to higher polishing rate [Bie99]. Abrasive particles in suspension may tend to agglomerate to form larger particles. The stability of the suspension indicates how long the agglomerated particles may remain suspended before settling out of the suspension. Good stability indicates minimal agglomeration and a uniform particle size distribution. Uniform particle size distributions are desirable to minimize surface damage.

Though mechanical grinding by the abrasive particles alone can provide planarization, this is not desirable because of extensive surface damage after polishing. Alternatively, chemicals alone cannot achieve planarization since most chemical reactions are isotropic on the wafer surface [Ste97]. The chemical components that may be present include oxidizers, complexing agents, pH buffering agents, corrosion inhibitors, dispersion agents, etc. These chemicals have specific roles in creating an easily removable surface layer on the material. An oxide layer formed on metal surfaces assist in achieving planarization. A passivation layer is utilized to maintain a low chemical removal (etching) rate from the recessed area. Stable CMP slurries are achieved either by the control of pH or by the addition of stabilizing reagents. The synergistic interaction of both mechanical and chemical interactions causes material to be easily removed from the surface of the wafer with low defectivity. Therefore, it is important to determine the extent of the chemical activity on the wafer surface and the conditions under which the mechanical abrasion takes place.

## Polishing Pad

The polishing pad is important in determining polishing rate and planarization ability of a CMP process. Figure 2-7 illustrates the images of pads manufactured by Rodel [Rod03]. Pads are spherical in shape and its diameter is dependent on wafer size. The diameter of pads is increased with the increase of diameter of wafer to be polished.



Figure 2-7. Schematic illustration of CMP pads manufactured by Rodel [Rod03].

The pad surface performs two primary functions during CMP: (1) pores in the pad aid in slurry transport, and (2) the polymeric foam cell walls of the pad are responsible for removal of reaction products from the wafer surface [Jai94a]. The pad thus influences both the chemical and mechanical aspects of CMP. In general, polishing pads are composed of polyurethane because polyurethane chemistry allows the pad characteristics to be tailored to meet specific mechanical property needs [Jai94b].

Specific gravity indicates the pad porosity; the lower the specific gravity, the higher the porosity [Ste97]. Porosity is an important property due to two primary reasons: (1) the

pores aid in slurry transport and (2) the pore walls aid in the removal of reaction products from the polishing site [Jai94a].

Table 2-1. Pad properties [Rod03].

| Pad      | Specific Gravity | Compressibility | Hardness        |
|----------|------------------|-----------------|-----------------|
| Suba IV  | 0.3              | 16 %            | 55 (Shore A)    |
| Suba 500 | 0.34             | 12 %            | 65 (Shore A)    |
| IC-60    | 0.7              | N/A             | 52-60 (Shore D) |
| IC-1000  | 0.6-0.8          | 2.5 %           | 57 (Shore D)    |

Hardness and compressibility have been found empirically to affect planarity. The harder and more non-compressible the pad, the less it will bend and conform to the wafer surface to remove material at the low regions. However, some flexibility of the pad is also required to avoid any possible breakage of wafers during polishing. Stacked pads have been introduced to meet these demands. Figure 2-8 shows a SEM cross-section of Rodel's composite polishing pad consisting of two pre-stacked films. The bottom is Suba IV pad and the upper is IC 1000 pad. As seen in Table 2-1, Suba IV pad is softer and more compressible than IC 1000 pad. The bottom soft pad (Suba IV) enables the composite structure of the pad to conform to the wafer shape due to its low hardness and high compressibility. The top stiffer pad (IC 1000) maintains a wide planar area while polishing patterned wafers, which assists in obtaining global planarity. The surface topography of the pad is tailored to meet the slurry transport demands.

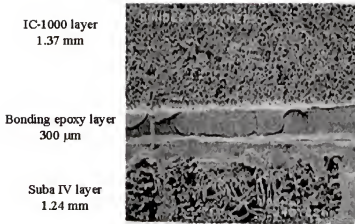


Figure 2-8. SEM cross-section of IC 1000/Suba IV stacked polishing pad ( $40\times$ ) [Obe98].

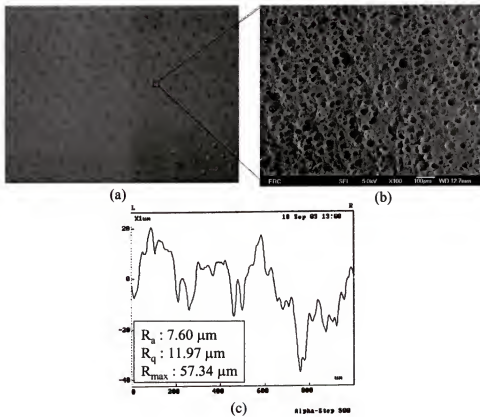


Figure 2-9. IC1000 polishing pad; (a) optical microscopy, (b) SEM micrograph, and (c) profilometer scan of cross-section of pad surface.

Figure 2-9 shows optical and SEM images of an IC 1000 polishing pad with the cross section measured by profilometer. The optical image shows the periodically arranged macro-pores on the pad surface. The SEM image magnified from the seemingly macroscopically flat area in the optical image illustrates a large number of micro-pores randomly distributed. Therefore, slurry transport is achieved by combined interaction of both macro and micropores. As seen in figure 2-9, the height distribution of the top surface area of the pad is non-uniform and very rough. This is confirmed by the surface roughness measurements ( $R_q = 11.97\mu\text{m}$ ,  $R_a = 7.60\mu\text{m}$ ) of top surface area in polishing pad. It is known that the pad surface roughness is important in determining polishing rate and planarity [Yu93, Jai94-2, Ren94]. Ren *et al.* [Ren94] have demonstrated that polishing rate increases with pad roughness. Yu *et al.* [Yu93] have measured pad roughness and proposed a removal mechanism based on the distribution of surface asperity heights (asperities are high points in the pad surface). While the down pressure is applied to the interface between pad and wafer, some portions of the pad asperities are thought to be in contact with the wafer surface and the contact area is expected to increase with increasing down pressure. In addition, the abrasive particles are trapped and released from the pad surface continuously at the points of contact during polishing [Kir94]. It is apparent that surface roughness and porosity of pad determine the relative rate of slurry transport to the surface, material transport away from the surface, and the contact area of the pad to the surface. Thus, it is important to optimize pad surface roughness and porosity, and to maintain these over the useful life of the pad. During polishing, however, the surface of the pad can undergo plastic deformation so that the surface becomes smoother and the pores fill with pad material, which is referred to as





Figure 2-10. SEM images of Suba IV pad surface (150 $\times$ ). (a) Before polishing (new pad) (b) After polishing (glazed) [Ste97].

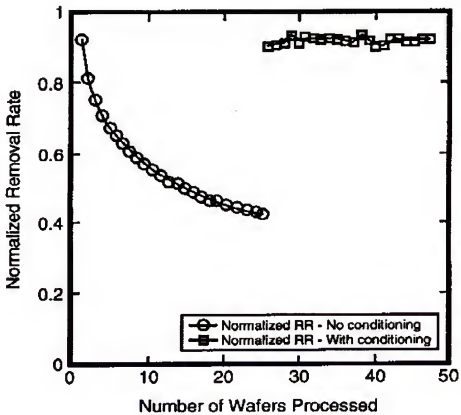


Figure 2-11. The effect of pad glazing and conditioning on polishing rate [Jai94a].

glazing [Jai94a]. Figure 2-10 depicts the surface of glazed pads. Glazing is undesirable since it leads to a decrease in polishing rate [Jai94a]. Figure 2-11 shows the effect of pad glazing on polish rate over time. The polishing rate decays approximately logarithmically with time until the surface is refreshed by a conditioning technique. Conditioning techniques are commonly performed on pads to maintain the roughness and porosity of the pad surface.

### **Materials to Be Polished**

Material selection in integrated circuits (ICs) is important to achieve high performance of microelectronic device. The high performance of ICs can be achieved by decreasing the RC time delay. As seen in Equation 2.5, to decrease RC time delay, resistivity ( $\rho$ ), dielectric constant ( $\epsilon$ ), or line length ( $l$ ) should be decreased. Resistivity and dielectric constant are terms related to material selection and line length is dependent on the structure of ICs. Therefore, multilevel interconnection structures with metal interconnects of low resistivity and dielectric materials of low dielectric constant have been developed for high performance of microelectronic devices.

The successful application of the CMP process in ICs began with multilevel interconnecting structures employing SiO<sub>2</sub> as the inner layer dielectric, chemical vapor deposited (CVD) tungsten as the via fill metal, and sputtered aluminum as the planar interconnection metal [Moy89]. Initial process developments in CMP focused on SiO<sub>2</sub> and tungsten layers [Utt91, Kau91]. Since then, a variety of metals and their alloys such as Al, Cu, Ta, Ti, TiN, and W, and dielectric materials including SiO<sub>2</sub> and SiO<sub>2</sub> doped glasses, Si<sub>3</sub>N<sub>4</sub>, polymer, and polysilicon are applied to multilevel interconnection structures. As mentioned earlier, decreasing the resistivity in metal interconnects plays an

important role in decreasing RC time delay. Table 2-2 shows resistivities for interconnect conducting materials [Mur93, Ste97].

Table 2-2. Low resistivity materials for interconnect conductor materials [Mur93, Ste97].

| Metal             | Bulk Resistivity<br>( $\mu\Omega\text{-cm}$ ) | Thin Film Resistivity<br>( $\mu\Omega\text{-cm}$ ) |
|-------------------|---|--|
| Ag                | 1.6   |  |
| Au                | 2.4   | 4.1  |
| Al                | 2.65  | 2.7  |
| Cu                | 1.7   | 1.8 – 2.1  |
| Mo                | 5.2   | 7.5 – 12   |
| W                 | 5.6   | 10 – 14  |
| WSi <sub>2</sub>  | 12.5  | 26 – 100   |
| TiSi <sub>2</sub> | 16.7  | 17 – 25  |
| MoSi <sub>2</sub> | 21.6  | 40 – 100   |
| TaSi <sub>2</sub> | 38  | 35 – 60  |

The most commonly used metals in IC manufacturing are the aluminum alloys since aluminum is a good conductor with a resistivity of  $2.66 \mu\Omega\text{-cm}$ . Among the candidates, only silver, copper, and gold has a resistivity lower than aluminum. Gold is favorable for its high resistance to corrosion and electromigration; however it shows only a marginal improvement in resistivity with a value of  $2.35 \mu\Omega\text{-cm}$ . Although silver shows the best resistivity value ( $1.59 \mu\Omega\text{-cm}$ ), silver has several disadvantages: (1) it is a very fast diffuser in  $\text{SiO}_2$  [Mcb86], (2) finding barriers to silver diffusion into the  $\text{SiO}_2$  and

silicon has proven difficult [Mur91], (3) silver has poor electromigration performance due to its low melting point [Li94]. Gold and silver dramatically affect the device's electronic properties due to the two deep levels introduced into the silicon band gap [Sze81]. Therefore, copper appears to be the most attractive candidate among all the metals with lower resistivity than aluminum. Its resistivity is  $1.67 \mu\Omega\text{-cm}$ , which is approximately 50 % lower than currently used aluminum alloys. In addition, copper has a higher melting point (1356 K) than aluminum (933K), leading to greater electromigration resistance [Li94]. As interconnection dimensions are scaled, copper with its higher electromigration resistance is required. There are, however, several challenges which must be resolved before metal can be fully accepted into IC manufacturing. First, copper exhibits deep levels in the silicon band gap and copper impurities in  $\text{SiO}_2$  lead to leakage [Sze81]. The degradation in the electronic properties of the silicon and  $\text{SiO}_2$  can be prevented using several barrier materials such as tantalum, tantalum nitride, and silicon nitride [Wan94]. The second challenge for copper is its susceptibility to corrosion. Third, the traditional method of metal patterning, using reactive ion etching (RIE), is not practical for copper due to the lack of copper compounds with high vapor pressures at relatively low temperatures [Ste97]. Thus, new methods of achieving the copper pattern (dual damascene process) have been introduced in IC fabrication, causing the CMP process to gain attractiveness in the semiconductor industry. The advantages of this process are no metal etching required, no interface resistance between the vias and lines, single step deposition of copper, and a globally planarized surface after CMP. This means that the subsequently deposited dielectric will also be planarized, and thus will not have to undergo CMP, leading to a reduction in the number of process steps. The dual

damascene process steps and two-step copper CMP process are schematically shown in Figure 2-12 [Jac98]. I would suggest starting new parameters here. Selection of interlayer dielectric (ILD) materials with low dielectric constant can reduce RC time delay. The need for new ILD materials arises from the relatively high dielectric constant ( $k$ ) of silica. The currently used ILDs are mostly chemical vapor deposited  $\text{SiO}_2$  with dielectric constant between 3.9 and 6.0 depending on the doping (fluorine or boron) and water content of silica.

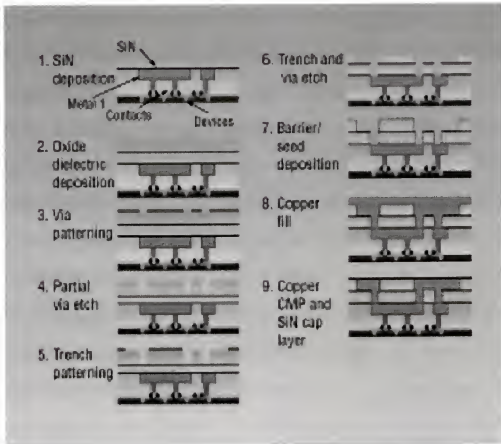


Figure 2-12. Process flow of dual damascene process for copper interconnection [Jac98].

To utilize low-k dielectric materials as new ILD materials, important requirements should be fulfilled: the dielectric constant should be lower than 3, should be thermally stable in 400–450°C range, moisture adsorption less than 1%, good adhesion to metal, mechanically stable, planarization behavior, plasma etching behavior, etc. The most promising candidates for low-k ILD materials are either organic or inorganic, and can be applied by spin-on or chemical vapor deposition (CVD) methods.

Table 2-3. The most promising candidates for low-k ILD materials [Chi99].

| Application method          | ILD material (Company)                                    | Dielectric constant (k) |
|-----------------------------|---|-------------------------|
| <b>CVD</b><br>Inorganic     | SiO <sub>2</sub>  | 4.1                     |
|                             | FSG F <sub>y</sub> SiO <sub>x</sub> (Silicon oxyfluoride) | 3.4 – 4.1               |
|                             | Black Diamond (Applied Materials)                         | 2.2 – 2.7               |
|                             | Methyl-doped SiO <sub>2</sub> (Trikon Technology)         | 2.6 – 3.0               |
| Organic                     | Parylene AF4 (Novellus (Alpha))                           | 2.25                    |
|                             | PTFE (DuPont)   | 1.9                     |
| <b>Spin-On</b><br>Inorganic | Nanoglass (AlliedSignal etc)                              | 1.3 – 2.5               |
|                             | MSQ methyl silsesquioxane (Dow Corning)                   | 2.7                     |
|                             | HSQ hydrogen silsesquioxane (Hitachi, EKC & Ashian)       | 2.9 – 3.1               |
| Organic                     | Silicon-based polymer (AlliedSignal)                      | 2.8 – 3.0               |
|                             | BCB, SiLK (Dow Chemical)                                  | 2.65                    |
|                             | Porous organosilicates (IBM)                              | 2.2 and lower           |
|                             | PTFE (W.L. Gore Speedfilm)                                | 4.9                     |

Among them, Black Diamond, SiLK, BCB, poly(arylene) ether, and Flare are favored low-k dielectric materials, and many studies have been conducted on these new materials. Table 2-3 contains a list of potentially useful low-k ILDs [Chi99].

### **Polishing Mechanism in Metal CMP**

#### **Tungsten CMP**

Metal polishing mechanisms appear to be considerably different from dielectric polishing. The first mechanism specifically proposed for metal CMP was that of Kaufmann *et al.* [Kau91] who proposed a relatively straightforward two-step mechanism, focusing on tungsten polishing. The first step is the formation of passive oxide layer on the metal surface, and the second step is the abrasion removal of the passive oxide layer by the abrasive in the slurry. The bare metal, when immediately exposed to the oxidizer, is repassivated. The passivation of metal in the slurry plays a very important role in CMP performance, by either forming native metal oxides on the surface using oxidizers such as  $H_2O_2$  [Mue99] and  $K_3Fe(CN)_6$  [Bie99]. Biemann *et al.* [Bie98] demonstrated the formation of a protective oxide layer on the tungsten surface by rubbing the surface using the pin-on-disk method. As shown in Figure 2-13, the current was decreased to near zero due to the formation of a passive oxide layer on the surface during the motionless stage, whereas when the fresh metal surface was exposed to the slurry by rubbing, current increased as the oxidation reaction started on the bare tungsten surface [Bie98]. A passivating oxide layer may be formed on the surface of tungsten in very short time scales during polishing. Biemann *et al.* [Bie98] also observed via *in situ* electrochemistry that the tungsten surface is fully passivated by the tungsten oxide layer in milliseconds as illustrated in Figure 2-14.

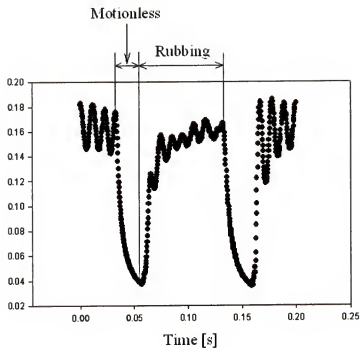


Figure 2-13. Current recorded for one stroke during the tribological experiments for anodic applied potential (+2V) in 0.5M  $\text{H}_2\text{SO}_4$  for a sphere motion cycle of 0.2 second [Bie98].

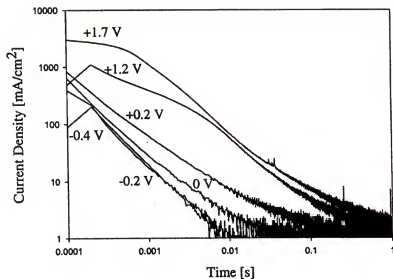


Figure 2-14. Anodic current as a function of time for tungsten measured in 0.5M  $\text{H}_2\text{SO}_4$  at various potentials [Bie98].



Therefore, the formation of a passivated oxide layer and the dynamic nature of this layer are key issues in understanding tungsten polishing mechanisms. In this regard, more extensive studies are required to understand the tungsten polishing mechanism.

### **Copper CMP**

Copper is the most attractive material for interconnects in MLI. As the dual damascene technology is successfully introduced into the IC fabrication industry, Copper CMP has become the indispensable process for planarization of copper. Generally, in all copper CMP processes, an oxidizer is used to etch copper. Carpio *et al.* have investigated the CMP slurry chemistries in various media [Car95]. In acidic media, an inhibitor, benzotriazole (BTA), is used to control the polishing rate and avoid isotropic etching [Kau00a, Kau00b]. Some of the advantages of an acidic process are the high selectivity of copper to silicon dioxide (selectivity greater than 100 is achievable) and excellent corrosion protection provided by residual BTA to the underlying copper long after polishing. One of the drawbacks of this process is the possible corrosion of the polishing equipment caused by the oxidizers in the slurry at low pH conditions [Ste97].

For neutral and alkaline media, copper can be passivated according to the Pourbaix diagram [Pou74]. In this case a passivation layer is used to reduce the isotropic etching of recessed regions on an uneven surface. In neutral polish slurries, it is reported that  $H_2O_2$  can be utilized as an oxidizer and the selectivity of copper to silicon dioxide of 70 is achieved [Sta95]. For alkaline media, ammonia ( $NH_3$ ) is utilized as a complexing reagent, forming complexes with copper ions. The disadvantage of this process is the undesirably low selectivity of copper to silicon dioxide. The chemistry of copper and alumina suggest that the mechanism for copper removal is the mechanical removal of copper, followed by the dissolution of abraded copper particles. Lee [Lee03] suggested

that polishing rate is significantly dependent on the mechanical properties of top surface layer. In his paper, material removal rate is proportional to the elastic modulus of the top surface layer that is changed by the kinds and concentration of chemical additives.

Copper can be polished with various abrasives, in the presence of various suppressants and with a wide range of oxidizers over a wide pH range. Because of the very rigorous demands of copper damascene CMP, and the incomplete current understanding, research efforts focused on copper are still growing.

### **Polishing Mechanism in Oxide CMP**

Oxide CMP is one of the most widely used CMP process with the most fundamental studies having been performed in this area. Oxide CMP has been described as an enabling technology because the high degree of planarization generated with CMP eases the burden of advanced lithography and etch processes [Lan92]. However, a CMP process that is not stable and well controlled is likely to result in more problems than solutions. In order to develop stable CMP processes and to control these processes in manufacturing, a good understanding of the process fundamentals are required.

In oxide CMP, water plays an important role because it provides the chemical component of the polish. Figure 2-15 shows a result in which the glass is indented in various liquids with a Knoop indenter under a 100g load for 30sec. Here, indentation under water also leads to water entry; however, water entry does not occur with indentation under other liquids [Tom94]. Cook [Coo90] suggests that water entry under the load imposed by the indenter is similar to water entry under the load imposed by the abrasive particle.

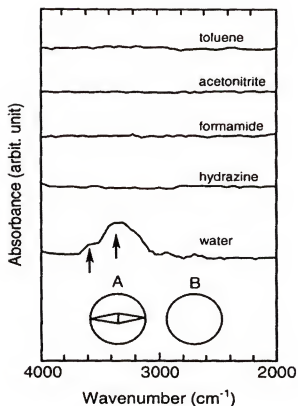


Figure 2-15. Penetration of different liquids into a glass surface during indentation [Tom94].

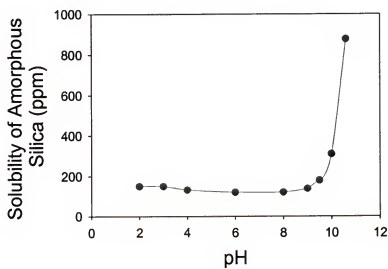
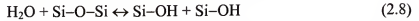
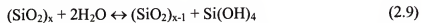


Figure 2-16. Solubility of amorphous silica particles [Ale54].

Water entry into the oxide surface weakens the glass network by breaking Si–O bonds. As a consequence, the hardness of the glass surface is reduced by water entry. The general reaction for the interaction of Si–O and H<sub>2</sub>O as follows [Ile79]:



Water diffusion into the oxide leads to the breaking of Si–O bonds within the hydrated layer, forming Si–OH bonds. Near the bulk, most of the Si–O bonds in the hydrated layer will be linked to the glass network, forming Si–O–Si links. Near the oxide surface, however, many of the Si–O bonds will be hydrated. The rate of this reaction is believed to be controlled by the diffusion of water into silica structure [Dor73]. The diffusion coefficient of water in silica at ambient conditions and neutral pH were measured to be quite low [Nog84, Lan85]. A significant increase in the diffusion rate of water into the silica structure occurs at high pH (> pH 9.0). Iler [Ile79] reported a three orders of magnitude increase in silica dissolution rate as the pH value was increased from 2 to 11. This behavior is explained based on the OH<sup>-</sup> ion acting as a catalyst for attack by water on the silica network [Bud61]. Once all of the Si–O bonds for a given Si atom are hydrated, Si(OH)<sub>4</sub> is formed which is highly soluble in water at high pH (>10) as seen in Figure 2-16. The overall reaction is given by:



Reaction (2.8) and (2.9) are accelerated by the compressive stress imposed into the surface by the abrasive particle. This is supported by Ito and Tomozowa's observation in which dissolution of silica increased significantly as a function of increased pressure from 50 to 250 MPa [Ito81]. Other investigations suggest that strain fields generated by the abrasive particles diffuse water into the surface and then accelerate the chemical

reaction of the water with the glass network, which initially breaks down the glass network in the hydrated layer and eventually leads to dissolution of the network at the surface and a subsequent high removal rate [Nog84].

Trogolo *et al.* [Tro94] revealed the evidence of a chemically or structurally modified surface layer formed on the silica surface layer after CMP using transmission electron microscopy (TEM) and Fourier-transform infrared (FTIR) spectroscopy. The cross-sectional TEM micrographs of the silica surface after CMP shows a two phase modified surface region. The first is a 2 nm surface region possessing lower density than the bulk, which is confirmed by grazing X-ray reflection [Nev80]. Adler observed a short-range repulsion on silica surface by atomic force microscopy (AFM) interaction force measurements [Adl01]. He suggested that this phenomenon might be due to the swelling of the silica surface as a result of water diffusion into structure, forming a gel-layer (top surface layer softer than the silica itself). This result is in agreement with the results of Tomozawa *et al.* [Tom94] in which silica hardness was observed to decrease drastically with the increasing water content. It can be concluded that the physical and mechanical properties of bulk silica are altered by the addition of water. These characteristics enable us to believe that the presence of a modified surface layer will affect the CMP performance such as polishing rate, surface defectivity, and planarization etc.

As a practical application to oxide CMP, the effects of slurry abrasives on polishing rate were studied. Even though slurry abrasive size and concentration is critical in determining CMP performance, the effect that abrasive size and concentration has on polishing rate is not clear. It has been suggested that the oxide polishing rate increases

with both abrasive size and concentration [Jai94a]. However, other reports find that glass polishing is constant with abrasive size [Coo90, Siv92], even decreases with abrasive size [Izu79]. Our previous work suggests two polishing mechanisms in silica CMP [Bie98].

One is a contact area based mechanism by

$$A \propto C_0^{\frac{1}{3}} \cdot \phi^{-\frac{1}{3}} \quad (2.10)$$

where A is the contact area,  $C_0$  is abrasive concentration, and  $\phi$  is the abrasive diameter.

In this model, polishing rate increases with the increase of abrasive concentration and the decrease of abrasive size, which was observed experimentally on tungsten CMP. The other is an indentation volume based mechanism by

$$V \propto C_0^{-\frac{1}{3}} \cdot \phi^{\frac{4}{3}} \quad (2.11)$$

where V is the indentation volume. According to this indentation volume based mechanism, polishing rate increase with a decrease in abrasive concentration and an increase in abrasive size. This mechanism was observed via silica polishing experiments. This mechanism becomes predominant at low concentration or for larger abrasive size in silica polishing [Mah00]. In the micro- and nano- scale, polishing rate is significantly dependent on interfacial interactions at the pad-particles-wafer interface. The change in particle size and concentration also alters the interfacial interaction during CMP. Friction force is a function of interfacial interactions or the contact behavior between two materials. Therefore, understanding the principles of friction force are critical to achieve high CMP performance.

## Friction in CMP

### Principles and Causes of Friction

Friction is the resistance to motion that exists when a solid object tangentially slides or rolls with respect to the surface of another that it touches [Sci03]. Amonton [Amo1699] presented two basic friction laws that are referred to as “Amonton’s laws”. The first law states that friction is independent of the apparent area of contact between the contacting bodies, and the second is that friction force is proportional to the normal load. Coulomb [Cou1785] also introduced a third law, that states kinetic friction is nearly independent of the speed of sliding, but this law has a smaller range of applicability than the first two laws. The first law of Amonton makes it possible to assume that the resistive force per unit area of contact is constant since friction is related to the real area of contact. Thus

$$F = As \quad (2.12)$$

where  $F$  is the friction force,  $A$  is the real contact area,  $s$  is the specific friction force—the friction force per unit area. The second law of Amonton is that the friction force is proportional to the normal load ( $L$ ). Therefore, it can be expressed as follows:

$$F = \mu L \quad (2.13)$$

where  $\mu$  is a constant known as the “coefficient of friction”. It should be noted that  $\mu$  is a constant only for a given pair of sliding materials under a given set of conditions.

In addition to the principle of friction, the cause of friction is reviewed below. Friction force is not only affected by the interaction which occurs between the opposing surfaces in the case of wafer-pad interaction, but also is caused by the phenomena which occur on materials surfaces. There are two main surface interactions causing friction. One

is asperity interlocking and the other is macro-displacement. Figure 2-17 illustrates the schematic of asperity interlocking. It is noted that the relative motion cannot take place without deformation of the asperities [Edw68, Gre55]. Mahajan *et al.* [Mah99a] suggested that asperity interlocking plays an important role in the contact between pad and wafer surface for particle free CMP condition.

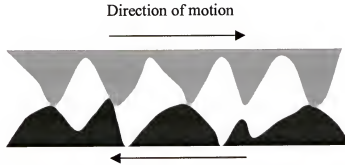


Figure 2-17. Schematic of interlocking in two different surfaces.

Macro-displacement is presented in Figure 2-18. When a hard sphere A is loaded against a relatively soft flat surface B, relative motion takes place by displacing material B. In the presence of abrasive particles between pad and wafer, the interaction of a single particle on a wafer surface is considered as macro-displacement. Brown *et al.* [Bro81] predicted material removal from the contact between a single particle and wafer surface, which is referred to as macro-displacement. When two surfaces are forced together, they somewhat attach due to contact. This adhesion is one form of surface interaction causing friction [Bow64]. Furthermore, friction force is dependent on the chemical environments in the aqueous medium due to the formation of adsorption layers, the change of mechanical properties on the surface by adsorption of molecules, and the formation of a third layer on the surface via tribochemical reaction. The formation of an adsorption layer can be explained by the adhesion theory concerning the mechanism of friction between



two solids. According to adhesion theory [Bow64], the shear stress at the interface between two solids will be reduced with an increase in the rate of adsorption of a molecular layer, resulting in a decrease in material removal through a reduction of the friction force.

## Direction of motion

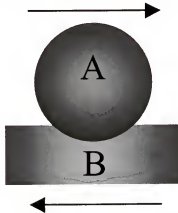


Figure 2-18. Schematic of macro-displacement.

The change of mechanical properties by adsorption is referred to as a chemo-mechanical effect. The mechanical strength of a solid surface is altered by the adsorption of extraneous molecules in an aqueous medium. The species and the concentration of the molecular adsorbed layer play an important role in determining the mechanical properties of a solid surface. It is suggested that the rupture stress ( $\sigma$ ) of the solid be related to the surface energy ( $\gamma$ ) as follow [Oro 55]:

$$\sigma \approx \left( \frac{E(\gamma + P)}{C} \right)^{\frac{1}{2}} \quad (2.14)$$

where  $E$  is Young's modulus,  $P$  is surface plastic work, and  $C$  is depth of micro-crack on the surface. In brittle materials such as ceramics ( $\gamma \gg P$ ), rupture stress ( $\sigma$ ) is lowered with a reduction in surface energy ( $\gamma$ ).

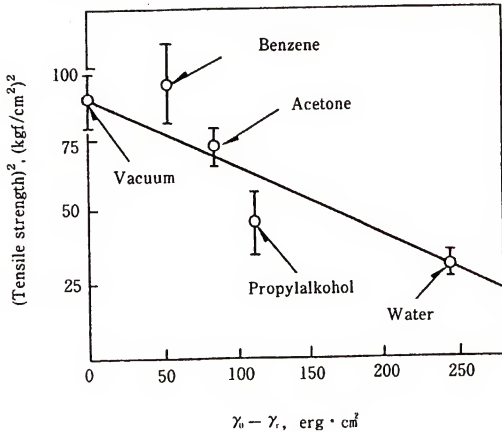


Figure 2-19. Relation between tensile strength and surface energy decrease of fused silica in various atmospheres [Ham65].

Hammond *et al.* [Ham65] verified this equation by experimental showing a relation between tensile strength and surface energy decrease (difference between surface energy of solid in vacuum ( $\gamma_0$ ) and in vapor ( $\gamma_v$ )). In Figure 2-19, the mean tensile strength of fused silica in various vapors is plotted versus the corresponding decrease of the surface energy. It is seen that the experimental results were consistent with Equation 2.14.

Tribochemical reactions are a peculiar chemical reaction produced due to friction at sliding surfaces [Hei84]. Chemical reaction due to friction results in the formation of a layer consisting of a third material, which differs from the initial materials on the sliding surfaces. This tribochemical reaction is thought to enhance lubrication by the formation of reaction products at the sliding surface, which reduce friction [Sas92].

### **Friction during Chemical Mechanical Polishing**

The removal of material is achieved by both contact of both pad and particles with the wafer surface for dynamic CMP conditions. Friction also takes place at the interface of pad, particles, and wafer due to the contact interaction. The analysis of friction can provide an insight into understanding the various contact mechanisms for dynamic CMP conditions. During CMP, the contact regime can be defined as direct (asperity), partial (semi-direct), and indirect (hydroplating) contact by the dependence of friction coefficient on slurry viscosity, platen velocity, and down pressure [Moo99]. The load is solely carried by the interacting asperities in the direct contact regime, leading to high friction. The surfaces separated by the fluid lubrication film in the indirect contact regime result in low friction. And, the semi-direct contact regime stipulates that the load is carried by the interacting asperities and the fluid lubrication film. These relationships are originated from the Stribeck curve that defines contact modes for journal bearings [Ava95]. Figure 2-20 shows the Stribeck curve and lubrication in journal bearings. In the Stribeck curve, friction force is plotted as a function of oil viscosity, shaft velocity, and bearing pressure, resulting in determination of three contact regimes (asperity contact, partial contact, and hydrodynamic contact).

Runnel *et al.* [Run94a] demonstrated the existence of the fluid layer at the pad-wafer interface and determined fluid film thickness between convex type wafer and flat pad as a

function of platen velocity, slurry viscosity, and down pressure during polishing. The fluid film thickness ( $h$ ) is determined as follows:

$$h = H_0 \left( \frac{vV}{P} \right)^{\frac{1}{2}} \quad (2.15)$$

where  $V$  is the platen velocity,  $H_0$  is constant at steady state ( $V=0$ ),  $v$  is the fluid viscosity, and  $P$  is the down pressure.

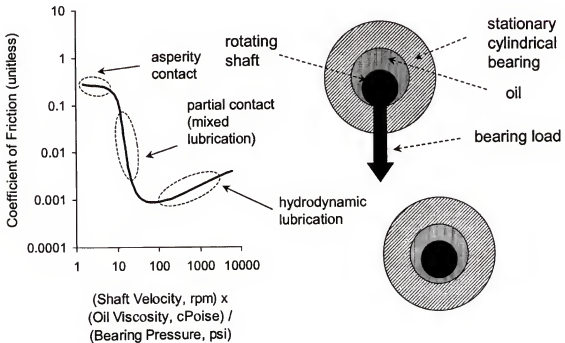


Figure 2-20. Lubrication in Journal bearing & the Stribeck curve [Ava95].

Figure 2-21 presents fluid film thickness and friction coefficient plotted as a function of slurry viscosity, platen velocity, and down pressure during CMP. It was found that the increase of fluid film thickness resulted in the reduction of contact area between wafer and pad asperities, leading to lower friction force in the direct and semi-direct contact regimes. However, the friction coefficient increases with fluid film thickness in the indirect contact regime because load is carried by fluid pressure. It was also suggested

that the contact between a single particle and wafer surface and the fraction of particles bonding to glass surface are responsible for determining the friction force during the direct contact regime [Coo90]. An operational definition of the friction force ( $F$ ) for this condition is shown as:

$$F = \pi r_c^2 f_b \frac{E}{10} \quad (2.16)$$

where  $\pi r_c^2$  is the contact area between polishing particle and the glass surface,  $f_b$  is the fraction of the contact area in which bonding occurs (1%), and  $E/10$  is an estimate of the theoretical fracture strength of network bonds.

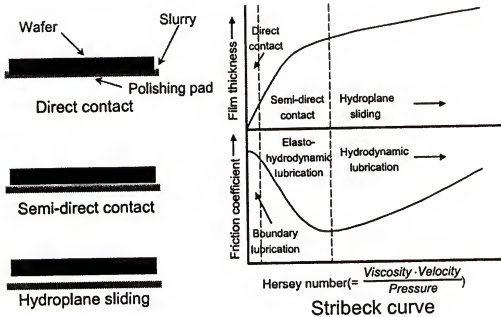


Figure 2-21. Characteristic of slurry film thickness [Dor01].

From the Equation 2.16, it is suggested that chemically active polishing particles such as  $\text{CeO}_2$  generate higher friction force than inert materials such as diamond because  $\text{CeO}_2$  has a large fraction of surface species bonding to the glass [Coo90].

Bhushan *et al.* [Bhu95] analyzed CMP mechanisms during the semi-direct contact regime by maintaining a thin fluid film between the pad and the wafer, thus reducing the role of the asperities in the pad. In this regime, it was found that chemical reactivity of oxide is more important than mechanical abrasion, and CMP process parameters are independent of material removal rate. This semi-direct contact model is hardly applicable to real CMP processes because it is difficult to control the thickness of the fluid film between the pad and the wafer. Mahajan *et al.* [Mah99b] studied the effect of chemical additives (pH and ionic strength) on friction in the absence of slurry particles. They suggested that the reduction in the friction force is caused by the increase of electrostatic repulsion force for the condition of high pH and low ionic strength. These results make it possible to estimate the interfacial interaction mechanism between the pad and the wafer. However, real CMP conditions consist of three bodies including pad, particles, and wafer. Therefore, *in situ* friction force measurements for three body conditions are required to investigate the interfacial interaction and then delineate polishing mechanism occurring for real CMP conditions.

### **Modeling of Chemical Mechanical Polishing**

The models of material removal rates of CMP are developed respectively for four varying approaches. The first is a phenomenological approach based on results of the CMP process. Preston presented the first mechanical model, which empirically related the removal rate to the work done by the friction force [Pre27]. In his works, experimental evidence showed that the amount of material removed in time ( $t$ ) has a linear relationship with the work done by the friction force ( $\text{Friction force} \times \text{Distance}$

traveled in time,  $t$ ). From this experimental relationship, material removal rate (thickness of the material removed at a given unit of time) is given by:

$$M.R.R = C_p P V \quad (2.17)$$

where  $C_p$  is known as Preston coefficient which is proportional to the coefficient of friction,  $P$  is the down pressure, and  $V$  is the relative velocity between pad and wafer.

Although Preston's equation has been used to predict overall material removal rate, it fails to predict material removal rate for a wide range of process parameters such as the slurry chemistry, particle size, and particle concentration etc.

The second approach is based on the theory of fluid hydrodynamics. This approach assumes slurry erosion to be the main material removal mechanism and neglects mechanical abrasion by particles at the interface of the three bodies. Based on the effect of slurry erosion on material removal, Runnel and coworkers developed a feature-scale erosion model that linked chemical effects modeled on the particle scale to process conditions modeled at the wafer scale [Run94b]. The equation based on feature-scale erosion model is as follows:

$$M.R.R. = C_p \sigma \tau \quad (2.18)$$

where  $C_p$  is the Preston like coefficient,  $\sigma$  is the normal stress tensor due to the down pressure, and  $\tau$  is the shear stress due to slurry flow activated by relative motion between pad and wafer. In this approach, they presented the existence of a hydrodynamic fluid film thickness and hydrodynamic pressure in a rigid and flat polishing pad system. It was believed that hydrodynamic force is responsible for material removal alone. However, they did not show any experimental results concerning material removal. In addition, real

chemical mechanical polishing is conducted on a soft and grooved pad in direct contact condition, resulting in deviations from the feature scale erosion model.

The third approach makes use of the theory of contact mechanics. Greenwood and Williamson [Gre66, Gre67] determined the real contact area of surface asperities from the distribution of asperity heights and the deformation law for a single asperity. Yu *et al.* [Yu93] applied a statistical asperity model to characterize the surface roughness of the polishing pad. A feature-scale polishing model was developed using the distribution of surface asperity heights. According to this feature-scale polishing model, material removal rate is proportional to the contact area (A).

$$\text{M.R.R.} = K_2 A V \eta \int_d^{d+h} \int_0^\infty a \Phi_\beta \Phi_z d\beta dz \quad (2.19)$$

where  $K_2$  is a material constant,  $A$  is nominal pad area,  $V$  is the platen velocity,  $\eta$  is the asperity density,  $d$  is the separation based on asperity heights,  $h$  is the separation based on surface height,  $a$  is the contact area, and  $\Phi_\beta$  and  $\Phi_z$  are Gaussian distributed variations in asperity height  $\beta$  and radius  $z$ . This theoretical approach suggested that the contact area between pad asperity and wafer surface was critical in determining material removal rate. This feature scale contact model is used to explain polishing at the device feature level [Yu93]. However, the effect of particles and the chemically modified layer on material removal rate was not included in this model. Therefore, characterization of the effect of the chemically modified layer on material removal rate and the contact of particles between pad and wafer is required to consolidate the feature-scale polishing model.

The fourth approach is built on the theories of contact mechanics and fluid dynamics. Tichy *et al.* [Tic99] suggested the existence of subambient hydrodynamic



pressure between a nearly rigid pad and wafer surface based on the highly idealized one-dimensional model and experimental determination of suction fluid pressure. Shan *et al.* [Sha00] also predicted the existence of the subambient and positive pressure at the interface between steel and plain pad. Though they suggested the existence of a subambient fluid pressure at the interface of wafers and plain pads, they didn't show any relationship between subambient pressure and material removal rate to support the existence of subambient fluid pressure during CMP processes. A further limitation is the lack of applicability of subambient fluid pressure to a CMP process because the grooved pad used restricts subambient pressure values from being applied to the interface of pad and wafer surface.

All models mentioned above have several critical limitations: (1) over simplification without experimental proofs, (2) no consideration of micro and nano-scale effects, (3) no predictability of slurry performance, and (4) simple fitting parameters to match experimental data. Therefore, a more sophisticated CMP model which accounts for the output parameters such as surface finish, planarity, and selectivity is required for optimized CMP performance.

## CHAPTER 3

### STUDY OF FRACTIONAL SURFACE COVERAGE OF ABRASIVE PARTICLES DURING CHEMICAL MECHANICAL POLISHING

#### **Introduction**

The ultra large scale integrated (ULSI) circuit structure is vital in modern semiconductor fabrication technology. Newly developed planarization technologies for ULSI circuit structures have been successfully utilized for integrated circuit (IC) manufacturing [Ste97]. Chemical mechanical polishing (CMP) is established as an important step for achieving global and local planarization of wafer surfaces for current semiconductor fabrication technology. The CMP process has been used for interlayer dielectric planarization [Bar98, Rut95], shallow trench isolation [Dav89], and damascene technologies [Baj02]. Although CMP has been extensively developed in the semiconductor industry, the fundamental knowledge of the effect of the numerous CMP process variables on polishing performance is lacking.

An understanding of the nature of contact between particles and the wafer to be polished is essential to maintain the strict process requirements for manufacturing current and future generation IC chips. Particularly in oxide CMP, particles play a significant role in achieving desired CMP performance such as high material removal rate, minimal number of surface defects, and local and global planarization via mechanical abrasion and chemical modification of the wafer surface [Sin02a]. A more in-depth understanding of the effect of CMP process variables (down pressure, particle size and concentration

etc.) on particle-pad-wafer interactions will greatly enhance the fundamental knowledge of the oxide CMP process.

In spite of its importance, experimental validation of CMP theories is critically lacking. Greenwood *et al.* [Gre66, Gre67] analyzes the contact of a nominally flat surface using the statistical model of peak asperities. Their results suggested that the real area of contact is directly proportional to down load and is independent of the apparent area. Yu *et al.* [Yu93] developed the statistical asperity model reporting two results: (1) real contact area is proportional to down load, (2) real pressure of pad in contact with wafer is weakly dependent on the applied down pressure. Assuming that a uniform distribution of asperities exists and that these asperities are elastically deformed, Zhao *et al.* [Zha99b] suggested that polishing rate is proportional to the real contact area between the pad and wafer. Furthermore, they also noted that the real contact area has a nonlinear relationship with pressure. Our previous results showed that the ions introduced into the interface between the pad and wafer surface causes a reduction of electrostatic repulsion force between them, leading to an increase in the contact area, and thus a higher friction force [Mah99]. Besides the contact area between pad and wafer, the number of particles introduced into the interface between pad and wafer is critical for high CMP performance. Cook [Coo90] theoretically defined the fractional surface coverage of particles as the particle fill fraction ( $K$ ) on the whole wafer. The particle fill fraction ( $K$ ) between two hard surfaces can be expressed as follows:

$$K = \frac{\sqrt{3} \cdot P \cdot r^2}{2 \cdot F_p} \quad (3.1)$$

where  $P$  is the polishing pressure,  $r$  is the radius of particle, and  $F_p$  is the force per individual particle. Zhang *et al.* [Zha98, Zha99a] used the particle fill fraction ( $K$ ) to determine the polishing force for a single particle in the partial contact mode. Ahmadi *et al.* [Ahm01] predicted the number of particles uniformly distributed on a wafer surface using the particle fill fraction ( $K$ ). Though particle fill fraction ( $K$ ) has been used to predict material removal rate, pressure per particle, and the number of particles between two hard surfaces, it is hardly applicable to a real CMP process because the two opposing surfaces are made of soft compliant polymers and a hard flat wafer [Shi98].

In this study, we report the effect of down pressure, particle size, and solids loading on *in situ* lateral friction force under real CMP conditions. Based on the friction force response, the relative contact area of both particles in contact with the wafer, and that of pad contacting with wafer have been investigated to predict the fractional surface coverage of particles in contact with the wafer during polishing.

### Experimental

The abrasive particles used for this study were 0.2 and 1.0  $\mu\text{m}$  spherical sol-gel silica particles obtained from Geltech Corporation. Slurries were formulated to 0.2 wt.%, 2 wt.%, 5 wt.%, 10 wt.%, and 15 wt.% by mixing de-ionized water and abrasive particles. The agglomerated particles were broken down to primary particles using a Fisher Scientific ultra sonic cleaner. The slurries were adjusted to pH 10.5 using 0.1 M  $\text{HNO}_3$  and 0.1 M  $\text{NaOH}$ . A Coulter LS 230 light scattering instrument with a small volume module was used to analyze the particle size. Rodel IC 1000/Suba IV stacked pads were used for all experiments, and were conditioned using a Grid-Abrade Diamond pad conditioner before each experiment. Sapphire [0001] 0.8  $\times$  0.8 in. was used as the wafer

to be polished, which provides the same surface polishing condition due to the fact that sapphire material is not removed by silica abrasives at room temperature [Gut78].

*In situ* lateral friction force measurements were carried out to investigate the effect of CMP process variables on the relative contact area of particles in contact with pad and wafer. A schematic of the instrument used to measure the *in situ* lateral friction force is shown in Fig. 3-1. This *in situ* friction force measurement tool was assembled on a tabletop Struers Rotopol 31 polisher. The unit consists of a cylinder-type aluminum block on which the samples to be polished were mounted. It is designed to rotate by the difference of the linear velocities of the wafer sample and the rotating platen. Movement is restricted to one direction only.

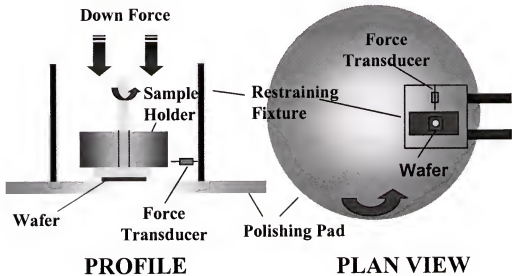


Figure 3-1. Schematic presentation of *in situ* lateral friction force instrument.

The sample mount was then loaded with desired weights to give the pressure of 2 psi and 4 psi. The applied lateral force was measured by a force transducer (Sensotec

model 31 load cell), and its output was transferred to a data acquisition computer system with a data sample taken every 250 ms. The polishing platen was run at a constant speed of 150 rpm translating to an average linear velocity of 110cm/sec.

## Results and Discussion

### Particle Size and Size Distribution in CMP Slurries

The particle size and size distribution are critical when seeking to control material removal rate, planarity, and defect density.

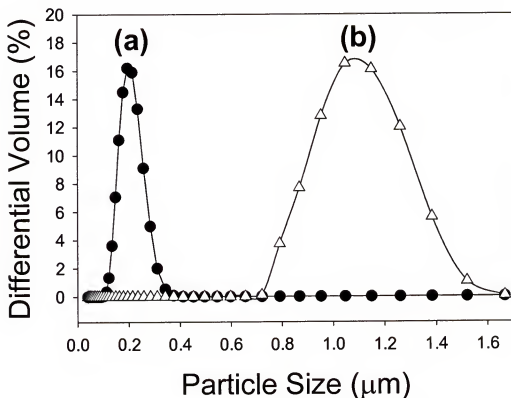


Figure 3-2. Size distributions of particles measured by dynamic light scattering (a) mean diameter (0.204μm), standard deviation (0.0444μm), (b) mean diameter (1.087μm), standard deviation (0.899μm).

The change of particle size and size distribution leads to a change in contact area and indentation depth of particles into wafer surface, resulting in a change in the polishing performance. In particular, in oxide CMP, the material removal mechanism is determined

by particle size and size distribution [Mah99]. The increase of particle size by agglomeration has not only a detrimental effect on the wafer to be polished but also changes the polishing mechanism [Hay95]. Therefore, careful control of particle size and size distribution is very important for obtaining desired CMP performance and must be accurately monitored. Figure 3-2 shows the size and size distribution of silica particles.

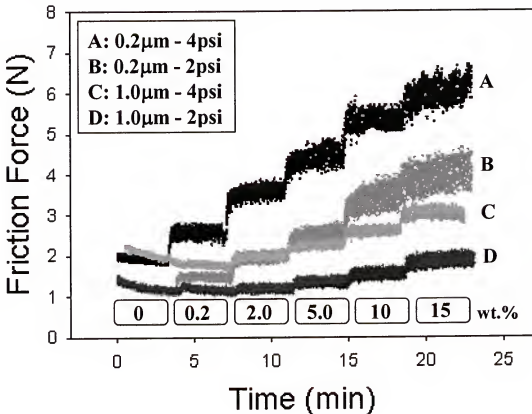


Figure 3-3. *In situ* lateral friction force as a function of time for different down pressure, particle size, and solids loading.

A single peak in the particle size distribution demonstrates that silica particles are well dispersed at pH 10.5. Abrasive particle mean diameters measured by light scattering method are agreement with the mean diameter values provided by Geltech company. At

this pH, high electrostatic repulsion forces between slurry particles are responsible for slurry dispersion.

### **Effect of Down Pressure, Particle Size, and Solids Loading on Friction Force**

Figure 3-3 shows the *in situ* lateral friction force as a function of time for different down pressures, particle sizes, and solids loading. As the solids loading was increased every four minutes, friction force response increases in a step like manner. At a given down pressure, particle size, and solids loading, friction force is relatively constant. This fact suggests that if process variables (e.g., down pressure and platen velocity) and slurry variables (e.g., particle size and solids loading) remain unchanged, the total contact area at the pad-particles-wafer interface remains constant. Based on the adhesion friction theory, friction force ( $F$ ) is described as [Hal75]:

$$F = A \cdot S \quad (3.2)$$

where  $A$  is the real area of contact and  $S$  is the specific friction force (friction force per unit area). If the slurry conditions remained unchanged, then  $S$  can be expected to be a constant. In this regard, the dependence of friction force on contact area may now be demonstrated by changing the process variables and measuring the *in situ* friction force response.

Figure 3-4 shows the friction force as a function of solids loading at different down pressures and particle sizes. The solids loading dependence of the friction force for 0.2  $\mu\text{m}$  silica particles is found to be sublinear, whereas friction force linearly increases with solids loading for 1.0  $\mu\text{m}$  silica particles. This suggests that the characteristics of interfacial contact between 0.2  $\mu\text{m}$  silica particles and the wafer differs from the case of 1.0  $\mu\text{m}$  silica particles and wafer.



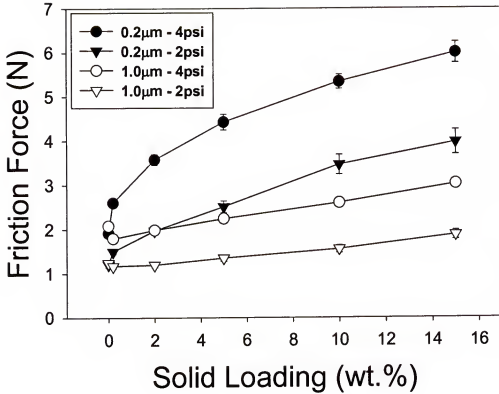


Figure 3-4. *In situ* lateral friction force as a function of solids loading for different down pressure and particle size.

This difference in the interfacial contact area may be responsible for the variance in the surface coverage of particles in contact with a wafer. A sublinear response of friction force demonstrates nearly complete coverage of particles at high solids loading; however, a linear response of the friction force to changes in solids loading is due to only partial coverage of particles. At a given solids loading, a decrease in particle size results in an increase in the friction force response. For a single particle in contact with a wafer, the larger the particle the larger the contact area. Hertzian contact mechanics shows that the contact radius of a single particle in contact with a wafer is proportional to particle diameter [Her1896]. In this regard, the number of particles available for polishing increases with decreasing particle size for fixed solids loading condition, leading to a

large total contact area for all particles in contact with the wafer. For real CMP conditions, polishing is carried out by large amounts of particles in contact with the wafer. Therefore, determining the number of particles is an important factor in determining the dynamic contact area during CMP.

It is also shown that the friction force increases with solids loading for fixed down pressure, platen velocity, and particle size. This dependence of friction force on solids loading can be explained by an increase in the number of particles in contact with the wafer. The increase in solids loading increases the number of particles available for polishing on the wafer surface, also increasing the total contact area of particles leading to higher friction force.

In the absence of particles, the measured friction force at 4 psi is 1.63 times higher than that at 2 psi. An increase in the down pressure causes compression of pad asperities, increasing the total area of the pad in contact with the wafer. In the presence of particles, as the down pressure increases, this compression of pad asperities exposes a larger number of particles to the wafer surface. Therefore, increasing the number of particles available for polishing yields a higher total interfacial contact area which is responsible for the increase in the measured friction force.

### **Comparison of Friction Force for a Fixed Number of Particles**

In order to compare the friction force per particle, the number of particles per unit volume ( $\text{cm}^3$ ) was calculated from solids loading (0.2 wt.%, 2 wt.%, 5 wt.%, 10 wt.%, and 15 wt.%), particle density ( $2.1 \text{ g/cm}^3$ ), and particle size ( $0.2 \mu\text{m}$  and  $1.0 \mu\text{m}$ ). The number of  $0.2 \mu\text{m}$  silica particles per unit volume ( $\text{cm}^3$ ) is around 125 times more than  $1.0 \mu\text{m}$  silica particles for a fixed solids loading condition. Figure 3-5 shows the friction

force as a function of the number of particles per unit volume ( $\text{cm}^3$ ) for different down pressure and particle sizes. At a given particle size, the friction force increases as number of particles increases. The increase of friction force may be assumed to be due to the increase in the number of particles in contact with wafer. Figure 3-5 shows a detailed comparison of the friction force as a function of number of particles.

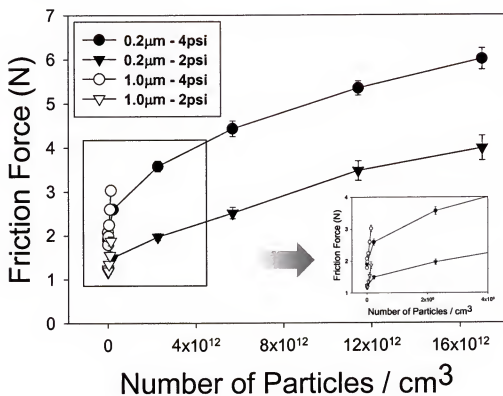


Figure 3-5. *In situ* lateral friction force as a function of the number of particles per unit volume ( $\text{cm}^3$ ) for different down pressure and particle size.

It is shown that the friction force response for 1.0  $\mu\text{m}$  particles is more pronounced than that for 0.2  $\mu\text{m}$  particle. This means at a given solids loading that the increase in particle size increases the interaction area of particles in contact with wafer, leading to a higher friction force. It is verified from the Hertzian equation that the contact area of 1.0  $\mu\text{m}$  single particle is 2.92 times larger than 0.2  $\mu\text{m}$  single particle [Her1896].

An insert to Figure 3-5 also shows that the slope in friction force vs. the number of particles curve for 1.0  $\mu\text{m}$  particles is much higher than that of 0.2  $\mu\text{m}$  particles. This can be attributed to the cumulative increase of interaction area due to the increase in the number of particles. It should be made clear that calculations for number of particles are based on slurry conditions not for actual total number of particles at the pad-wafer interface.

### **Fractional Surface Coverage of Particles in Contact with Wafer to be Polished**

When silica particles are introduced between the polishing pad and sapphire wafer, the surface of the sapphire wafer is not removed because silica particles are much softer than the sapphire wafer. This is confirmed by Vicker's hardness test in that hardness of fused silica is 540  $\text{kg/mm}^2$  and the hardness of sapphire ( $\text{Al}_2\text{O}_3$ ) is 2370  $\text{kg/mm}^2$ , respectively [Ric71]. Thus, it can be thought that friction force arises only from the mechanical interactions between particles and pad asperities against the wafer surface, and fractional surface coverage of particles in contact with wafer can be calculated by observing the change in the *in situ* friction force.

For the rule of friction based on Amonton's principle [Amo1699], the friction force ( $F$ ) and down load ( $L$ ) have the following relationship.

$$F = \mu \cdot L \quad (3.3)$$

where  $\mu$  is the coefficient of friction. The pressure ( $P$ ) applied against the wafer surface can be written as follows:

$$L = P \cdot A \quad (3.4)$$

where  $A$  is the area of contact Combining Equation (3.3) and Equation (3.4), friction force ( $F$ ) can be determined by the following relationship.

$$F = \mu \cdot P \cdot A \quad (3.5)$$

The total friction force equals the sum of the friction force ( $F_\phi$ ) due to the particles in contact with pad and wafer, and the friction force ( $F_p$ ) of pad in contact with wafer as follows:

$$F = F_\phi + F_p = \mu_\phi \cdot P_\phi \cdot A_\phi + \mu_p \cdot P_p \cdot A_p \quad (3.6)$$

We can assume that the real contact pressure ( $P_{con}$ ) remains unchanged ( $P_{con} = P_\phi = P_p$ ) because the conventional CMP pads used in IC fabrication are soft compliant polymers [Shi98]. Thus, friction force can be expressed as follows:

$$F = P_{con} \cdot (\mu_\phi \cdot A_\phi + \mu_p \cdot A_p) = A_{con} \cdot P_{con} \cdot (f \cdot \mu_\phi + (1-f) \cdot \mu_p) \quad (3.7)$$

where  $A_{con}$  is total area contacting the wafer surface, and  $f$  (fractional surface coverage of particles in contact with pad and wafer) is  $A_\phi/A_{con}$ . Fractional surface coverage ( $f$ ) of particles embedded on the pad and wafer can be expressed by

$$f = \frac{F_t - \mu_p \cdot P_{con} \cdot A_{con}}{\mu_\phi \cdot P_{con} \cdot A_{con} - \mu_p \cdot P_{con} \cdot A_{con}} \quad (3.8)$$

In the absence of particles ( $f=0$ ), the friction force was measured and may be attributed to the contact area of the pad in contact with the wafer. In the presence of particles ( $f \neq 0$ ), friction force can be determined as a function of the ratio of the contact area of particles in contact with wafer to the contact area of pad in contact with wafer (the fractional amount of particles between pad asperities and wafer). Friction force measured at 35 wt.% was selected as the saturated value because friction force changed only slightly from 15 wt.% to 35 wt.% as shown Table 3-1. This maximum friction force value and Equation 3.8 make it possible to estimate the fractional amount of slurry particles

actually in contact with the wafer. Figure 3-6 shows the normalized fractional surface coverage as a function of down pressure, particle size, and solids loading. Fractional surface coverage of particles increases monotonically with solids loading and has a strong dependence on particle size. At a given solids loading, a greater fraction of 0.2  $\mu\text{m}$  slurry particles actually contact the wafer surface.

Table 3-1. *In situ* lateral friction force with down pressure and particle sizes for 35wt. % solids loading.

| Down Pressure (psi) | Particle Size ( $\mu\text{m}$ ) | Friction force at 35 wt.% (N) |
|---------------------|---------------------------------|-------------------------------|
| 2psi                | 0.2                             | 4.00 ( $\pm$ 0.32)            |
|                     | 1.0                             | 2.09 ( $\pm$ 0.21)            |
| 4psi                | 0.2                             | 6.43 ( $\pm$ 0.45)            |
|                     | 1.0                             | 3.44 ( $\pm$ 0.24)            |

Although the interaction area per particle is higher for a 1.0  $\mu\text{m}$  particle, the total contact area is larger for 0.2  $\mu\text{m}$  particles due to the large number of particles in contact with the wafer surface. At a given particle size, the applied down pressure does not affect the fractional surface coverage. This finding suggests that increasing the down pressure enlarges the total area of the pad in contact with wafer and increases simultaneously the number of particles contacting the wafer due to the softness and flexibility of commercial CMP pads. Thus, the fractional amount of particles in contact with the wafer remains unchanged over this down pressure range investigated.

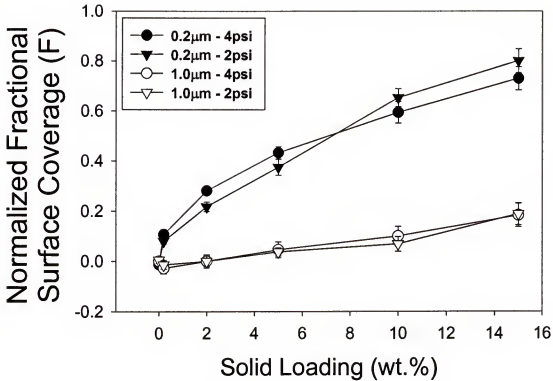


Figure 3-6. The normalized fractional surface coverage ( $f$ ) of particles in contact with wafer.

### Summary

The manner in which  $\text{SiO}_2$  particles contact a sapphire wafer has been investigated in order to validate the contact mechanism of particles during oxide CMP. In the absence of particles between pad and wafer, the increase in the down pressure applied to the wafer leads to an increase in the total area of pad in contact with the wafer, causing an increase in the measured friction force. In the presence of particles between pad and wafer, friction force is a function of down pressure, particle size, and solids loading. Increasing either down pressure or solids loading leads to an increase in the number of particles in contact with the wafer, resulting in a higher measured friction force. For a fixed solids loading condition, the decrease in particle size leads to an increase in total contact area of

particles in contact with the wafer, resulting in a higher friction force. An equation for fractional surface coverage of particles has been established for CMP with conventional soft pads. It is verified that the fractional surface coverage of particles is independent of down pressure, and increases with solids loading. The decrease of particle size leads to an increase in the total contact area of particles in contact with wafer, leading to a higher fraction of slurry particles in contact with the wafer. These results are in agreement with physical observations of CMP with soft commercial pads and will be used to provide further insight into oxide CMP polishing mechanisms.



## CHAPTER 4

### STUDY OF INTERFACIAL CONTACT VARIATION DURING CHEMICAL MECHANICAL POLISHING (CMP)

#### Introduction

Chemical Mechanical Polishing (CMP) has emerged as the most variable technology for the planarization of metal and dielectric films in the microelectronic device fabrication industry [Ste97]. The miniaturization of microelectronic devices has been the driving force for the development of CMP as a planarization technique. CMP is used to remove the excess metal (i.e., Cu and W) or dielectric (i.e., SiO<sub>2</sub>) produced by deposition techniques and to achieve global planarization [Bie99, Sin02]. In recent years, the rapid advances in the microelectronic industry have required more understanding of CMP principles for desired CMP performance.

The success of the CMP process depends upon an understanding of polishing mechanism and principles. Especially critical is the interfacial contact behavior during the polishing process. For CMP, interfacial contact is studied in terms of two conditions: the first is contact in the absence of particles and the second is contact in the presence of particles. In the absence of particles, Yu *et al.* [Yu03] has statistically studied the contact between pad and the wafer as a function of down pressure. Zhao *et al.* [Zha00] has also developed an asperity micro-contact model to determine the transition from elastic deformation to plastic deformation of a single asperity in contact with a rigid smooth surface. Furthermore, the contact area of pad (IC1000) was determined as a function of down pressure employing Fourier transform infrared / attenuated total internal reflection

spectroscopy (FTIR/ATR), proposing that pad contact area has a linear relation with down pressure [Bas03]. Considering that the elastic contact area between a pad asperity and the wafer is proportional to the two-thirds power of the applied pressure, the pressure dependence of the polishing rate for CMP with a soft pad has been elucidated [Shi98]. In the presence of particles, the contact area of particles between two rigid surfaces was theoretically estimated as a function of particle size and solids loading. Total contact area increases with solids loading increase and decreases with particle sizes increase [Bie98]. Several attempts to characterize pad-wafer interfacial contact and the interfacial contact of particles between two rigid surfaces have been reviewed here; however, the true nature of interfacial contact at the pad-particles-wafer interface is not yet fully understood. In order to achieve optimized CMP performance, a most fundamental understanding of the mechanisms of particle contact at the pad-wafer interface is needed.

In this study, an interfacial contact model for particles embedded into a soft pad was developed and validated by *in situ* friction force measurements.

## Experimental

*In situ* lateral friction force measurements were conducted to measure friction force obtained from the interaction of pad, particles, and a flat wafer. As shown in Figure 3-1, An *in situ* lateral friction force measurement instrument that is assembled on a Struers Rotopol 31 polisher was utilized to observe friction force arising from the pad-particles-wafer interface. The friction force was detected by a Sensotec model 31 load cell whose output data were recorded every 250 ms. Friction forces were measured at a constant down load of 2.7 psi (14.5 N) and a constant platen speed of 150 rpm (110 cm/sec). The sample to be polished was sapphire of  $0.8 \times 0.8$  square inch ( $2 \times 2$  cm<sup>2</sup>), and Rodel IC

1000/Suba IV stacked pads were utilized for all experiments. A Grid-Abrade diamond pad conditioner was used to abrade the pad before each test. The abrasive particles used for this study were Levasil (50CK, 50CK-V1, and 100K) silica slurries provided by Bayer Company. The pH was adjusted to 10.5 using 0.1M  $\text{HNO}_3$  and 0.1M NaOH. The sizes of particles in silica slurry were analyzed using a Honeywell Microtech UPA 150 particle size analyzer utilizing the dynamic light scattering technique.

### **Modeling of Contact Area**

#### **Contact between A Rigid Flat Surface and Single Particle**

Delineation of the contact area between a wafer and a single particle embedded into a soft pad is crucial in understanding the CMP mechanism. As was presented in the previous chapter, the variation of particle size and solids loading leads to a change in the contact area of particles in the polishing process, affecting the CMP performance. In this regard, a contact model is established in order to determine the contact area between a rigid flat wafer surface and a single particle embedded into soft pad, resulting in an estimation of the contact behavior during CMP. The interfacial contact area was calculated based on the next three assumptions.

1. A particle participating in polishing process is spherical in shape with an average radius (R).
2. A particle is embedded into soft pad due to the difference of the elastic modulus between two materials (i.e.,  $E_{\text{Silica}} = 71.6 \text{ GPa}$  [Law75],  $E_{\text{IC 1000 Pad}} = 27 \text{ MPa}$  [Mod96]).
3. Real particles are never completely rigid, and on coming into contact they deform elastically under the influence of any externally applied load [Isr00].

Figure 4-1 shows a two-dimensional interfacial image of a flat rigid wafer in contact with a single particle embedded into a soft pad under an applied down force ( $P$ ). Upon application of an applied down force, a single particle embedded into a soft pad is elastically deformed against a flat rigid wafer, producing a circular region of contact under the condition of force equilibrium ( $P = F$ ).

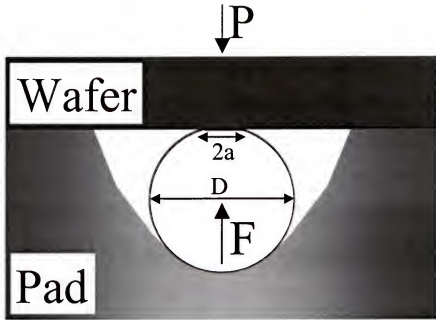


Figure 4-1. Two-dimensional interfacial contact of a single particle with a rigid wafer and a pad.

Hertz [Her1896] showed that the diameter of the contact area,  $2a$ , is dependent on the magnitude of the down force, the diameter of particle, and the elastic properties of the particles and the flat wafer as follows:

$$a^3 = \frac{3}{8} \cdot F \cdot D \cdot \left[ \frac{1 - \nu_1^2}{E_1} + \frac{1 - \nu_2^2}{E_2} \right] \quad (4.1)$$

where  $a$  is the radius of the contact area,  $F$  is the down force normal to the contact area,  $D$  is the diameter of a single particle,  $E$  is Elastic modulus, and  $\nu$  is the Poisson's ratio; the subscripts differentiate between particle and wafer. The contact area between a single particle and the wafer can be given by:

$$A_s = \pi a^2 = \pi \left( \frac{3}{8} \cdot F \cdot D \cdot \left[ \frac{1 - \nu_1^2}{E_1} + \frac{1 - \nu_2^2}{E_2} \right] \right)^{\frac{2}{3}} \quad (4.2)$$

For the equilibrium state, it is found that the contact area between a rigid flat wafer and a single particle embedded into the soft pad is a function of down force, particle diameter, and the elastic modulus.

#### **Number of particles participating in contact at the interface**

In the previous chapter, a relation which gives the fractional amount of slurry particles expected to be at the pad-wafer interface was presented. However, for a micro-contact model, the actual number of particles participating in contact at the interface is a critical factor needed to predict total contact area of particles and polishing rate [Zha01b]. The number of particles can be calculated based on the following two assumptions.

- 1 Spherical particles with average radius of  $R$  are uniformly distributed in the slurry
2. The area density of the particles embedded into the polishing pad is the same as that in the slurry.

Let  $\alpha$  be volume concentration of the particles in the slurry. Then

$$\alpha = \frac{C_0}{\rho} \quad (4.3)$$

where  $C_0$  is the slurry concentration and  $\rho$  is the density of slurry. An average volume of an individual particle ( $\beta$ ) is given by

$$\beta = \frac{1}{6} \cdot \pi \cdot D^3 \quad (4.4)$$

Since the volume density ( $\gamma$ ) of the slurry particles is given by

$$\gamma = \frac{\alpha}{\beta} \quad (4.5)$$

then

$$\gamma = \frac{6 \cdot C_0}{\pi \cdot \rho \cdot D^3} \quad (4.6)$$

Let  $\chi$  be the area density. Then

$$\chi = \gamma^{\frac{2}{3}} = \left( \frac{6 \cdot C_0}{\pi \cdot \rho \cdot D^3} \right)^{\frac{2}{3}} \quad (4.7)$$

Therefore, the number of particles ( $N_p$ ) participating in the contact can be calculated by

$$N_p = A_r \cdot \chi = A_r \cdot \left( \frac{6 \cdot C_0}{\pi \cdot \rho \cdot D^3} \right)^{\frac{2}{3}} \quad (4.8)$$

where  $A_r$  is the real contact area between pad and the wafer. It is reported in an earlier modeling and experimental proof that the real contact area,  $A_r$ , linearly increases with the applied pressure, and remains unchanged under a constant applied down load [Yu93, Bas03]. Total contact area of particles in contact with wafer ( $A_t$ ) is related to the number of particles ( $N_p$ ) and the contact area of a single particle ( $A_s$ ) by

$$A_t = A_s \cdot N_p = A_r \cdot \left( \frac{9 \cdot \pi^{\frac{1}{2}} \cdot F \cdot C_0}{4 \cdot \rho \cdot D^2} \left[ \frac{1 - \nu_1^2}{E_1} + \frac{1 - \nu_2^2}{E_2} \right] \right)^{\frac{2}{3}} \quad (4.9)$$

When the process variables (i.e., down load and platen velocity etc.) and chemical variables (i.e., ionic strength and pH etc.) remain unchanged, it can be assumed that the real contact area ( $A_r$ ), density of slurry particles ( $\rho$ ), elastic modulus ( $E$ ) and Poisson's

ratio ( $v$ ) of slurry particles and wafer may remain unchanged. For a CMP process with a soft pad, down pressure per single particle ( $F$ ) does not markedly change when further particles are added because most particles are embedded into the pad under the applied down pressure [Shi98]. Therefore, for constant down pressure, platen velocity, and chemical condition (i.e., ionic strength and pH etc.), total contact area ( $A_t$ ) can be given by

$$A_t \propto D^{-\frac{4}{3}} \cdot C_0^{\frac{2}{3}} \quad (4.10)$$

When process variables and slurry (chemical) variables are kept constant, total contact area is found to be a function of particle diameter and solids loading which has been demonstrated using a  $\text{SiO}_2$  slurry and sapphire substrate.

#### **Friction Force Based on the Interfacial Contact**

Friction force ( $F_f$ ) can be expressed as follows [Hal75]:

$$F_f = F_u \cdot A_t \quad (4.11)$$

where  $F_u$  is the friction force per unit area which remains constant under constant chemical conditions. If the chemical conditions of the slurry system are kept constant, the friction force will be solely dependent on the contact area between the two surfaces [Mah99]. Friction force can be given by

$$F_f \propto A_t \quad (4.12)$$

thus

$$F_f \propto R^{-\frac{4}{3}} \cdot C_0^{\frac{2}{3}} \quad (4.13)$$

This theoretical relation of friction force shows that friction force has a non-linear relation with particle size and solids loading. It is expected from this theoretical

estimation that smaller particles and high solids loading lead to high friction force due to the formation of a large total contact area due to larger fraction of slurry particles available for polishing.

### Results and Discussion

The silica slurries used in these experiments were composed of amorphous silica particles with no organic solvent and surfactant added. Figure 4-2 shows the size distribution of silica particles diluted in DI water at pH 10.5.

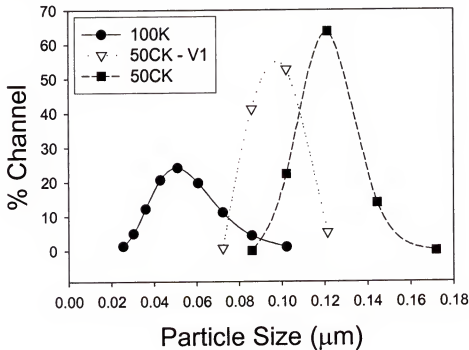


Figure 4-2. Particle size distribution for different lots of silica particles diluted in DI water at pH 10.5.

The mean volume diameter distribution and standard deviation of diameter are shown in Table 4-1. Levasil (50CK) shows an average particle diameter of 0.11 μm, which is the largest among three samples. The particle size distribution of Levasil (100K) is 0.0065 μm, which is the broadest among the three slurry samples. Figure 4-3 shows



SEM images of Levasil abrasive silica particles. Individual particles are spherical in shape, confirming assumption number 1, and are observed to possess a uniform distribution generally.

Table 4-1. Variation in size of particles by light scattering techniques

| Particle type | Mean volume distribution diam.( $\mu\text{m}$ ) |
|---------------|---|
| 100K          | 0.0482 ( $\pm 0.0065$ )                         |
| 50CK – V1     | 0.0882 ( $\pm 0.0048$ )                         |
| 50CK          | 0.1105 ( $\pm 0.0054$ )                         |

Additionally, the SEM images containing 100K abrasive particles show the smallest abrasive particles of which mean size is less than 20 nm. The existence of extremely small sized abrasive particles in 100 K slurry explains the large standard deviation in mean volume diameter of 100 K abrasive particles presented in Table 4-1. Figure 4-4 shows the friction force as a function of time for the different particle sizes. During the initial 30 sec, friction force was measured while de-ionized water flowed into the pad-wafer interface. Friction forces measured for the different particle sizes were normalized by friction force measured with DI water.

When solids loading conditions are kept constant, friction force only slightly changes with time. This is because the number of particles which flows into the pad-wafer interface for a period of each solids loading remains unchanged. As solids loading was changed for a given particle size, friction force also varied due to an increase in the number of particles in contact with wafer. In order to describe the dependence of particle size and solids loading on friction force, friction force vs. solids loading was redrawn

from Figure 4-4. Figure 4-5 shows the friction forces and their fitting as a function of solids loading for different particle sizes.

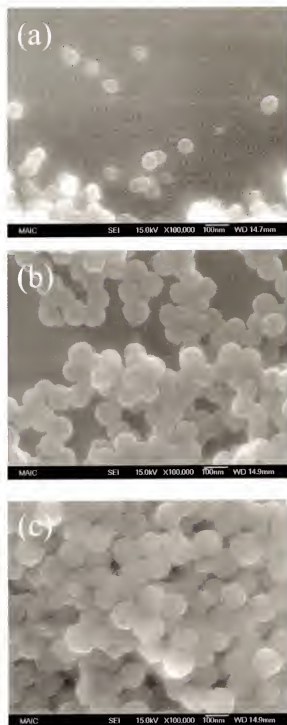


Figure 4-3. SEM images of abrasive particles: (a) 100K, (b) 50CK-V1, and (c) 50CK.

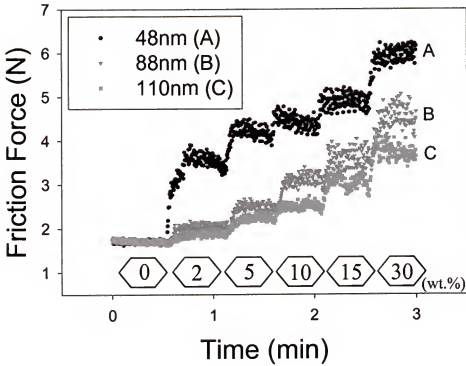


Figure 4-4. Friction force as a function of time for various particle sizes. Solids loading is varied every 30 sec.

The fitted data also shows that friction force has a non-linear dependence on solids loading. Based on the fitting graphs of Figure 4-5, friction force ( $F$ ) can be expressed as:

$$\begin{aligned}
 F_f &= F_{\text{absence-of-particles}} + F_{\text{presence-of-particles}} \\
 &= 1.7 + K \cdot \phi^{-2.67} \cdot C_0^b
 \end{aligned}
 \quad (4.14)$$

where  $K$  is a constant ( $= 47930$ ),  $\phi$  is the diameter of particle (nm),  $C_0$  is the solids loading (wt.%),  $b$  is a constant related to solids loading (i.e., 0.3 for 48 nm, 0.68 for 88 nm, and 0.77 for 110 nm). In the absence of particles, friction force obtained by the pad-wafer contact is found to be 1.7 N. In the presence of particles, as seen in Equation 4.14, friction force is a function of particle size and solids loading.

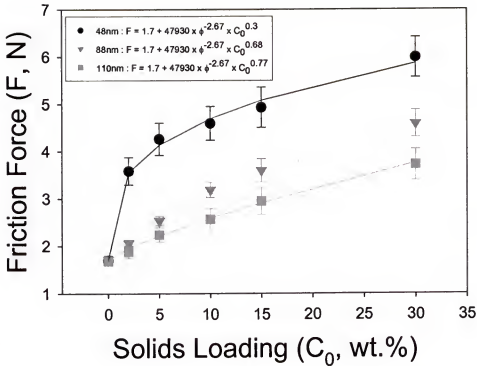


Figure 4-5. Friction force as a function of solids loading for different particle sizes.

A silica slurry with smaller particle size and high solids loading yields the maximum friction force observed. The dependence of particle size and solids loading on friction force is in agreement with theoretical estimations, which are described in Equation 4.13, with slight discrepancies in dependence of friction force on particle size and solids loading. In spite of slight discrepancies, which may be due to inherent experimental errors and size distribution of slurry particles, the dependence of friction force on particle size and solids loading provides insight into the contact behavior of particles in the polishing process. The estimation of the fundamentals of particle contact between pad and the wafer will contribute to further understanding of the polishing mechanism and will enhance our ability to predict the CMP performance given a set of process variables.

### Summary

A contact area model has been developed to predict the interfacial contact area between abrasive spherical particles and a flat wafer surface as a function of particle size and solids loading. Theoretically, it was found that the total contact area between particles and a flat wafer surface increases with the increase of solids loading and the decrease of particle size. Therefore, high friction forces may be achieved for the condition of high solids loading of small particles. This contact area model is generally consistent with the variation in friction force arising from the pad-particles-wafer interface. These observations not only provide an insight into the polishing mechanism, but they also present the basis of slurry design for optimization of the CMP process

## CHAPTER 5

### DYNAMIC CONTACT CHARACTERISTICS DURING CHEMICAL MECHANICAL POLISHING (CMP)

#### Introduction

Chemical mechanical polishing (CMP) has emerged as the vital process in fabricating a multilevel interconnected ultra large scale integrated (ULSI) circuits [Ste97]. The introduction of CMP in ULSI circuits fabrication makes it possible to eliminate topographic variation created by deposition processes and to achieve global and local planarization. CMP performance is determined by dynamic contact at the pad-particles-wafer interface during CMP. Most knowledge of dynamic contact is originated from the Stribeck curve that defines three contact regimes (asperity contact, mixed contact, and hydrodynamic contact) for ball bearings [Ava95]. Based on the Stribeck curve, Moon [Moo99] reported three contact regimes that detail the influences of fluid film thickness on friction coefficient in the CMP process. Several CMP models related to contact regimes and fluid film thickness have been developed. Runnel et al. [Run94] exhibited the existence of the fluid layer at the pad-wafer interface and suggested that hydrodynamic force alone is responsible for material removal rate for the indirect contact regime during CMP. Bhushan et al. [Bhu95] analyzed CMP mechanisms under the semidirect contact region by maintaining a thin fluid film between pad and wafer, thus reducing the role of the asperities in the pad. On the other hand, Cook [Coo90] suggested in glass polishing that wafer are polished by direct contact of particles on wafer surface. Yu [Yu93] also theoretically showed that contact area between pad and wafer is linearly

proportional to down force. In spite of the progress in the effort to estimate the dynamic contact behavior at the pad-particles-wafer interface, many studies are limited to the contact of a single particle on the wafer surface or contact between pad and wafer in the absence of particles.

In this study, we have investigated the dynamic contact as a function of platen velocity and down pressure using *in situ* lateral friction force measurements.

### Experimental

Levasil silica slurry (35.5wt.%) of 100nm obtained from Bayer Corporation was diluted to 0.5 wt.%, 2 wt.%, 5 wt.%, 10 wt.%, and 15 wt% in order to observe the effect of particle concentration on friction force. The slurries were adjusted to pH 10.5 using 0.1M  $\text{HNO}_3$  and 0.1M  $\text{NaOH}$ . Particle size of the slurry was analyzed using a Honeywell Microtrac UPA 150 particle size analyzer, which utilizes the dynamic light scattering technique. Slurry viscosity was measured using PAAR PHYSICA MCR 300 Rheometer to investigate the effect of slurry dilution on viscosity. Rodel IC 1000/Suba IV stacked pads were used for *in situ* lateral friction force measurements, and they were conditioned using a Grid-Abrade Diamond pad conditioner before each experiment. The speed of the polishing platen was changed from 90 rpm (an average linear velocity of 66 cm/sec) to 180 rpm (an average linear velocity of 132 cm/sec) for each experiment. Slurry flowing rate remained constant at 100 mL/min.

*In situ* lateral friction force measurements were carried out to investigate the dynamic contact between pad, particles and wafer, or between pad and wafer.

As seen in Figure 3-1, a friction force measurement tool was assembled on a tabletop Struers Rotapol 31 polisher. The down pressures of 2.7 psi (17.845 kPa), 3.5 psi (23.132 kPa), and 5.0psi (33.046 kPa) were loaded on a cylinder-type aluminum block on which

the wafer to be polished was mounted. The output data is taken every 250 msec, and is transferred to a data acquisition system by a force transducer (Sensotec model 31 load cell). For these experimental conditions, material is not removed from the sapphire wafer [0001] by the silica particles. Therefore, the same surface conditions exist for each experimental run.

### Results and Discussion

The size distribution of silica particles is shown in Figure 5-1. Particle size analysis shows that silica slurries are well dispersed and have no agglomeration at pH 10.5.

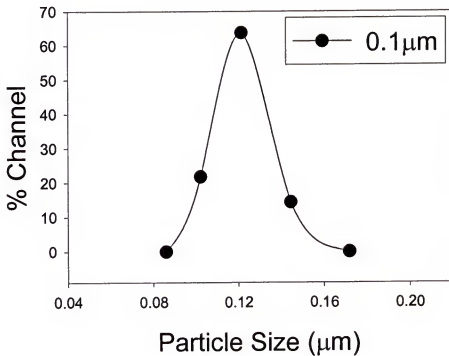


Figure 5-1. Size distribution of abrasive particles measured by dynamic light scattering technique.

Figure 5-2 shows *in situ* lateral friction force as a function of time for different solids loading and platen velocities. During the initial 30 sec, de-ionized water was



utilized as baseline slurry for this experiment. Based on the friction force response by the de-ionized water, friction force response changed due to variation in solids loading and platen velocity has been normalized. After the initial 30 sec, platen velocity was changed every 30secs for different solids loading. Depending on platen velocity and solids loading, friction force response was seen to change in a step like manner.

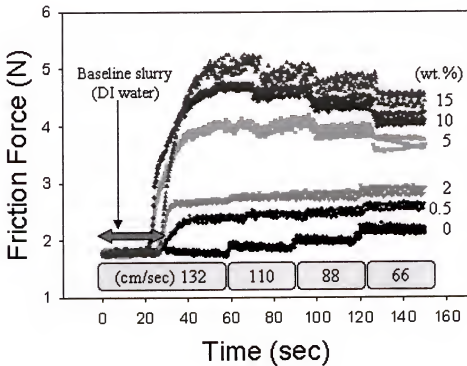


Figure 5-2. Friction force as a function of time for different platen velocity and solids loading.

Figure 5-3(a) shows friction forces as a function of platen velocity for different solids loading, which is redrawn from Figure 5-2. Friction force decreased with platen velocity for low solids loading (less than 2wt.%) and it increased with platen velocity at high solids loading (more than 5wt.%).

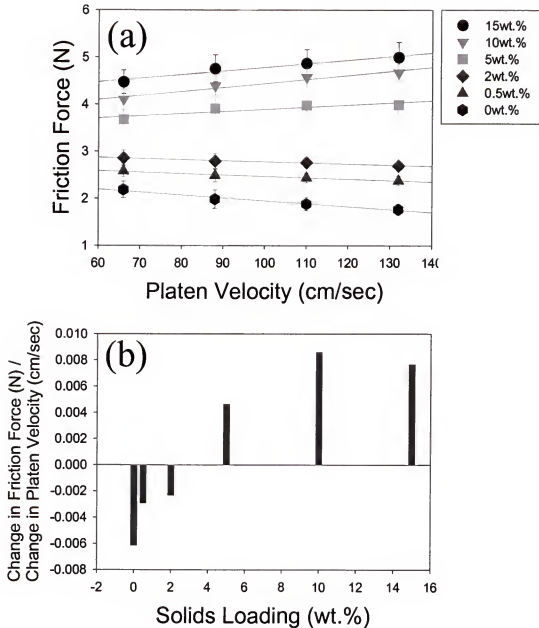


Figure 5-3. (a) Friction force as a function of platen velocity for different solids loading, (b) slope in friction force vs. platen velocity as a function of solids loading.

Based on Figure 5-3(a), the slopes in the friction force vs. velocity curve were redrawn in Figure 5-3(b). Figure 5-3(b) shows the slopes in the friction force vs. velocity curve as a

function of solids loading. The range of solids loading for which the transition from negative to positive takes place is between 2wt.% and 5wt.%.

For either semi-direct contact or direct contact regimes, it is known that friction force is inversely proportional to fluid film thickness [Moo99]. Runnel et al. determined fluid film thickness for the condition where a set of  $h$  (fluid film thickness) and  $\theta$  (the angle of inclination between pad and wafer), which satisfy the zero gimbal moment conditions [Run94]. Therefore,  $\theta$  is an important factor needed to determine fluid film thickness, leading to the change in friction force [Sch79]. In our experimental condition,  $\theta$  has been assumed to remain constant because the cylinder-type aluminum block on which the wafer to be polished is mounted is fixed to maintain a constant tilting condition. In this regard, fluid film thickness ( $h$ ) is suggested as follows [Run94]:

$$h = H_0 \left( \frac{v \cdot V}{P} \right)^{\frac{1}{2}} \quad (5.1)$$

where  $V$  is the platen velocity,  $H_0$  is a constant at steady state ( $V=0$ ),  $v$  is the slurry viscosity, and  $P$  is the down pressure. Figure 5-4 shows the effect of solids loading on slurry viscosity. It is seen that slurry viscosity is independent of solids loading in these shear rate ranges. Therefore, fluid film thickness can be limited to a function of platen velocity and down pressure. Friction force ( $F$ ) between two contacting bodies is determined by shear strength ( $\sigma$ ) and real contact area ( $A_r$ ) as follows [Jon85]:

$$F = \sigma \cdot A_r \quad (5.2)$$

Shear strength can be substituted with following approximation used for tribological approximations for slider bearings [Dav91].

$$\sigma = \frac{v \cdot V}{h} \quad (5.3)$$

Friction force can now be defined using the following relationship by combining Equation (5.1), Equation (5.2), and Equation (5.3).

$$F = \left(\frac{1}{H_0}\right) \cdot (v \cdot V \cdot P)^{\frac{1}{2}} \cdot A_r \quad (5.4)$$

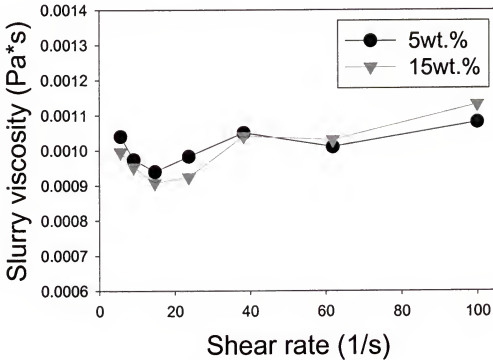


Figure 5-4. Effects of solids loading on slurry viscosity.

When down pressure and slurry viscosity remains unchanged, friction force is a function of platen velocity and real contact area. In the absence of particles, the real contact area between the polishing pad and wafer surface decreases with increasing platen velocity due to the increase of fluid film thickness, resulting in low friction force. Even though shear strength increases with increasing platen velocity, the role of shear

strength seems to be negligible for particle-free conditions. For low solids loading (less than 2wt.%), friction force decreased with platen velocity. This indicates that the area of particles contacting with the wafer is smaller than that of pad in contact with the wafer. Therefore, the negative trends of slopes in the friction force vs. velocity curve were not changed by the addition of small amount of particles at low solids loading (less than 2wt.%). However, for high solids loading (more than 5wt.%), the slopes in friction force vs. velocity curve are positive.

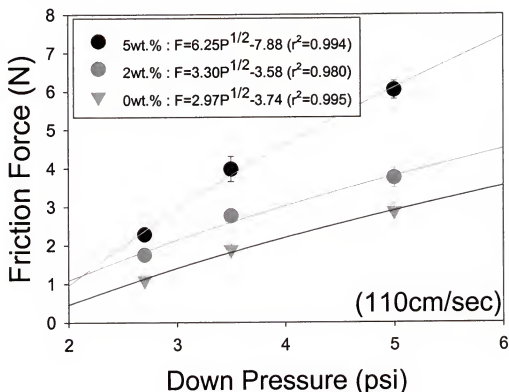


Figure 5-5. Friction force as a function of down pressure for different solids loading.

This suggests that shear strength is more significant than contact area at the pad-particles-wafer interface. Despite the decrease in contact area, friction force increases due to the increase of shear strength. Regardless of solids loading, the slope in friction force vs.

platen velocity curve generally increases with solid loading as shown in Figure 5-3. This indicates that shear strength increases with solids loading. In other words, shear strength is proportional to the number of particles between pad and the wafer to be polished. When slurry viscosity, platen velocity, and solids loading remain unchanged, friction force is thought to be a function of down pressure. Figure 5-5 shows the effect of down pressure on friction force for different solids loading. Friction force sub-linearly increases with down pressure having one-half power dependence on down pressure. This result is well in agreement with the relationship in Equation 5.4. The increase of shear strength by increasing down pressure is thought to be a significant factor in the increase in friction force.

### Summary

Dynamic contact at the pad-particles-wafer interface was studied as a function of platen velocity and down pressure for different solids loading (0wt.%~15wt.%) using *in situ* lateral friction force measurements. The decrease of friction force with platen velocity in the absence of particles is due to the decrease of dynamic contact area between pad and wafer. At low solids loading condition (less than 2wt.%), the contact area of particles contacting with wafer is smaller than that of pad in contact with wafer. Thus, the role of particles is negligible in this condition, resulting in a negative slope for friction force vs. platen velocity curve. At high solid loading (more than 5wt.%), the enhancement of friction force with platen velocity is due to the increase of shear strength caused by the enhancement of sliding speed of particles, leading to positive slope in friction force vs. platen velocity curve. Shear strength increases with down pressure, raising the friction force, which is confirmed by observing the effect of down pressure on

friction force. To this point the fractional surface coverage has been estimated , along with a relation to predict the particles a the pad-wafer interface. Also, the description of dynamic contact behavior has been presented.

## CHAPTER 6

### STUDY OF PH EFFECTS ON SILICON DIOXIDE DIELECTRIC CHEMICAL MECHANICAL POLISHING (CMP)

#### Introduction

Chemical mechanical polishing (CMP) is the process utilized most extensively to remove topographic variations and to achieve global and local planarization during microelectronic device fabrication [Ste97, Sin02a]. The miniaturization of microelectronic devices has necessitated the growing role of CMP in the semiconductor industry. The CMP is a complex process achieved by synergistic interactions of mechanical abrasion and chemical reaction at the pad-particles-wafer interface [Sin02b]. During mechanical abrasion, the removal of material and planarization results from the direct contact of the wafer against the pad and the particles embedded into the pad [Bro81, Co090]. Chemical reactions through the solvent behavior of the slurry are responsible for the physical and mechanical properties of the thin surface layer formed during dielectric and metal CMP [Mic82, Tro94, Kau91]. It has been demonstrated that the desired performance (i.e., global planarization, good surface finish, and high removal rate) of CMP is achieved by an appropriate balance of synergistic interaction arising from mechanical abrasion and chemical interaction [Lee02]. In order to optimize the CMP process, a mechanistic understanding of chemical and mechanical interactions involved in the polishing process is necessary.

The CMP of dielectric silica has long been an important step for planarization in multilayer interconnects (MLI) or shallow trench isolation (STI). The polishing



mechanism of dielectric silica needs to be understood in order to achieve desired CMP performance. The mechanism controlling CMP is manifested in the contact response at the pad-particles-wafer interface and physical properties at the surface and near-surface level. The physical properties of the near surface layer formed on silicon dioxide are significantly dependent on the slurry conditions. Tomozawa *et al.* [Tom02] noted that the decrease in microhardness of silica glass with water content is due to the diffusion of water into the surface of silica glass. Hammond *et al.* [Ham11] reported that fracture strength of silica decreases with water because surface free energy is lowered by the increase of the amount of water content. Nevot *et al.* [Nev80] has examined the existence of the near surface of silica reporting the existence of a modified layer with density lower than the bulk using grazing X-ray reflection. Trogolo *et al.* [Tro94] revealed the evidence of a physically modified near surface thin layer of silica produced at pH 10.5 using transmission electron microscopy (TEM). The effect of pH on the polishing rate of silica by colloidal silica has been investigated [Izu82]. Polishing rate remained constant for  $\text{pH} \leq 11$ , but began to increase rapidly for  $\text{pH} \geq 11$ , conversely the solubility of silica increases drastically with the increase of pH at approximately pH 10 [Ale54]. The chemical effect in silica polishing is in doubt since the solubility of silica does not correspond with polishing rate of silica glass. The variation of pH in silica CMP is complicated by agglomeration of colloidal silica, the modification of sub surface, and surface charge, making it difficult to investigate the chemical effect on polishing of dielectric silica. Well-dispersed non-agglomerated abrasive silica particles are required to investigate the chemical effect on polishing of dielectric silica. In this study, we investigated the polishing behavior of dielectric silica using non-agglomerated

amorphous silica particles in order to validate the polishing mechanism of dielectric silica.

### **Experimental**

The abrasive particles used for this study were Levasil (50CK) colloidal silica particles obtained from Bayer Company. The average diameter of as-received silica particles was approximately 110 nm. The chemical characterization of the as-received silica slurry was conducted using Fourier-transform infrared (FTIR) spectroscopy. Silica slurry of 35.5 wt.% was diluted to 10 wt.% for polishing experiments and friction force measurements. The pH of diluted silica slurry was adjusted with 0.1 M NaOH and 0.1 M HNO<sub>3</sub> to reach pH 2, pH 5, pH 9, and pH 10.5. For each pH condition, size and size distribution of silica particles were analyzed using a Honeywell Microtech UPA150 particle size analyzer utilizing the dynamic light scattering technique. Zeta potential measurements were carried out using a ZetaPlus manufactured by Brookhaven Instruments Corporation. In order to measure the solubility of silica deposited on silicon wafer by plasma enhanced chemical vapor deposition (PECVD), dipping test was conducted at various pH conditions. Finally, the interaction forces between silica particle and silica wafer were obtained from a Nanoscope III Atomic Force Microscopy (AFM) provided by Digital Instruments Company. The silica particle of 25  $\mu\text{m}$  radius was attached to the tip of the AFM cantilever and the force between it and the flat silica surface was measured. The interaction force was measured from the deflection of the cantilever and the distance was controlled by the extension of a piezoelectric drive. The AFM has a displacement resolution of 0.1 nm and force sensitivity of  $\sim 0.2$  nN.

Polishing experiments were conducted to investigate the material removal mechanism using a Struers Rotapol 31 polisher. The polishing samples were clipped to  $1.5 \times 1.5$  square inch from 8 inch silicon wafer on which silica (thickness is  $2.0 \mu\text{m}$ ) was deposited by a plasma enhanced chemical vapor deposition (PECVD) technique. The thickness of silica layer was measured by a J. A. Woollan Variable Angle Spectroscopic Ellipsometry (WVASE) before and after polishing to calculate the polishing rate. An IC1000/Suba IV stacked pad was utilized as a polishing pad, and a Grid-Abrade diamond conditioner was used to abrade the pad before each test. The flow rate of slurry was fixed at 100 ml/min. The rotation speed of pad and wafer was 110 cm/sec and down pressure was adjusted to 7.5 psi, 10.5 psi, and 15 psi. Surface topography produced after CMP was measured using a Digital Instruments Nanoscope III AFM.

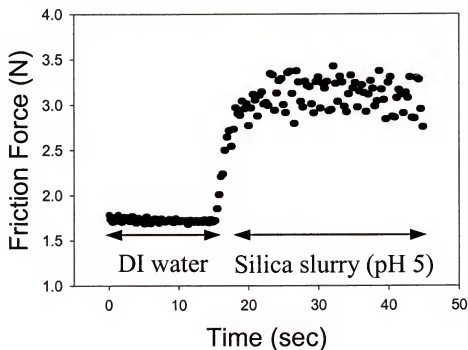


Figure 6-1. Friction force as a function of time at down pressure of 2.5 psi.

*In situ* Lateral friction force measurements were carried out to detect friction force due to interactions at the pad-particles-wafer interface. As seen in Figure 3-1, the tool used to measure the friction force was mounted on the Struers Rotopol 31 tabletop polisher. A Sensotec model 31 load cell was used to detect the friction force with a data collection acquired every 250ms. Friction samples were clipped to 1.0 × 1.0 square inch from the same 8 inch silica wafer used for polishing experiments. Down pressures of 2.5 psi, 3.5 psi, and 5.0 psi was applied during friction force measurements. Figure 6-1 shows the friction force as a function of time for down pressure of 2.5 psi. The friction force was measured during 45 sec intervals for each run. De-ionized water was utilized as a baseline condition during the initial 15 sec. During the next 30 sec, it was shown that the variation of friction force was detected by the addition of silica slurry.

### Characterization of Slurry

#### Chemical Analysis

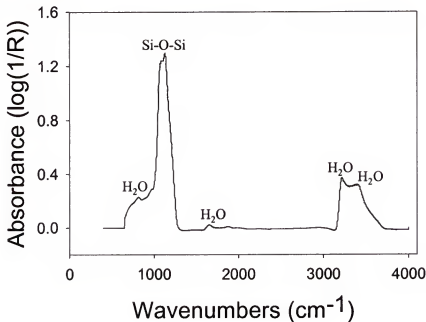


Figure 6-2. FTIR spectrum of as received colloidal silica slurry.

The Levasil (50CK) silica slurry was characterized using FTIR. Figure 6-2 shows the FTIR spectra of the as-received Levasil (50CK) colloidal silica slurry. The FTIR spectrum contains the absorption peak characteristics of the Si-O-Si bonds in silica slurry at 1129 and 1000  $\text{cm}^{-1}$  [And74]. The adsorption peaks of 3383  $\text{cm}^{-1}$ , 3221  $\text{cm}^{-1}$ , and 812.58  $\text{cm}^{-1}$  corresponds to the background adsorption peaks detected by de-ionized water. Note that no organic solvent and surfactant were detected, which is in agreement with slurry characteristics provided by Bayer Company [Sta03].

#### Particle Size Analysis

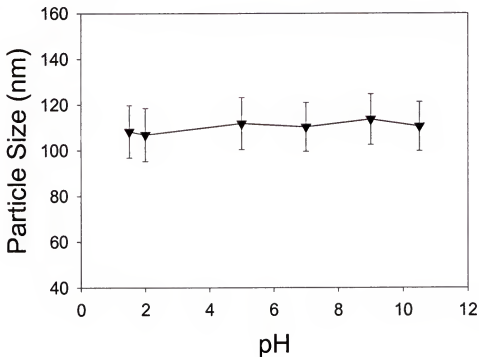


Figure 6-3. Particle size and size distribution of colloidal silica as a function of pH.

The size and distribution of silica particles was detected by the light scattering method. As seen in Figure 6-3, particle size and size distribution remained unchanged with pH over the range of pH 1.5 to pH 10.5. This enables us to investigate the polishing behavior occurring between non-agglomerated particles and wafer. Figure 6-4 shows

SEM images of abrasive silica particles dispersed at pH 10.5. This image confirms the particle size measured by light scattering methods and shows that particles are spherical in shape. Based on particle size analysis mentioned above, Table 6-1 shows quantitative values of average particle diameter measured by light scattering and SEM, respectively.

Table 6-1. Variation in size of supplied abrasive particles.

| Particle type | Mean volume distribution diam. ( $\mu\text{m}$ ) <sup>a</sup> | Standard deviation ( $\mu\text{m}$ ) <sup>a</sup> | Average diam. ( $\mu\text{m}$ ) <sup>b</sup> | Standard deviation ( $\mu\text{m}$ ) <sup>b</sup> |
|---------------|---|---|--|---|
| 50CK          | 0.1105  | 0.0107  | 0.1163                                       | 0.0132  |

a Obtained by dynamic light scattering measurements

b Determined by scanning electron microscopy (SEM)

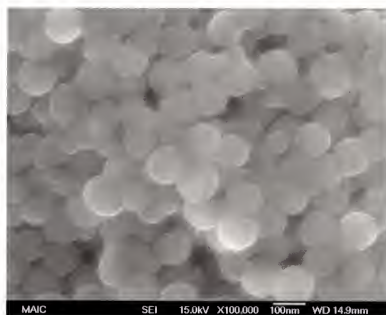


Figure 6-4. SEM image of colloidal silica particle dispersed at pH 10.5.

The mean volume particle diameter measured by light scattering is well in agreement with the average particle diameter measured by SEM imaging. These results

illustrate that spherical silica abrasive particles are dispersed in aqueous media over the pH range from pH 1.5 to pH 10.5.

### Solubility of Silica

Figure 6-5 shows the solubility of silica as a function of pH. The left side denotes the solubility of amorphous silica particles and the right side represents the solubility of a PECVD silica wafer. The surface area of silica wafer is a  $10^{-4}$  times smaller than that of amorphous silica particles, making a difference in the degree of solubility.

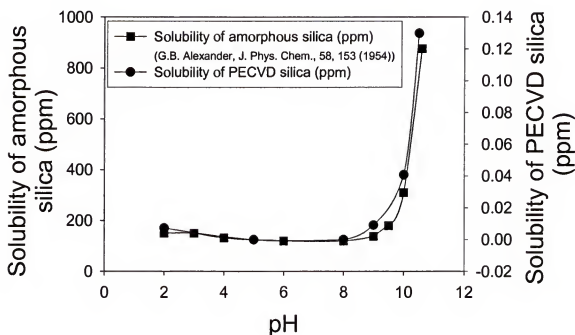


Figure 6-5. Solubility of amorphous silica particle and silica wafer as function of pH.

Regardless of the surface area, it was observed that the solubility of silica changes little at low pH conditions (less than pH 9). For  $\text{pH} \geq 9$ , however, the solubility of silica steeply increased with increase of pH. This suggests that solubility of silica is significantly dependent on the pH range. These dissolution tendencies are important factors to consider when seeking to understand the polishing behavior of silica polishing. As the pH

of the slurry and the solubility of  $\text{SiO}_2$  increase, the tendency for polished  $\text{SiO}_2$  to dissolve and/or remain in solution increases. Jairath *et al.* [Jai94] shows considerable increases in oxide polishing rate with pH for silica-based slurries when the pH of the slurries higher than 9.5. This result demonstrates the need for a more complete study of pH effect in oxide CMP. Based on the solubility of silica, polishing mechanism for silica CMP will be described here.

## Results and Discussion

### Effects of pH on Polishing Rate

Surface characteristics of dielectric silica are varied by water-silica reactions. The reaction between siloxane bonds ( $\text{Si-O-Si}$ ) and water determine the surface properties of silicon dioxide during polishing.

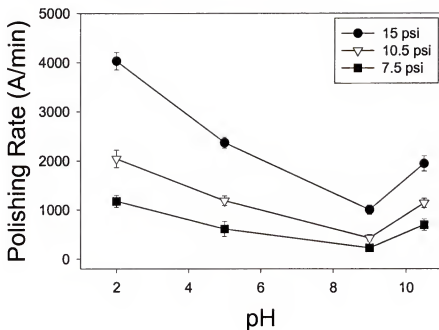
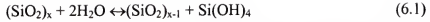


Figure 6-6. Polishing rate as function of pH for various down forces.

This reaction is described as a reversible depolymerization reaction whose expression is given as follows [Ile79]:





Polishing of dielectric silica is achieved by breaking the Si-O bonds through chemical and mechanical interaction occurring at the pad-particles-wafer interface.

Figure 6-6 presents the polishing rate as function of pH for various down pressures.

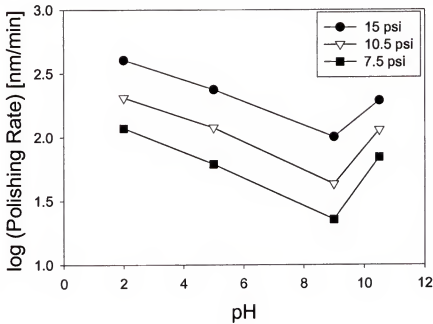


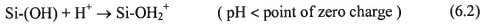
Figure 6-7. Log plot of silica polishing rate vs. pH for different down force.

In order to validate the effect of down force on polishing rate at each pH condition, Figure 6-7 was redrawn to log scale. As seen in Figure 6-7, regardless of pH, polishing rate increased with increasing down pressure. This suggests that polishing rate is generally proportional to down pressure at the same polishing rate at each pH range. For a given down pressure, with increasing pH, polishing rates decreases, and then increases with the transition occurring at pH 9.

It was noted that the solubility of silanol ( $\text{Si}(\text{OH})_4$ ) in water is significantly increased at a pH of more than 10.0 [Ale54], allowing dissolution ahead of the particle

without redeposition at the trailing edge, thus favoring the dissolution reaction in the forward direction resulting in material removal [Coo90]. In this regime silica simply dissolves, entering solution as a silicate anion. Thus, solubility effects appear to be responsible for increases in the polishing rate. At a pH of less than 10.0, the solubility of silanol ( $\text{Si}(\text{OH})_4$ ) in water remained unchanged with pH [Ale54]. It is clear that polishing rate is not a function of solubility of dielectric silica for  $\text{pH} \leq 10$ . In this regime, electrostatic interactions between the silica particles and the surface of silica wafer may play a role in determining the polishing rate [Raj97, Mah99].

The surface of depolymerized silica is charged with the nature of charge depending on the pH as follows [Par65]:



In order to determine the nature of charge, the zeta potential of Levasil silica slurry was measured. Figure 6-8 shows the measured zeta potential of silica slurry with pH, and the corresponding isoelectric point (IEP) is found to be less than pH 2.0. In addition, figure 6-9 presents the extent of the interaction forces between a single silica particle and a silica wafer as a function of separation distance for three pH conditions. Increasing the pH of the silica slurry increases the magnitude of the repulsive interaction force for a given separation distance. According to Figure 6-7, the polishing rate is greater at pH 2 than at pH 9. This decrease in polishing rate increase of pH causes an increase in the repulsive interaction force, which is in agreement with interaction force measurements. At each pH condition, the increase of down pressure raises the polishing rate pound for pound.

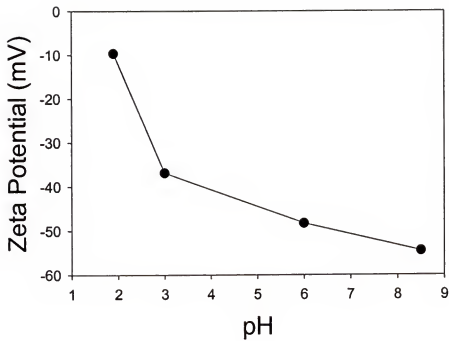


Figure 6-8. Zeta potential of silica slurry as a function of pH.

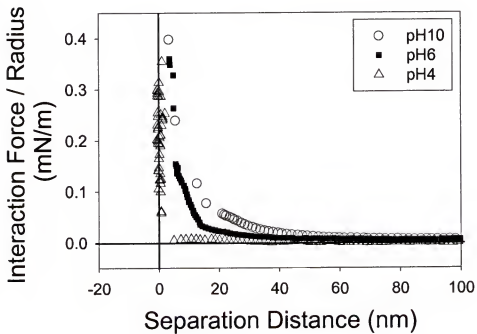


Figure 6-9. The interaction force between a silica particle 25  $\mu\text{m}$  in radius and a silica plate in 0.001 M sodium chloride solution as a function of pH.

This suggests that the variation of polishing rate due to changing down pressure is only related the interfacial contact of pad, particles, and wafer. As demonstrated in previous chapters, the increase of down pressure leads to an increase in contact area between pad and wafer and the number of particles in contact with wafer, thus resulting in higher polishing rates.

### **Effect of pH and pressure on friction force**

Friction is caused by phenomena that occurs on the surface of pad, particles, and wafer. Thus, friction characteristics are dependent on the physical and chemical properties of the surface. Figure 6-10 shows the friction force as a function of pH for down pressure of 35 psi. The friction force sub-linearly decreases with pH and exhibits the same trends with polishing rate for  $\text{pH} \leq 10$ . The decrease in friction force may be due to the variation of charge on the surface of silica. With increasing pH, both silica particles and silica wafer accumulate strong negative charges on the surface, causing a higher repulsive interaction force, which is confirmed by interaction force measurements via AFM. It has been noted that the friction force originating from the pad/wafer interface decreased with an increase of pH because the electrostatic repulsion force increased with pH [Mah99]. At a pH greater than 10.0, it was observed that friction force steeply decreases with the increase of pH. In this high pH regime, the variation of the friction force is opposed to that of polishing rate. As mentioned earlier, for  $\text{pH} \geq 10$ , the increase of polishing rate with pH is expected to be due to the formation of a soft gel-layer on the top surface of silica due to a significant increase of silica solubility. In addition, the increase of silica solubility at high pH is thought to play an important role in providing a superior lubrication effect.

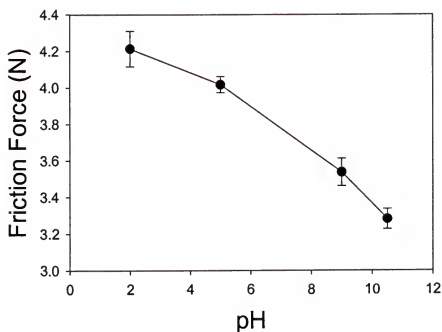


Figure 6-10. Friction force as a function of pH under the down pressure of 3.5 psi.

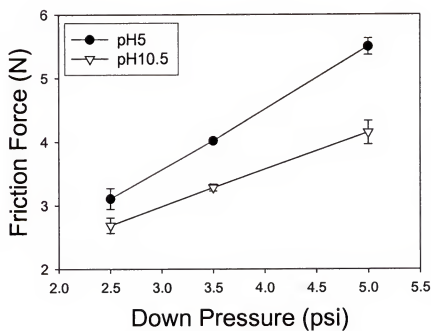


Figure 6-11. Friction force as a function of down pressure for different pH conditions.

Sasaki [Sas92] suggests a tribochemical reaction wear model that explained that hydroxides created by high pressure and high shear stress at a contact point play the same role as high viscosity lubricants on sliding surface and result in a favorable lubrication effects. Figure 6-11 shows the friction force as a function of down pressure for two pH conditions. The friction force increases with down pressure due to the increase of total contact area at the pad-particles-wafer interface. At all down pressure conditions, the friction force measured at pH 5 is higher than at pH 10.5. This result also indicates the presence of a soft gel layer. Based on friction force behavior, we can say that the reduction in friction force can be attributed to both the increase in repulsive interaction force and the formation of soft gel layer on the surface of silica.

#### Surface Analysis by AFM

The surface morphology and surface roughness as measured by AFM can provide further insight into the polishing mechanism. Surface roughness ( $R_s$ , the penetration depth of the particle into the surface) is given by [Coo90]:

$$R_s = \frac{3}{4} \phi \left( \frac{P}{2kE} \right)^{\frac{2}{3}} \quad (6.4)$$

where  $\phi$  is the particle diameter,  $P$  is the down load per particle,  $k$  is the particle concentration, and  $E$  is the elastic modulus of the wafer to be polished with abrasive particles. According to Equation 6.4, surface roughness is a function of elastic modulus of substrates. Elastic modulus is a measure of a material's resistance to deformation. Therefore, the case of a lower elastic modulus for the top surface is expected to lead to higher surface roughness. The variation in pH affects the mean surface roughness of the polished wafer surface, as shown in Figure 6-12. The mean surface roughness is almost

same for  $\text{pH} \leq 10$ ; however it increases as  $\text{pH}$  increases from 9 to 10.5. The solubility of silica could account for the observed variation in surface roughness. In addition, the change in solubility explains the effect of chemical environments on the top surface layer.

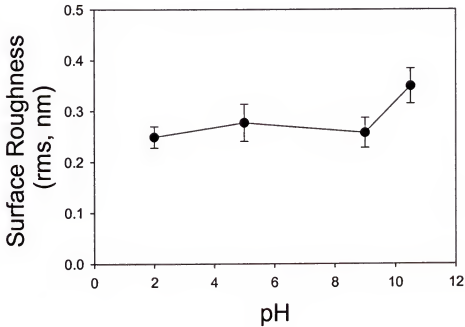


Figure 6-12. Surface roughness (RMS) of silica wafer polished with colloidal silica as a function of  $\text{pH}$  at down pressure of 10.5 psi.

For  $\text{pH}$  less than 10, particle size and solubility of silica remains unchanged, leading to a constant surface roughness, which is confirmed by Equation 6.4. At high  $\text{pH} \geq 10$ , the solubility of silica steeply increases with  $\text{pH}$  [Ale54]. Trogolo *et al.* [Tro94] reported top silica surface regions of low density produced at a  $\text{pH}$  of 10.5 through the phase contrast mechanism of TEM imaging. A grazing angle X-ray study of polished silica provided evidence of a silica surface region possessing a lower density than the bulk [Nev80]. Therefore, the elastic modulus of the modified surface layer on the silica surface may be lower than the bulk. At high  $\text{pH} (\geq 10)$ , The increase of surface roughness may be due to

the decreased elastic modulus of top silica surface, which is verified by Equation 6.4 at which surface roughness is inversely proportional to elastic modulus. Figure 6-13 shows AFM images and cross-section of silica wafer polished with silica slurry at a condition of pH 5 and pH 10.5, respectively. The scratches produced on the silica wafer demonstrate the characteristics of particle surface contact. Polishing is achieved by the sliding motion of particles, which was confirmed by a two-body contact mechanism [Abr91].

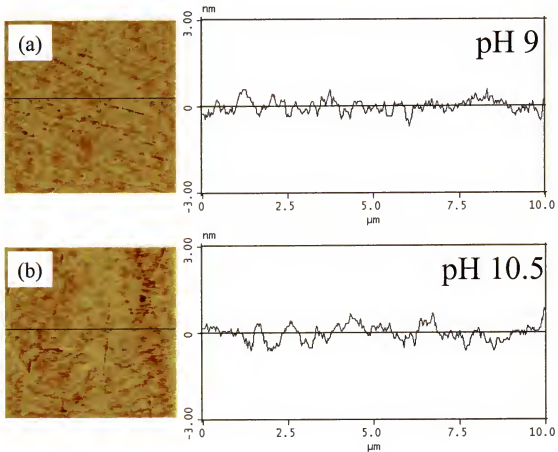


Figure 6-13 Overview and cross-section for the silica wafer polished with colloidal silica slurry of (a, top) pH 9 and (b, bottom) pH 10.5.

Based on the cross-sectional images, it can be noted that surface roughness produced at pH 10.5 is approximately 0.08 nm higher than at pH 9. Normally, the indentation depth



per particle at pH 10.5 is slightly deeper than at pH 9 due to the formation of soft gel-layer on top silica surface, yielding a higher surface roughness.

### **Summary**

The variation of silica polishing rate with pH is primarily due to the variation in interaction force between silica particles and a silica wafer, and the solubility of silica. With the transition at pH 10 above which solubility of silica is steeply increased, a significant variation of polishing rate, friction force, and surface roughness was observed. The increase in repulsive interaction force between silica particles and silica wafer indicates the lubricating effect of the chemically modified surface layer, leading to lower friction force and polishing rate. The high solubility of silica reduces friction force but it enhances polishing rate due to the formation of soft gel layer possessing a low density. It was also noted that surface finishes are affected by particle size and solubility of silica. When the particle size in the silica slurry remained unchanged, the adjustment of surface charge and physical properties of the silica surface have an important effect on polishing performance with such characteristics as polishing rate, interfacial friction force, and surface finish. These observations indicate that the polishing performance is a function of chemical and mechanical phenomena at the pad-particles-wafer interface.

## CHAPTER 7

### EFFECTS OF SLURRY PARTICLES ON SILICA CHEMICAL MECHANICAL POLISHING (CMP)

#### **Introduction**

As the minimum feature size of microelectronic device reaches the 100 nm technology node, chemical mechanical polishing (CMP) has become the best choice for global and local planarization [Ste97, Bey99, Sho00, Sin02a]. Global and local planarization makes it possible to produce a multilevel integrated circuit device by reducing the topography variation at the wafer scale. Without CMP, it would be impossible to fabricate complex, dense, and miniaturized integrated circuit devices. During the past decades, CMP has significantly advanced both in the development of sophisticated processing tools and in the formulation of slurries. In spite of these achievements, CMP remains one of least understood areas in microelectronic device fabrication processing.

Even though the characteristics of slurry particles (i.e., the shape, the size, and the concentration) are critical in determining CMP performance, the effect that the slurry particles have on polishing performance is not clear. For polishing of copper or ferrite, it was suggested that polishing rate is proportional to particle size and solids loading [Jai94b, Xie96]. Cook [Coo90] has presented data suggesting that polishing rate is independent of particle size for glass polishing. While, Izumitani [Izu79] suggested that polishing rate decrease with increasing particle size. Our previous work suggests two

polishing mechanisms in silica CMP [Mah99c]. One is a contact area based mechanism by which

$$A \propto C_0^{\frac{1}{3}} \cdot \phi^{-\frac{1}{3}} \quad (7.1)$$

where A is the contact area,  $C_0$  is the particle concentration, and  $\phi$  is the particle diameter. In this model, polishing rate increases with an increase in particle concentration and a decrease in particle size, which was observed during tungsten CMP [Bie98]. The other is an indentation-volume-based mechanism by which

$$V \propto C_0^{-\frac{1}{3}} \cdot \phi^{\frac{4}{3}} \quad (7.2)$$

where V is the indentation volume. According to this indentation-volume-based mechanism, polishing rate increases with decreasing particle concentration and increasing particle size. This mechanism was observed via silica polishing experiments [Mah99c].

In the micro- and nano-scale, polishing rate is significantly dependent on the dynamic contact of particles between the pad and the wafer. In order to examine the dynamic interfacial contact of particles during CMP, friction force measurement techniques and surface finish analysis are considered the most applicable methods for direct observation of contact phenomena [Mah99b]. Abrahamson *et al.* [Abr91] studied the material removal mechanism by loose abrasive particles (i.e., two-body contact) and compared with material removal mechanism by bonded abrasive particles (i.e., three-body contact). As seen in Figure 7-1, it was also reported that three-body contact produced a “shot-blast” appearance, while two-body contact yielded continuous scratches. Macmillan *et al.* [Mac74] studied the sliding frictional behavior under various chemical environments using pin-on-disk friction force measurements. Scratches by sliding motion

of particles were observed on the MgO surface. Previous results showed that electrostatic repulsion force between two surfaces and surface roughness played important roles in determining a friction force during polishing [Raj97, Ram00].

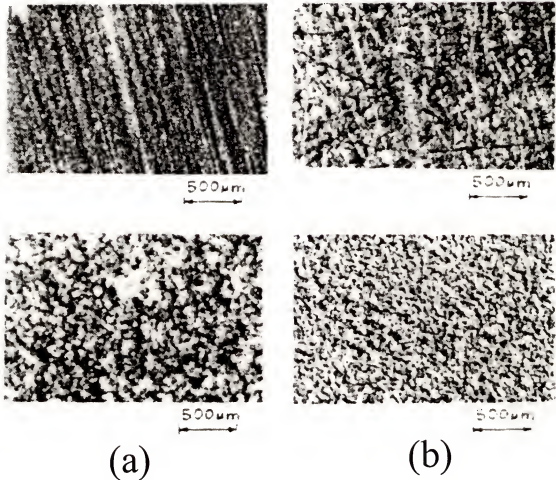


Figure 7-1. Wear patterns for (a) fused silica and (b) 1018 steel using two-body abrasion (top) and three-body abrasion (bottom) [Abr91].

This paper presents further validation of the polishing mechanism using sol-gel silica slurries. The effects of particle size and solids loading on friction force and surface finishes were delineated to understand the dynamic contact of particles during polishing.

## Experimental

CMP slurries were formulated by dispersing sol-gel silica particles from Geltech Corporation in de-ionized water. The average particle diameters provided by Geltech were 0.2, 0.5, 1.0, and 1.5  $\mu\text{m}$ . The solids loadings were varied from 0.5 wt.% to 30 wt.%. Slurries composed of sol-gel silica particles were dispersed using an ultrasonic bath, and they were stabilized by adjusting pH values to 10.5 with 0.1M NaOH and 0.1 M  $\text{HNO}_3$ . The average size and distribution of stabilized sol-gel silica particles were analyzed with a Coulter LS 230 instrument that uses a dynamic light scattering technique. In addition, the shape and size of the particles were determined by scanning electron microscopy (SEM) analysis.

Polishing samples were clipped to 1.5 $\times$ 1.5 square inches from a 8 inch p-type silicon wafer on which silica of about 2.0  $\mu\text{m}$  thickness was deposited by the plasma enhanced chemical vapor deposition (PECVD). IC 1000/Suba IV stacked pads (supplied by Rodel Inc.) were utilized as CMP pad, and a Grid-Abrade diamond pad conditioner was used to abrade the pad before each test.

A Struers Rotopol 31 tabletop polisher was used to polish samples. The following conditions were applied to each run: down pressure of 3.5 psi (23.132 kPa), polishing time of 30 seconds, slurry flow rate of 100 ml/min, and the rotation speed of 150 rpm (110 cm/sec). Polishing tests were repeated three times to ensure reliable results. Polishing rates were determined by measuring oxide film thickness on the samples before and after the polishing experiments, using a J. A. Woollam variable angle spectrometry ellipsometer (WVASE). A Digital Instruments Nanoscope III Atomic Force Microscopy (AFM) was used to characterize the surface finishes of the polished samples.

*In situ* friction force measurements were carried out to investigate the contact behavior at the pad-particles-wafer interface. As seen in Figure 3-1, an *in situ* friction force measurement tool was mounted on an aforementioned Struers Rotopol 31 tabletop polisher. A Sensotec model 31 load cell was used to measure the friction force, and was connected to a data acquisition system, with a data point received every 250 ms. Experimental conditions of *in situ* friction force measurements were the same as the process conditions of polishing experiments. Friction force was measured during 1 minute for each run. During the initial 15 sec, de-ionized water was utilized as a baseline condition. During the next 45 sec, the variation of friction forces with slurry particles was determined.

## Results and Discussion

### Analysis of Shape and Size of Silica Particles

We directly observed the shape and size of sol-gel silica particles with scanning electron microscopy (SEM) and statistically detected the size and distribution of the silica particles with light scattering particle size analysis. As shown in Figure 7-2, the primary particles are spherical in shape and are similar in size. The average particle sizes measured from SEM micrograph are (a) 0.22  $\mu\text{m}$ , (b) 0.59  $\mu\text{m}$ , (c) 1.13  $\mu\text{m}$ , and (d) 1.62  $\mu\text{m}$ , respectively. These direct observations are statistically confirmed by light scattering particle size analysis. As shown in Figure 7-3, particle size distribution curves show single peaks with average particle diameters (standard deviation of particle size) of 0.20  $\mu\text{m}$  ( $\pm 0.05 \mu\text{m}$ ), 0.55  $\mu\text{m}$  ( $\pm 0.08 \mu\text{m}$ ), 1.09  $\mu\text{m}$  ( $\pm 0.16 \mu\text{m}$ ), and 1.53  $\mu\text{m}$  ( $\pm 0.22 \mu\text{m}$ ), respectively. The average particle size measured by SEM is analogous to that measured by light scattering methods. Both observations are well in agreement with the average

particle size that the company provides. These silica particles are well dispersed inside aqueous media for pH 10.5. Spherical shape and uniform size distribution of these silica particles will make it possible to distribute equally the particles in contact with the pad and wafer during CMP.

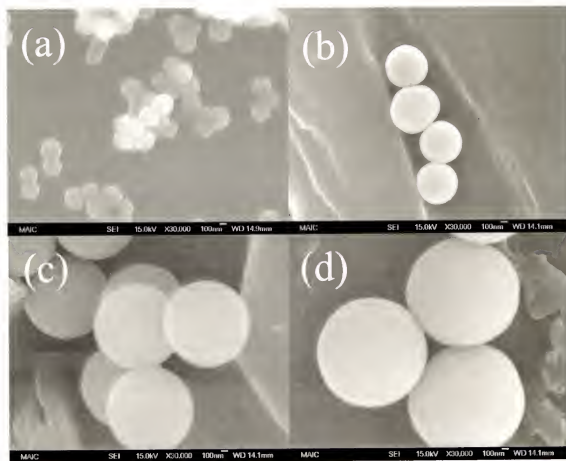


Figure 7-2. Scanning Electron Microscopy (SEM) images of silica particles with different particle size: (a) 0.2  $\mu\text{m}$ , (b) 0.5  $\mu\text{m}$ , (c) 1.0  $\mu\text{m}$  and (d) 1.5  $\mu\text{m}$ .

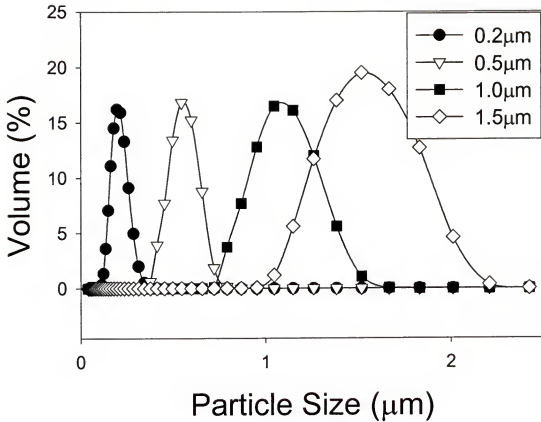


Figure 7-3. Size distribution of silica particles measured by dynamic light scattering.

#### Analysis of *In Situ* Friction Force

*In situ* monitoring of interfacial interaction between pad, particles, and wafer is essential to analyze the polishing mechanism. In this work it has been demonstrated that interfacial contact of pad, particles, and wafer is altered as particle size and solids loading are varied, resulting in a variation of friction force. Therefore, *in situ* friction force measurements can provide an insight into the polishing mechanism.

Figure 7-4 shows the friction force as a function of time for various solids loadings of 0.2 μm silica particles. During the initial 15 sec, the friction force was measured with just deionized water between the wafer and the pad. Friction force determined with



deionized water was considered as a baseline to compare the change of friction force using slurries including particles.

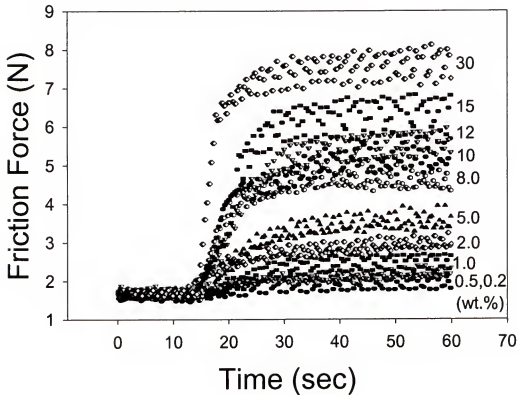


Figure 7-4. Friction force as a function of time for various solids loading of  $0.2\mu\text{m}$  silica particles.

Over the next 15sec, the slurry containing silica particles is flowed into the pad-wafer interface, elevating the friction force from a baseline to higher levels. Particles inserted into the interface between pad and wafer form the contact of three bodies (pad, particles, and wafer), enhancing the friction force. Finally, average friction forces were saturated with time in the range from 30 sec to 60 sec. Particles embedded into a soft pad slide on the wafer surface at a constant speed, causing a constant friction force. While particles are in contact with the wafer, friction force increases with the increase of solids loading.

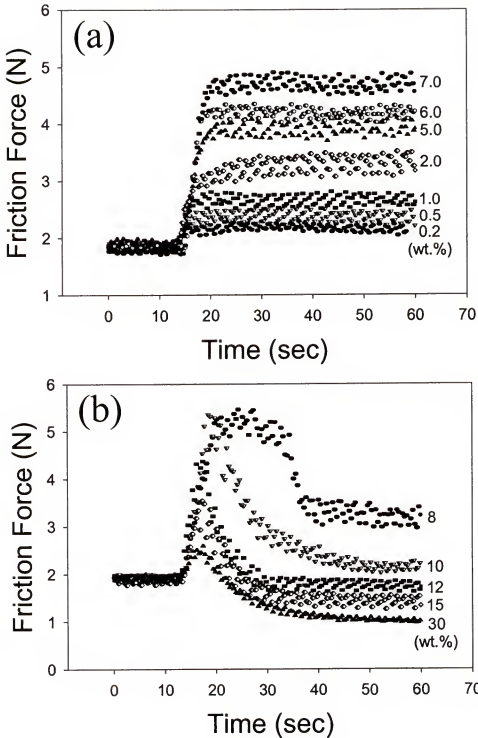


Figure 7-5. Friction force as a function of time for 0.5  $\mu\text{m}$  silica particles: (a) Low solids loading (less than 7 wt.%), (b) High solids loading (more than 8 wt.%).

The increase of solids loading leads to an increase in the number of particles in contact with wafer, enlarging the total contact area of particles between the wafer and pad. Therefore, the increase of friction force due to an increase in solids loading is due to an increase of contact area between wafer and particles embedded into the pad for sliding of particles, which will be confirmed by AFM analysis. Figure 7-5 shows the friction force as a function of time for various solids loadings of 0.5  $\mu\text{m}$  silica particles. As shown in Figure 7-5(a), friction force increased and then remains unchanged with time for low solids loading (less than 7 wt.%). Friction force also increased with the increase of solids loading. This observation in friction force indicates that particles in contact with the wafer are sliding and the number of particles in contact with the wafer increases with an increase of solids loading. The observed increase in friction force was in agreement with our previous results in which friction force was enhanced when solids loading was increased [Cho01]. As shown in Figure 7-5(b), friction force initially increased and then decreased with time for high solids loading (more than 8 wt.%). When slurry particles flow into the interface between the pad and the wafer, the coverage of slurry particles between the pad and the wafer increases to reach the saturated value at which lubrication begins. The insertion of particles into the pad-wafer interface initially enhanced friction force, which is due to the collision of sliding particles with high friction coefficient. The observed decrease in friction force in the presence of spherical silica particles indicates that the slurry possesses a lubrication effect due to the rolling of silica particles. The friction forces produced by rolling are much lower than that by sliding, which is in agreement with the theoretical principles concerning rolling [Bhu02].

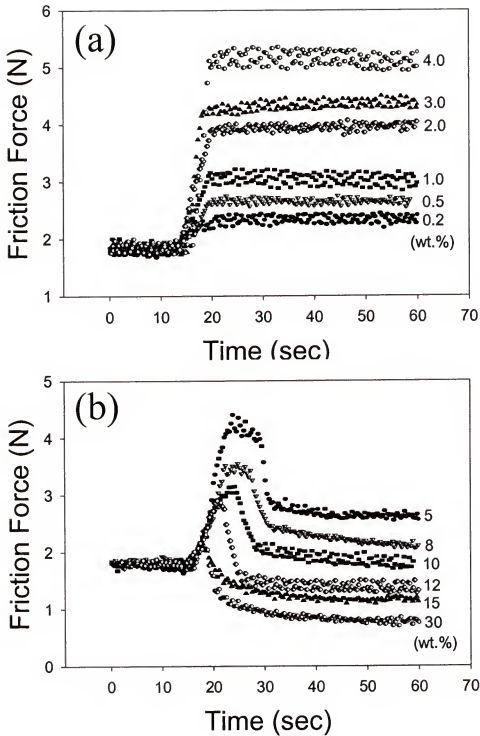


Figure 7-6. Friction force as a function of time for 1.0  $\mu\text{m}$  silica particles: (a) Low solids loading (less than 4 wt.%), (b) High solids loading (more than 5 wt.%).

It was also reported that the lubrication effect due to rolling motion took place in the presence of a layer of “Bucky ball bearings” [Mye99]. When spherical ball bearings roll between two flat surfaces, friction force was found to decrease with time. It was also observed in Figure 7-5(b) that friction force decreased with increasing solids loading. This observed decrease in friction force is in opposition to the frictional behavior shown in Figure 7-5(a). This also indicates an alteration of the interfacial dynamic contact behavior due to a change in solids loading. Figure 7-6 shows the friction force as a function of time for various solids loading of 1.0  $\mu\text{m}$  silica particles. As shown in Figure 7-6(a), for low solids loading (less than 4 wt.%), the friction force remained unchanged with time in the presence of slurry particles. Compared to friction force by 0.5  $\mu\text{m}$  silica particles, the transition between the sliding and the rolling behavior decreases from 7 wt.% to 4 wt.%, which is due to an increase of rolling probability due to an increase in particle size [Bhu02]. Otherwise, when the small silica particles (e.g., 0.2  $\mu\text{m}$ ) were used, an evidence of rolling behavior was not observed using *in situ* friction force measurement. Figure 7-6(b) shows the friction force as a function of time with high solids loading (more than 5 wt.%). The friction force initially increased due to addition of slurry into the pad-wafer interface and then gradually decreased with time. This frictional behavior is analogous to that produced by 0.5  $\mu\text{m}$  silica particles of high solids loading. Friction force measured with 5 wt.% and 8 wt.% silica particles showed two frictional regions: one is a high frictional force region (i.e., sliding region) between 20 sec and 30 sec and the other is the low frictional force region (i.e., rolling region) between 30 sec and 60 sec. These two regions indicate the transition from sliding to rolling of particles between the

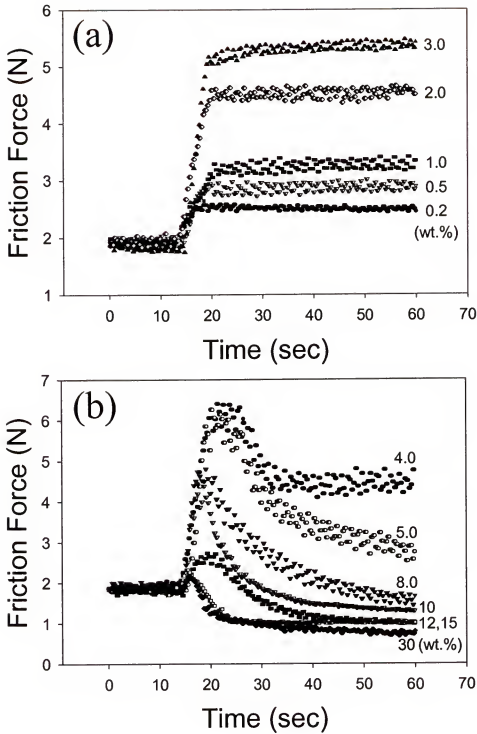


Figure 7-7. Friction force as a function of time for 1.5  $\mu\text{m}$  silica particles: (a) Low solids loading (less than 3 wt.%), (b) High solids loading (more than 5 wt.%).

pad and the wafer. It is interesting that the sliding region decreases with increasing solids loading. This also suggests that sliding is a main contact motion for low solids loading and rolling is a dominant contact motion for high solids loading. Figure 7-7 shows the friction force as a function of time for different solids loading of 1.5  $\mu\text{m}$  size silica particles. As seen in Figure 7-7(a), friction force remains unchanged with time for slurry flowing, which indicates particles are undergoing sliding motion for the solids loading (less than 3 wt.%). It is also shown that 3 wt.% is the maximum solids loading for sliding motion. Compared to the friction force measured with 1.0  $\mu\text{m}$  silica particles, maximum solids loading for sliding decreased from 4 wt.% to 3 wt.%. This result indicates that large particles start rolling motion at lower solids loading condition. Figure 7-7(b) shows the friction force as a function of time for high solids loading (more than 4 wt.%) of 1.5  $\mu\text{m}$  silica particles. The friction force obtained at 4 wt.% showed the combined frictional behavior of sliding and rolling. For high solids loading (more than 5 wt.%), the friction force decreased with time, indicating rolling of particles. Figure 7-8 shows the friction force as a function of solids loading for different particle sizes, which was redrawn from the graph of friction force vs. time (Figure 7-4 ~ Figure 7-7). For sliding conditions, the friction force increased with an increase in solids loading and particle size. While, in rolling conditions, the friction force decreased with an increase in solids loading and particle size. It is clear that the response of friction force to solids loading and particle size is dependent on the dynamic condition of slurry particles. In the case of sliding slurry particles, the effect of solids loading and particle size on friction force can be explained as follows. The increase of solids loading leads to an increase in the number of particles contacting the pad and the wafer, and it also leads to an increase in the fractional surface

coverage. The increase of particle size results in an increase in the particle's indentation depth into the wafer [Coo90, Zha01]. Increase in the friction force may be attributed to an increased indentation depth of particles along with increased solids loading at the pad-wafer interface.

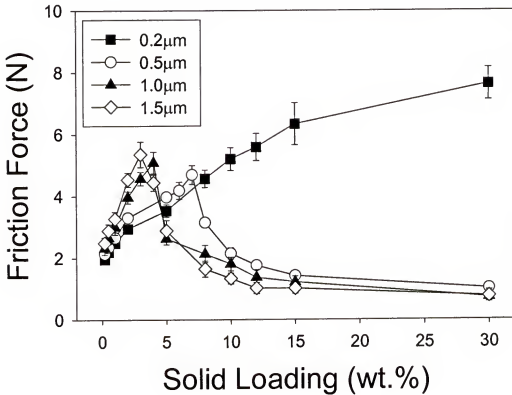


Figure 7-8. Friction force as a function of solids loading for different particle sizes.

As the dynamic motion of particles transits from sliding to rolling, the response of friction force to solids loading and particle size were varied. When a single particle is rolling on the flat surface, the rolling friction force ( $F$ ) is given by [Tim51]:



$$F = \frac{3}{16} \cdot N \cdot \frac{\varepsilon}{R} \cdot \left[ \frac{3}{4} \cdot N \cdot R \left( \frac{1 - \nu_1^2}{E_1} + \frac{1 - \nu_2^2}{E_2} \right) \right]^{1/3} \quad (9.3)$$

where  $N$  is the down force per particle,  $\varepsilon$  is the coefficient related to hysteresis loss during rolling motion,  $R$  is the radius of particle,  $\nu$  is the poisson's ratio,  $E$  is the elastic modulus, and 1 and 2 represent the particle and wafer, respectively. According to equation (9.3), rolling friction force is directly proportional to the four-thirds power of down force per particle and inversely proportioned to the two-thirds power of the radius of particles. As seen in Figure 7-8, rolling takes places at larger particle size conditions (i.e., 0.5  $\mu\text{m}$ , 1.0  $\mu\text{m}$ , and 1.5  $\mu\text{m}$ ). For rolling conditions, the increase of solids loading may lead to a decrease in down force per particles, reducing friction force. Figure 7-8 also showed that an increase in particle size resulted in a decrease in the friction force. Consequently, for rolling conditions, the friction force is in agreement with rolling friction force as expressed in Equation (9.3). Therefore, friction force measured during rolling conditions may be termed rolling friction force.

### Surface Finish Analysis

The surface finish of polished samples can be considered as surface topography produced during CMP. Surface topography of polished samples has been measured by Atomic Force Microscopy (AFM) during which surface images are taken by scanning the sample relative to the probing tip and measuring the deflection of the cantilever as a function of lateral position at the atomic level [Mey92]. Figure 7-9 shows over-view images of a wafers polished with 0.2  $\mu\text{m}$  silica particles for different solids loading: (a) 0.5 wt.%, (b) 5 wt.%, (c) 15 wt.%, and (d) 30 wt.%. Randomly distributed scratches have been detected in all the images investigated. As seen in Figure 7-4, for this small particle

size condition (i.e.,  $0.2\ \mu\text{m}$  silica particles), it was known that material removal was achieved by sliding of slurry particles. Therefore, scratches were produced due to the sliding of slurry particles along wafer surface.

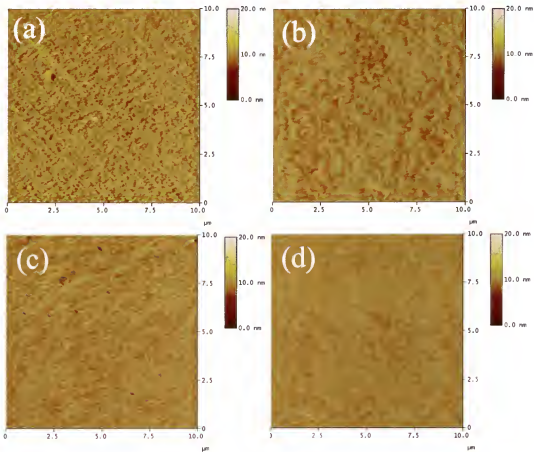


Figure 7-9. AFM over-view images for the wafer polished with  $0.2\ \mu\text{m}$  Geltech silica particles of different solids loading: (a) 0.5 wt.%, (b) 5 wt.%, (c) 15 wt.%, and (d) 30 wt.%.

These observed scratches are also in agreement with those produced by two-body contact, as shown in top images of Figure 7-1 [Abr91]. This indicates that material removal is achieved by the sliding of particles embedded into the pad. It was also observed that the number of scratches produced on the wafer decreased with increasing solids loading. From the difference of surface topography between 0.5 wt.% and 30 wt.%, it can be

easily detected that the increase in solids loading leads to the formation of smoother surface.

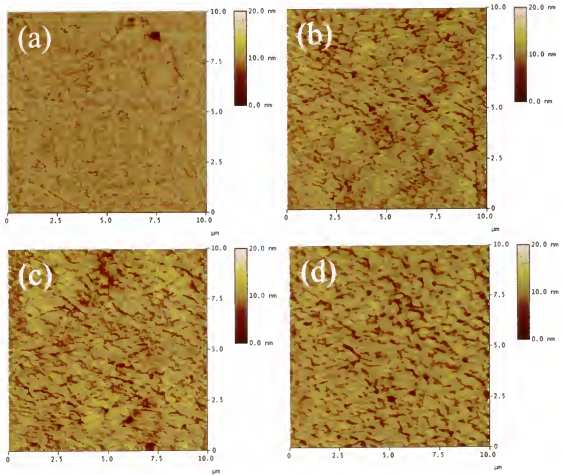


Figure 7-10. AFM over-view images for the wafer polished with 0.5  $\mu\text{m}$  Geltech silica particles of different solids loading: (a) 0.5 wt.%, (b) 5 wt.%, (c) 15 wt.%, and (d) 30 wt.%.

Figure 7-10 showed over-view images of wafers polished with 0.5  $\mu\text{m}$  silica particles for different solids loading: (a) 0.5 wt.%, (b) 5wt. %, (c) 15 wt.%, and (d) 30 wt.%. When solids loadings were low, many scratches were shown on the wafer surface. These observed scratches were similar to the images detected of wafers polished with 0.2 $\mu\text{m}$

silica particles. On the other hand, when solids loadings were high (i.e., 15 wt.% and 30 wt.%), “shot-blast” surfaces were produced on the wafer surface instead of scratches. These observed “shot-blast” appearances were in accordance with the images produced by three-body contact that was shown in bottom of Figure 7-1 [Abr91]. Similar contact images were observed on surfaces produced by a rolling sphere for three-body contact [Tim51]. In addition, as seen in Figure 7-5(b), the decrease of friction force due to rolling of slurry particles was observed. This indicates that rolling particles move freely between the pad and the wafer yielding “shot-blast” appearance. It is interesting to observe the existence of intermediate solids loading condition (i.e., 5 wt.%). For the intermediate condition of solids loading, scratch images were observed together with “shot-blast” appearance. This means that material is removed by two different dynamic motions (i.e., sliding and rolling) during polishing. As seen in Figure 7-5(b), *in situ* friction force measurements detected the coexistence of two dynamic contact motions at 8 wt. %. In spite of the different critical solids loading at which two dynamic contact motions coexist, it is interesting to detect the transition between sliding and rolling. Figure 7-11 shows over-view images of a wafer polished with 1.0  $\mu\text{m}$  silica particles for different solids loading: (a) 0.5 wt.%, (b) 2 wt.%, (c) 15 wt.%, and (d) 30 wt.%. An over-view image of the wafers polished with 0.5 wt.% particles show a large number of scratches. As mentioned previously, it can be thought that scratches are produced due to the sliding motion of particles. Small numbers of “shot-blast” features appear in series together with scratches on the surface of wafers polished with 2wt.% particles (Figure 7-11(b)) in which significant plastic deformation is shown along a band 0.3 to 0.5  $\mu\text{m}$  wide. These tracks also exhibit significant cracking and caterings. These plastic deformations, which

were not shown on wafers polished with small particles (i.e., 0.2  $\mu\text{m}$  and 0.5  $\mu\text{m}$ ), may only be produced by large silica particles. Macmillan *et al.* [Mac74] also showed a similar SEM picture of the track that was produced by a sliding sapphire ball. An over-view image of a wafer polished with 15 wt.% and 30 wt.% particles clearly showed a series of “shot-blast” regions, which indicates the rolling of particles observed during the three body contact.

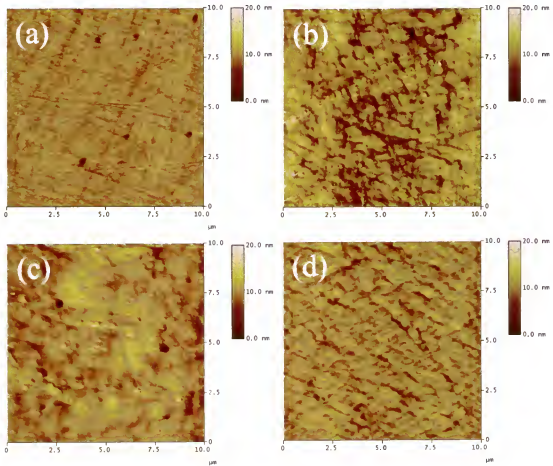


Figure 7-11. AFM over-view images for the wafer polished with 1.0  $\mu\text{m}$  Geltech silica particles of different solids loading: (a) 0.5 wt.%, (b) 2 wt.%, (c) 15 wt.%, and (d) 30 wt.%.

Figure 7-12 shows over-view images of a wafer polished with  $1.5\ \mu\text{m}$  silica particles for different solids loading: (a) 0.5 wt.%, (b) 2 wt.%, (c) 15 wt.%, and (d) 30 wt.%. For 0.5 wt.%, surface finishes with a lot of scratches are apparent. However, over-view images of a wafer polished with 2 wt.% particles shows a predominance of “shot-blast” regions rather than scratches. For 15 wt.%, instead of scratches, a mostly “shot-blast” appearance is observed on the wafer surface. Also, over-view images of a wafer polished at 30 wt.% show a smooth wafer surface with a shallow “shot-blast” appearance.

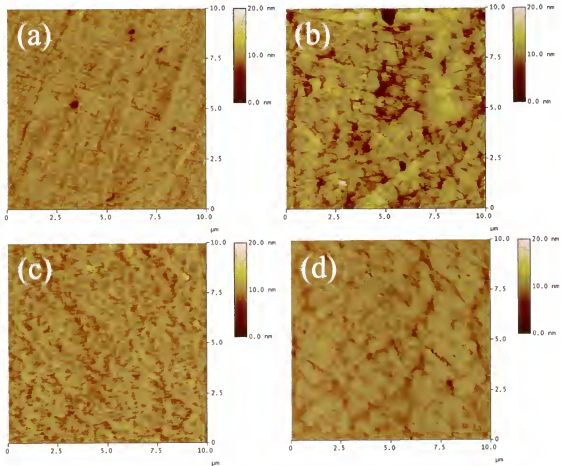


Figure 7-12. AFM over-view images for the wafer polished with  $1.5\ \mu\text{m}$  Geltech silica particles of different solids loading: (a) 0.5 wt.%, (b) 2 wt.%, (c) 15 wt.%, and (d) 30 wt.%.

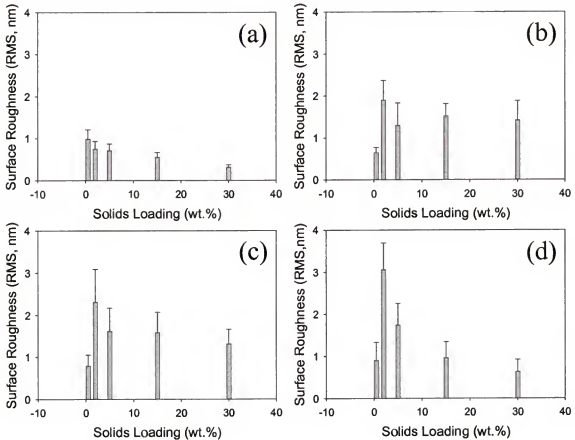


Figure 7-13. Surface roughness (Root Mean Square) as a function of solids loading for various particle sizes: (a) 0.2  $\mu\text{m}$ , (b) 0.5  $\mu\text{m}$ , (c) 1.0  $\mu\text{m}$ , and (d) 1.5  $\mu\text{m}$ .

Figure 7-13 shows the surface roughness (RMS, nm) as a function of solids loading for various particle sizes: (a) 0.2  $\mu\text{m}$ , (b) 0.5  $\mu\text{m}$  (c) 1.0  $\mu\text{m}$ , and (d) 1.5  $\mu\text{m}$ . For 0.2  $\mu\text{m}$  silica particles, surface roughness decreased with an increase in solids loading. On the other hand, for low solids loading of 0.5  $\mu\text{m}$ , 1.0  $\mu\text{m}$ , and 1.5  $\mu\text{m}$  silica particles, surface roughness increased with an increase in solids loading. The aforementioned roughness results were obtained during sliding conditions. For sliding conditions, surface roughness produced due to polishing with small particles is different from that of large particles. The increase in solids loading of small particles (i.e., 0.2  $\mu\text{m}$ ) leads to an increase in the total contact area. It was noted that local bonding during contact results in weakening of

binding forces at the surface, which allows material to be removed at the atomic level [Mor87]. The layer contact area is expected to enhance the kinetics of the chemical reaction by assisting in increasing the solubility of silica species, resulting in low surface roughness [Izu79]. The increase in solids loading of large particles (i.e., 0.5  $\mu\text{m}$ , 1.0  $\mu\text{m}$ , and 1.5  $\mu\text{m}$ ) results in the increase of surface roughness. For low solids loading of large particles, the observed increase of surface roughness may be due to the small number of particles. Total bonding area between silica particles and a silica wafer decreases with an increase in particle size. Mechanical contacts may be predominant for large particles. For a low solids loading of large particles, it is thought that the number of scratches increases with an increase in solids loading, leading to an increase in surface roughness. For rolling conditions (more than 5 wt. % of 0.5  $\mu\text{m}$ , 1.0  $\mu\text{m}$ , and 1.5  $\mu\text{m}$  silica particles), surface roughness decreased with an increase in solids loading, which is in agreement with the response of friction force to solids loading, as seen in Figure 7-8. Therefore, lubrication effect due to rolling particles is thought to reduce the surface roughness with solids loading.

### **Analysis of Polishing Rate**

In order to elucidate the mechanisms involved in silica polishing, the polishing rate was investigated as a function of particle size and solids loading. Figure 7-14 shows the polishing rate as a function of solids loading for various particle sizes at 3.5 psi. Polishing rate increased with the increase of solids loading for the 0.2  $\mu\text{m}$  silica particles. For 0.5  $\mu\text{m}$  silica particles, polishing rate shows a transition in polishing behavior at 5 wt.% of particles. Polishing with 1.0  $\mu\text{m}$  and 1.5  $\mu\text{m}$  silica particles produced the same transition behavior at lower solids loading of particle (i.e., 2 wt.%). According to *in situ* friction



force measurements and over-view images of polished wafer surface, the 0.2  $\mu\text{m}$  silica particles and the large particles (i.e., 0.5  $\mu\text{m}$ , 1.0  $\mu\text{m}$ , and 1.5  $\mu\text{m}$ ) at low solids loading achieved material removal via the sliding motions of slurry particles. The increase in the contact area of sliding particles leads to an increase in friction force and polishing rate, which yields no evidence of lubrication effects such as evidenced during rolling of slurry particles. For large particles (i.e., 0.5  $\mu\text{m}$ , 1.0  $\mu\text{m}$ , and 1.5  $\mu\text{m}$ ) at high solids loading, material is removed due to the rolling motions of slurry particles, which was confirmed by *in situ* friction force measurements and over-view images of polished wafer. The polishing rate decreased with increasing solids loading suggesting that lubrication effects due to rolling of slurry particles dominated when solids loading increased.

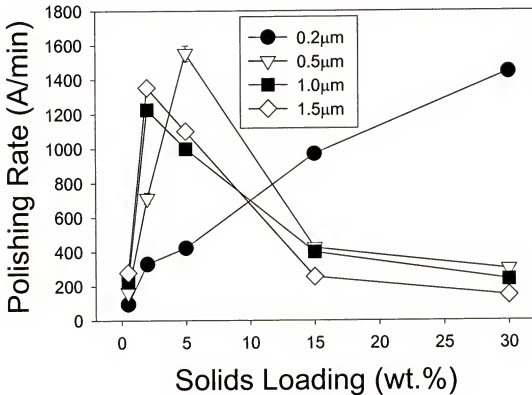


Figure 7-14. Polishing rate as a function of solids loading for different particle size.

For low solids loading (less than 2 wt.%), The increase of particle size leads to an increase in the polishing rate, which was achieved by sliding motions of slurry particles. *In situ* friction force measurements provided an insight into the interfacial contact of sliding particles. The increase in particle size results in an increase in the indentation depth per particle, which was confirmed by surface roughness (RMS) values. The increased indentation depth per particles may be responsible for the increase in friction force and polishing rate observed. For high solids loading (more than 15 wt.%), the increase of particle size leads to a decrease in polishing rate, which was due to rolling motions of slurry particles. Based on *in situ* friction force measurements, the lubrication effects of rolling particles increased with increasing particle size, thus leading to the reduction of friction force and polishing rate. These observations of varying polishing rate with particle size and solids loading suggested that various polishing mechanisms were involved in silicon dioxide CMP. It has been shown that by delineating dynamic motions of slurry particles at the pad-wafer interface appropriate criteria may be selected for robust slurry design for optimized CMP performance.

### Summary

The investigation into interfacial dynamic motion of silica particles during CMP provides critical information about silica polishing mechanisms. Polishing mechanisms of silica were elucidated via *in situ* friction force measurements and AFM images. The dynamic motion (sliding or rolling) of silica particles was detected via the friction force behaviors. AFM images exhibited that the effects of sliding motion of silica particles was scratch-type surfaces and that rolling motion of silica particles induced “shot-blast” appearance. From *in situ* friction force measurements and analysis of AFM images, it was found that polishing rate in silica CMP was dependent on the dynamic motion of silica

particles. For the sliding motion of particles, polishing rate is directly proportional to solids loading and particle size. For the rolling motion of particles, polishing rate is inversely proportional to solids loading and particle size. It was concluded that the opposite phenomena are results of dynamic motions of silica particles. The observed polishing behavior provides an insight into the polishing mechanism in silica CMP.

## CHAPTER 8

### EFFECTS OF COLLOIDAL SILICON DIOXIDE PARTICLES ON CHEMICAL MECHANICAL POLISHING (CMP) OF DIELECTRIC SILICON DIOXIDE

#### **Introduction**

Chemical mechanical polishing (CMP) has developed as the technique of choice to achieve global planarization of metal and dielectric films in the microelectronic fabrication industry. The CMP process consists of a resilient pad, wafer to be polished, and abrasive slurry [Ste97]. During the CMP process, a rotating wafer to be polished is pressed down onto a rotating polishing pad while slurry containing abrasive particles and chemical additives flows in between the pad and the wafer [Sin02a]. The synergistic interaction of mechanical abrasion and chemical reaction leads to material removal of the wafer, making the CMP process more complicated [Oli02]. Utilization of this synergistic interaction results in the desired CMP performance such as global planarization, low defect density, and appropriate removal rate, which is significantly dependent on polishing slurry conditions. Therefore, a more thorough understanding of the effect of the abrasives in the polishing slurry on the polishing mechanism is critical to achieving the desired CMP performance.

Throughout this work the impact of abrasive particles on interfacial interactions during CMP and their effect on CMP performance has been reported [Ste97]. The polishing rate, surface finish, and amount of surface defects are simultaneously affected by slurry particles [Bas00, Bie99]. The effects of particle size and solids loading on polishing rate and surface finish have been studied to understand the polishing

mechanism and achieve optimum polishing performance. Some have proposed that the increase in both particle size and solids loading leads to the increase of polishing rate [Jai94a, Jai94b], while others have suggested that polishing rate is increased with the decrease of particle size or is independent of particle size [Bie99, Co090]. Zhou et al. [Zho02] proposes that polishing rate increased with increasing solids loading and maximum polishing rate was achieved by the 80 nm colloidal silica particles. It was also suggested that the agglomeration of nano sized particles (e.g. 10 nm and 20 nm) have a detrimental effect on surface finish and polish at a lower rate. Li et al. [Li03] suggested that an increase in specific surface area of colloidal silica particles leads to an increase in silanol group concentration, resulting in a higher polishing rate. This indicates that the increase of polishing rate is due to an increase in the contact area of colloidal silica particles. Our previous studies exhibited two removal mechanisms depending on solids loading for various particle sizes [Mah99c]: one is a contact area based removal mechanism at which removal rate increased with an increase in the total contact area of particles in contact with wafer surface. The other is an indentation based removal mechanism at which removal rate increased with an increase in the indentation depth per particle. As appeared in previous works, it was shown that polishing performance such as polishing rate and surface finish is significantly related to particle size and solids loading. Even though previous works have provided some insight into the polishing mechanisms due to changing particle size and solids loading, there has been no consensus on the effects of particle size and solids loading on polishing performance. A major drawback is the lack of experimental validation of polishing mechanisms, and no investigation into the interfacial interactions during polishing.

This study continues the development of insight into the polishing mechanism of silicon dioxide chemical mechanical polishing by studying abrasive size and solids loading effects for slurries containing nano-sized colloidal particles. The effects of particle size and solids loading on polishing rate, surface finish, and friction force are described to further delineate the polishing mechanisms. An advanced micro contact polishing model is proposed by delineating the characteristics of interfacial contact of colloidal particles between the pad and the wafer during polishing.

### **Experimental**

Levasil abrasive silica slurries obtained from Bayer Company were utilized for this study. Slurries were diluted to 2 wt.%, 5 wt.%, 10 wt.%, 15 wt.%, and 30 wt.% by the addition of deionized water to the colloidal slurries provided by Bayer Company. The pH was adjusted to 10.5 using 0.1M  $\text{HNO}_3$  and 0.1M  $\text{NaOH}$ . The size and distribution of particles were measured using a Honeywell Microtech UPA 150 particle size analyzer which utilize light scattering techniques. The shape and size of particles were directly analyzed with Scanning Electron Microscopy (SEM). Polishing experiments were conducted using a Struers Rotopol 31 tabletop polisher. The process conditions for polishing tests were: down pressure (4.5 psi, 7.5 psi, 10.5 psi, and 15 psi), the rotation speed of pad and the wafer (110cm/sec), and flow rate of slurry (100ml/min). The polishing samples of  $1.5 \times 1.5$  square inch were prepared by clipping 8 inch silicon wafers deposited with silicon dioxide using plasma enhanced chemical vapor deposition (PECVD). An IC 1000/ Suba IV stacked pad was utilized as a polishing pad. The conditioning of the polishing pad was conducted using a Grid-Abrade diamond conditioner to maintain the roughness and porosity of pad surface. The polishing rate was

calculated from the thickness of silica layer measured by a J. A. Wollan Variable Angle Spectroscopic Ellipsometry (WVASE) before and after polishing. Surface topography and surface roughness of polished layers was characterized using a Digital Instruments Nanoscope III Atomic Force Microscopy (AFM).

The *in situ* friction force measurements were carried out to delineate the interfacial interaction of particles between pad and the wafer during CMP. The *in situ* friction force instrument was assembled on the Struers Rotapol 31 tabletop polisher, as shown in Figure 3-1. A data sample was acquired every 250 msec via a Sensotec model 31 load cell. The friction forces were measured under these conditions: down pressure (3.5 psi), the rotation speed of pad (110cm/sec), and flow rate of slurry (100ml/min). As seen in Figure 6-1, the friction forces were measured during 45 sec intervals for each run. De-ionized water was utilized as a baseline condition during the initial 15 sec. The variations of friction force due to the addition of slurry containing particles during the next 30 sec were normalized against the baseline.

## **Characterization**

### **The Size Characterization of Colloidal Silica Particles**

The size and size distribution of colloidal silica particles is critical in determining polishing performance. As can be seen in Figure 4-2, the particle size distribution measured by light scattering methods showed that the silica slurries were well-dispersed possessing monosized distributions. Table 4-1 shows the mean volume distribution diameter calculated from particle size measured via the light scattering technique. Particle size and size distribution were in agreement with the information that the company provided. As shown in Figure 4-3, the direct images of colloidal particles detected by scanning electron microscopy (SEM) suggested that colloidal particles were spherical in

shape. Particle sizes detected by SEM were in agreement with those measured via light scattering.

### Fundamentals of Characterization of Polished Surfaces

Surface quality is an indication of the expected yield and reliability of the interconnections. A rough interlayer dielectric (ILD) film is more susceptible to low breakdown strength and high leakage [Ste97]. Roughness is minimized by properly balancing the chemical and mechanical components of the CMP process.

Characterization of the polished wafer surface needs to be accompanied by polishing tests in order to optimize the polishing process. The average area and volume of particles in contact with the wafer were determined via two equations containing amplitude and texture parameters [Tho98]. Figure 8-1 shows the surface profile of cross-sectional area.

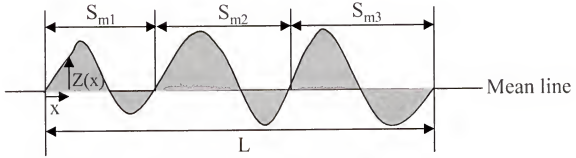


Figure 8-1. Surface profile of cross-sectional area of top surface

The amplitude parameter represents the average properties of a profile containing average surface roughness. Average surface roughness represented as root mean square (RMS) is given by:

$$R_q = \sqrt{\frac{1}{L} \int_0^L Z^2(x) dx} \quad (8.1)$$

where  $L$  is the evaluation length and  $Z(x)$  is the height function. Root mean square (RMS) of surface roughness is the variation in height from point to point on the surface



and indicates the average indentation depth of particles into wafer surface. The surface roughness parameter contains no information concerning the spatial or textural variation of the profile. It is important to describe the variation of relief in the plane of the surface. Texture parameters are utilized to distinguish between two profiles which are visibly different but for which all the amplitude parameters are the same. For texture parameters, the mean spacing of profile irregularities ( $S_m$ ) is given by the following equation:

$$S_m = \frac{S_{m1} + S_{m2} + S_{m3}}{n} \quad (8.2)$$

where  $n$  is the number of peaks per length of a profile. Along with  $R_q$ ,  $S_m$  is thought to be an important factor to characterize the surface finish produced during CMP.

## Results and Discussion

### Effects of Particle Size and Solids Loading on Polishing Rate

Figure 8-2 shows the polishing rate as a function of solids loading for three sizes of colloidal particles. Polishing test was conducted at the down pressure of 7.5 psi.

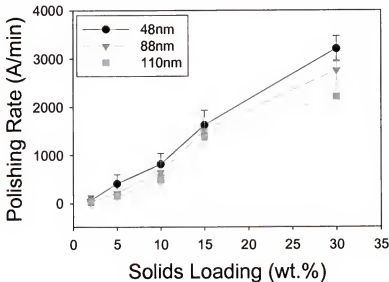


Figure 8-2. Polishing rate as a function of solids loading for various particle sizes under the condition of down pressure of 7.5 psi.

For a given down pressure, polishing rate was calculated as a function of particle size and solids loading. As seen in Figure 8-2, polishing rate increased with an increase in solids loading. Because an increase in solids loading leads to an increase in total contact area of colloidal particles in contact with wafer surface, an increase in solids loading results in an enhanced polishing rate. A decrease in particle size leads to an increase in polishing rate. For low solids loading ( $\leq 15$  wt.%), it is apparent that the difference in polishing rate due to particle size is small. For high solids loading of 30 wt.%, however, polishing rate significantly increased with a decrease in particle size. These differences in polishing rate suggested that the difference in contact area of particles in contact with wafer is large at high solids loading conditions. Based on Figure 8-2, the change in polishing rate due to particle size and solids loading is in agreement with a contact area based-model [Bie98]. According to the contact area-based model, polishing rate depends on the total contact area between the abrasive particles and the surface being polishing. The contact area as a function of particle size and solids loading is given by the following expression:

$$A \propto C_0^{1/3} \cdot \phi^{-1/3} \quad (8.3)$$

where  $A$  is the contact area,  $C_0$  is the solids loading, and  $\phi$  is the particle size. According to this model, it was found that the contact area of colloidal silica particles determined polishing rate. Zhou et al. [Zho02] exhibited similar results for the polishing by colloidal particles ( $\geq 80$  nm), which showed that polishing rate increased with a decrease in particle size and an increase in solids loading. For small colloidal particles ( $\leq 50$  nm), they expressed that polishing rate decreased with a decrease in particle size because the contact area decreased due to the agglomeration of colloidal particles. Consequently, it

was found that the area of colloidal silica particles in contact with the wafer played an important role in determining polishing rate.

### Surface Characterization (Solids Loading and Particle Size Effects)

Over-view images and cross-sectional profiles of the polished surface are an indication of surface finish produced by chemical mechanical polishing.

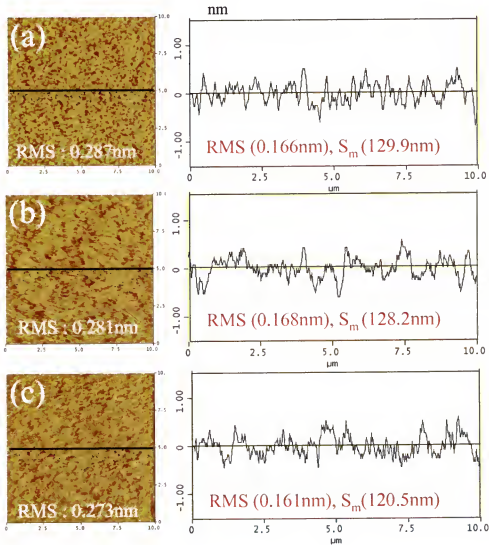


Figure 8-3. The over-view images and cross-section of silica wafer surface polished with colloidal silica particle having particle diameter of 88 nm for various solids loading: (a) 2 wt.%, (b) 5 wt.%, and (c) 15 wt.%.

Figure 8-3 depicts the over-view images and cross-section of a silica wafer surface polished with colloidal silica particles having particle diameter of 88 nm for various solids loading: (a) 2 wt.%, (b) 5 wt.%, and (c) 15 wt.%. The surface roughness (RMS) of the polished surface remained unchanged with an increase in solids loading. Cross sectional profile of polished surfaces also remains similar with changing solids loading. The surface roughness (RMS) and the mean spacing of profile irregularities ( $S_m$ ) remained constant with increasing solids loading. This indicates that down load per particle does not change with the change of solids loading. Therefore, it can be suggested that the wafer is in contact with the polishing pad and particles embedded into the pad simultaneously. An increase in solids loading leads to an increase in fractional surface coverage of particles between the pad asperities and the wafer, resulting in an increase in polishing rate. Figure 8-4 shows over-view images and cross-section of a silica wafer surface polished with colloidal silica particles having particle diameter of 48 nm and 110 nm for two solids loading conditions (10 wt.% and 30 wt.%). For particles with 48 nm and 88 nm diameters, surface roughness (RMS) and the mean spacing of profile irregularities ( $S_m$ ) also remained unchanged with solids loading. For each solids loading condition, surface roughness (RMS) and the mean spacing of profile irregularities ( $S_m$ ) increased with an increase in particle size. This suggests that an increase in particle size leads to an increase in area and volume of contact per particle. Even though the contact area and volume per particle increased with an increase in particle size, polishing rate decreased with increasing particle size, which indicates that the total area of particles in contact with the wafer is an important factor in determining polishing rate.

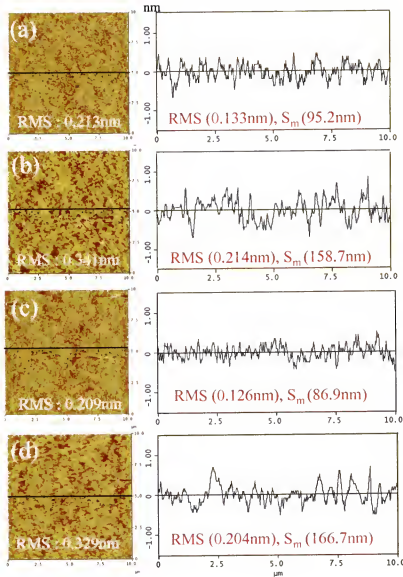


Figure 8-4. The over-view images and cross-section of silica wafer surface polished with colloidal silica particles for two solids loading conditions: (a) 10 wt. % (48 nm), (b) 10 wt.% (110 nm), (c) 30 wt.% (48 nm), and (d) 30 wt.% (110 nm).

### The *In Situ* Friction Force Measurements (Particle Size and Solids Loading Effects)

Friction force is a function of the interfacial contact behavior of particles. Friction force is a measure of how much contact the particles makes with the wafer surface, which is important in determining the abrasion mode. For a given solids loading, a change in particle size and solids loading leads to a variation in the interfacial contact behavior of

particles in contact with the wafer and the pad. Figure 8-5 shows the friction force as a function of solids loading for various particle sizes. For each solids loading condition, a decrease in particle size allows for an increase in friction force. This suggested that a decrease in particle size leads to an increase in the area of particles in contact with the wafer, resulting in higher friction force. For each particle size condition, an increase in solids loading enhanced friction force. Enhanced friction force due to the increase of solids loading may be due to an increase in total area of particles in contact with the wafer. In this regard, it is suggested that an increase in the number of particles present at the pad-wafer interface, leads to an increase in total area of particles contacting the wafer, resulting in an increase in friction force and polishing rate.

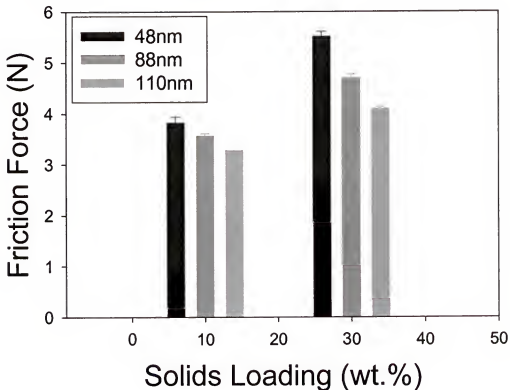


Figure 8-5. Friction force as a function of solids loading for various particle size at down pressure of 3.5 psi .

### Effects of Down Pressure on Polishing Rate

Polishing rate is significantly dependent on down pressure because a change in down pressure leads to a variation in interfacial contact at the pad-particles-wafer interface. Figure 8-6 shows a polishing rate as a function of down pressure for different particle sizes.

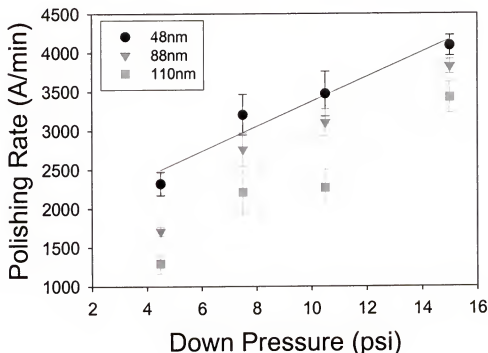


Figure 8-6. Polishing rate as a function of down pressure for various particle size.

Polishing rate was proportional to the down pressure and it increased with a decrease in particle size. For well-dispersed colloidal particles, the effect of particle size on polishing rate is in agreement with Zhou's work [Zho02]. According to Zhou's work [Zho02], agglomeration of colloidal silica particles leads to a lower polishing rate, while this work shows no such decrease in polishing rate due to use of well-dispersed slurries even for larger sizes. This assertion was confirmed by surface finish measurements. With

increasing down pressure, polishing rate increased, which follows the model of Preston [Pre27]. The model of Preston is given by the following equation:

$$MRR=KPV \quad (8.4)$$

Where MRR is the material removal rate, P is the down pressure, V is the relative polishing speed, and K is a system dependent parameters. When the relative velocity and chemical environments remains unchanged, polishing rate is expected to be a function of down pressure. As seen in Figure 8-6, polishing rate follows the model of Preston with only slight deviation. An optimum polishing rate may be obtained by tailoring the down pressure to desired levels.

#### **Surface Characterization (Down Pressure Effects)**

Surface finish indicates the manner of interfacial contact of particles during CMP. Large particles and agglomerated particles are expected to produce deep indentation depths and broad distances between peaks on the polished surface. The down pressure is expected to be a critical process parameter in determining surface roughness. Figure 8-7 illustrates over-view images and cross-section of polished surface for various particle sizes and down pressures. It was found that surface roughness (RMS) and the mean spacing of profile irregularities (Sm) remained unchanged with an increase in down pressure for a given particle size and only increased with an increase in particle size. Surface roughness, Rs, is the penetration depth of the particles into the surface, which is given by [coo90]:

$$R_s = \frac{3}{4} \cdot \phi \cdot \left( \frac{P}{2kE} \right)^{2/3} \quad (8.5)$$

where k is the particle concentration,  $\phi$  is the particle size, P is the down pressure, and E is the elastic modulus.



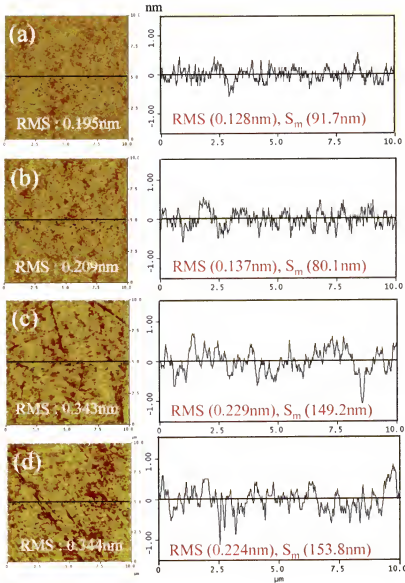


Figure 8-7. The over-view images and cross-section of silica wafer surface polished with 30 wt.% colloidal silica particles for two different particle sizes and solids loading conditions: (a) 4.5 psi (48 nm), (b) 15 psi (48 nm), (c) 4.5 psi (110 nm), and (d) 15 psi (110 nm).

According to Equation 8.5, it was expected that surface roughness is a function of particle size, down pressure, and elastic modulus. While chemical environments (e.g., pH) remained unvaried, elastic modulus ( $E$ ) of the top surface layer is thought to be a constant [Izu79]. For a constant particle size and chemical environment, the surface roughness is a

function of down pressure per particles. As shown in Figure 8-7, the effects of down pressure on surface roughness (RMS) and the mean spacing of profile irregularities ( $S_m$ ) indicates that down pressure per particle remained unchanged with an increase in applied down pressure. This suggests that an increase in down pressure leads to an increase in contact area between the pad and the wafer, allowing for a constant down pressure per particle embedded into the pad.

### **Proposed Interfacial Contact Model**

An interfacial contact model is being proposed to delineate the role of colloidal silica particles at the pad-particles-wafer interface during polishing. One is due to the particle size and solids loading effects on interfacial contact that occurs during polishing, and the other is due to the down pressure effect on interfacial contact of particles in contact with the wafer and the pad simultaneously.

### **Particle Size and Solids Loading Effects on Interfacial Contact**

Figure 8-8 shows a schematic diagram of the pad-particles-wafer interface as a function of particle size and solids loading. This interracial contact model was built on the basis of polishing rate, surface finish, and friction force measurements. For a given solids loading condition, the indentation depth of particles into the wafer surface and contact area per particle increases with an increase in particle size with smaller particles exhibiting higher polishing rates. Even though smaller particles produced a shallower indentation depth per particle into the wafer surface, total contact area of particles in contact with the wafer increase with a decrease in particle size. This suggested that polishing rate increased due to an increase in the total area of particles in contact with the wafer for a constant solids loading. For a given particle size, indentation depth per particle remained unchanged with an increase in solids loading.

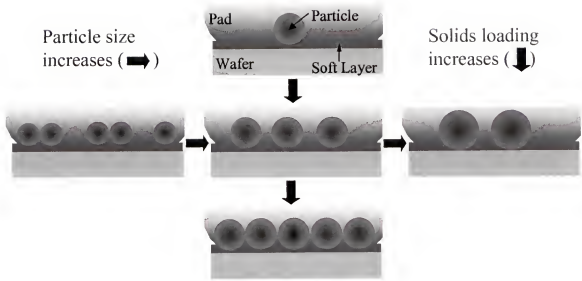


Figure 8-8. A schematic diagram of the interfacial contact at the pad-particles-wafer interface with the change of particle size and solids loading.

This is due to the fact that the pressure per particle remained unchanged with increasing solids loading. The wafer was in contact with the pad and the particles embedded into the pad simultaneously during polishing. Polishing rate increased with an increase in solids loading for constant particle size. An increase in solids loading leads to an increase in the number of particles in contact with the wafer, resulting in an enhanced polishing rate.

#### **Down Pressure Effects on Interfacial Contact**

Down pressure is a process input variable for CMP. The output parameters such as polishing rate, surface finish, and planarity are determined by modulating down pressure. Based on the polishing rate and surface finish of the polished wafer surface, the influence of down pressure on interfacial contact taking place during polishing is illustrated in Figure 8-9. With increasing down pressure, the asperities of the pad surface are

compressed, and the contact area between the pad and the wafer increases, allowing for larger pad-wafer contact area.

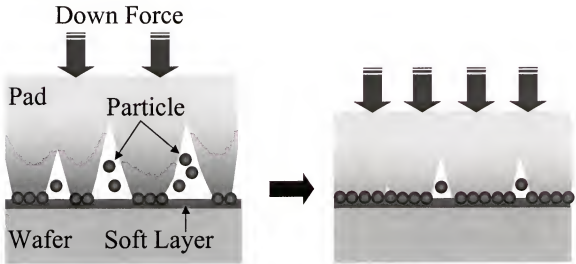


Figure 8-9. A schematic diagram of the interfacial contact at the pad-particles-wafer interface with the change of down pressure.

The lack of deviation in surface roughness when down pressure is varied is due to the fact that the indentation depth per particle remains unchanged. The pressure per particle remains the same because increasing the down pressure increases the fractional surface coverage causing a redistribution of pressure due to the simultaneous contact of the wafer with the pad and particles. Therefore, it can be concluded that the polishing rate increased with an increase in down pressure due to an increase in the number of particles in contact with the wafer. The particles assume some of the pressure formerly experienced by the pad.

### Summary

The interfacial interactions of colloidal silica particles between the pad and the wafer were studied to validate a polishing mechanism of dielectric silica. While nano-sized colloidal silica particles were inserted into the interface between the pad and the

wafer, the polished wafer surface was in contact with the pad and the particles embedded into the pad simultaneously during polishing, which was confirmed by surface finish such as surface roughness(RMS) and the mean spacing of profile irregularities ( $S_m$ ). In this regard, surface finish did not only remain unchanged with the change of solids loading and down pressure for a given particle size, but it increased with an increase in particle size. Polishing rate increased with the increase of solids loading and decreasing particle size, which is due to an increase in the contact area of colloidal particles between the pad and the wafer.

## CHAPTER 9

### SUMMARY

Chemical mechanical polishing (CMP) is accomplished by a variety of interfacial interactions taking place at the pad-particles-wafer interface. This complex interaction makes it difficult to understand polishing mechanism. Polishing performance including polishing rate, surface topography was found to be a result of physical and chemical interaction occurring at the pad-particles-wafer interface. This study focused on the investigation of interfacial interactions to understand the polishing mechanism and to obtain desired polishing performance.

The contact variations at the interface during polishing were examined through in situ friction force measurements. In the absence of particles, the contact area between the pad and the wafer increases with the increase of applied down pressure, leading to an increasing friction force. In the presence of particles, increasing down pressure and solids loading results in an increase in the number of particles in contact with the pad and the wafer, leading to an increase in friction force. At fixed solids loading, the decrease in particle size leads to an increase in total contact area of particles in contact with the wafer, causing a high friction force. Fractional surface coverage of particles was determined by friction force values and an equation was developed from the principles of friction force. Fractional surface coverage of particles is independent of down pressure, and increases with solids loading. Small particles have larger fractional surface coverage than larger particles at a given solids loading condition.

A micro contact area model was developed to predict the interfacial contact area between spherical particles and a flat wafer surface. The total contact area between particles and a flat wafer surface increases with the increase of solids loading and the decrease of particle size. This contact model is generally in agreement with *in situ* friction force measurements. High friction force was observed for the condition of high solids loading of small particles. From modeling and experiments, the contact variations of particles between the pad and the wafer were determined.

Dynamic contact at the pad-particles-wafer interface was investigated as a function of platen velocity and down pressure. For low solids loading condition (less than 2 wt.%), the contact area of particles contacting with the wafer is smaller than that of the pad in contact with the wafer. Thus the role of particles is negligible, resulting in the decrease of friction force with platen velocity. For high solids loading (more than 5 wt.%), the enhancement of friction force with increasing platen velocity is found to be due to the increase of shear strength caused by the increase of the sliding speed of particles. It was also found that the increase of shear strength by down pressure played an important role in raising the friction force.

In addition to physical contact variations, chemical interaction is also important for achieving desired CMP performance. The variation of silica polishing rate with pH is primarily due to the variation in interaction force between silica particles and a silica wafer, and the solubility of silica. The significant variation of polishing rate, friction force, and surface roughness was observed with the transition occurring at pH 10. The increase in repulsive interaction force between silica particles and silica wafer causes the lubrication effect, leading to low friction force and polishing rate. The high solubility of

silica reduces friction force but it enhances polishing rate due to the formation of a soft gel layer possessing a low density. Surface finishes are affected by particle size and solubility of silica. For low pH ( $\leq \text{pH}10$ ), when particle size remains unchanged, surface roughness did not show any change depending on pH. For high pH ( $\geq \text{pH}10$ ), however, surface roughness increases with the increase of pH due to gel layer formed due to high solubility of silica.

The dynamic motions (sliding motion or rolling motion) of spherical silica particles were elucidated through *in situ* friction force measurements and AFM images. For the sliding conditions of particles, friction force remains unchanged with time in the presence of particles, and surface topography of scratch-type was observed. For the rolling conditions of particles, friction force decreases with time in the presence of particles and the shot-blasted surface topography was evidenced. Sliding takes place in the condition of low solids loading and small particles. Rolling occurs in the condition of high solids loading and large particles. For sliding conditions, polishing rate increases with the increase of solids loading. The effect of particle size on polishing rate for sliding condition needs to be investigated in future works. For rolling conditions, polishing rate decreases with increasing solids loading and particle size. It is apparent that dynamic motion of particles in the CMP process is critical in determining polishing rate.

The interfacial contact of colloidal silica particles and its influence on polishing performance such as polishing rate and surface finish. For colloidal silica particles, the wafer surface was carried by both the pad asperities and particles embedded into the pad simultaneously. Smaller particles did not only produce lower surface roughness (RMS) and mean spacing of profile irregularities ( $S_m$ ), but it also higher polishing rate than



larger particles. It was apparent that polishing rate was significantly dependent on the contact area of particles in contact with the wafer during CMP.

## LIST OF REFERENCES

- Abr91 Abrahamson, G.R., Duwell, E.J., McDonald, W.J. (1991). J. Trib., **113**, 249
- Adl00 Adler, J.J., Singh, P.K., Patist, A., Rabinovich, Y.I., Shah, D.O., and Moudgil.B.M. (2000). Langmuir, **16**, 7255
- Ahm01 Ahmadi G. and Xia, X. (2001). J. Electrochem. Soc., **148** (3), G99
- Ale54 Alexander G.B. (1954). J. Phys. Chem. **58**,153
- Amo1699 Amontons, G. (1699). Acad. R. Soc., (Paris), 266
- And74 Anderson, D.R. (1974). *Analysis of Silicones*, A. Lee Smith, editor, Wiley-Interscience, New York, Chapter 10
- Ava95 Avallone E.A. and Baumeister, T. (1995). *Marks' Standard Handbook for Mechanical Engineers*, Tenth Edition, McGraw-Hill, New York, NY
- Baj02 Bajaj, R., Zutshi, A., Surana, R., Naik, M. and Pan, T. (2002). Mat. Res. Soc. Bull., **27**(10), 776
- Bar98 Barla, K., Gounelle, C., Lair, C., Lafarges, Y., Lasserre, V., Lis, S., Maddalon, C., Verove, C., Lous, E., Morand, Y., Passemard, G., Pires, F., and Demolliens, O. (1998). Proc. VMIC (Institute of Electrical and Electrons Engineers, Piscataway, NJ, 27
- Bas00 Basim, G. B., Adler, J.J., Mahajan, U., Singh, R.K., and Modugil, B.M. (2000). J. Electrochem. Soc., **147**, 3523
- Bas03 Basim, G.B., Vakarelski, I.U., and Moudgil, B.M. (2003). J. Colloid. Interface Sci, **263**, 506
- Bey99 Beyer, K. D. (1999). IBM Micronews, **5**, 40
- Bhu02 Bhushan, B. (2002). *Introduction to Tribology*, John Wiley & Sons, New York, NY
- Bhu95 Bhushan, M., Rouse, R., and Lukens J.E. (1995) J. Electrochem. Soc., **141** (11), 3845
- Bie98 Biemann, M. (1998). "Tungsten Chemical Mechanical Polishing," Master's Thesis, University of Florida

- Bie99 Biemann, M., Mahajan, U., and Singh, R.K. (1999). *Electrochem. Solid-State Lett.* **2**(7), 401
- Bla69 Black, J. R. (1969). *IEEE Trans. Electron Devices*, **ED-16**, 338
- Bow64 Bowden F.P. and Tabor D. (1964). *The Friction and Lubrication of Solids Pt II*. Oxford University Press
- Bro81 Brown N.J., Baker, P. C., and Maney, R.T. (1981). *Proc. SPIE Contemporary Methods of Optical Fabrication*, **306**, 42
- Bud61 Budd, S. M. (1961). *Phys. Chem. Glasses*, **2**, 111
- Car90 Carr, J. W. (1990). U.S. Patent 4,954,142
- Car95 Carpio, R., Farkas, J., and Jairath, R. (1995). *Thin Solid Films*, **266**, 238
- Chi99 Chiang, S.-K., and Lassen, C. L. (1999). *Solid State Technol.*, **42**, 42
- Cho01 Choi, W., Lee, S.-M., Singh, R. K. (2001). *Mat. Res. Soc. Proc. Symp.*, **337**, 89
- Coo90 Cook, L.M. (1990). *J. Non-Cryst. Solids*, **120**, 152
- Cou1785 Coulomb C.A. (1785). Miscellaneous paper
- Dan81 Dang, R. L. M., and Shigyo, N. (1981). *IEEE Electron Devices Lett.*, **EDL-2**, 196
- Dav89 Davari, B., Koburger, C., Furukawa, T., Taur, Y., Noble, W., Megdanis, A., Warnock, J., and Mauer, J. (1989). *IEDM Tech. Dig. (Institute of Electrical and Electronics Engineers, Piscataway, NJ*, 92
- Dav91 Davies, R.D., Arnell, P.B., and Whomes, T.L. (1991). *Tribology Principles and Design Applications*, Springer-Verlag, New York, 124
- Dor01 Dornfeld D. <http://www.lma.berkeley.edu> (2001)
- Dor73 Doremus, R. (1973). *Glass Science*, Wiley, New York, NY
- Edw68 Edwards C. M. and Halling, J. (1968). *J. Mech. Eng. Sci.*, **10**, 101
- Fuj88 Fujii, S., Fukumoto, M., Fuse, G., Ohzone, T. (1988). *Electron Devices, IEEE Transactions*, **35**, 11
- Gre55 Green, A.P. (1955). *Proc. R. Soc.*, **228**(A), 191
- Gre66 Greenwood J.A. and Williamson, J.B. (1966). *Proc. Royal Soc. A*, **395**, 300

- Gre67 Greenwood J.A. (1967). J. Lubrication Technology, Jan. 81
- Gut78 Gutsche, H. W. and Moody, J.W. (1978). J. Electrochem. Soc. **125** (1),136
- Hal75 Halling, J. (1975). *Principles of Tribology*, Macmillan Press Ltd., New York, NY
- Ham65 Hammond, M.L. and Ravitz, S.F. (1965). J. Am. Ceram. Soc., **46** (7), 329
- Hay95 Hayashi, Y., Sakurai, M., Nakajima, T., Hayashi, K., Sasaki, S., Chikaki, S., and Kunio, T. (1995). Jap. J. Appl. Phys. Part 1, **34**(2B), 1037
- Hei84 Heinike, G. (1984). *Tribochemistry*, Charlhanser Verlag Munchen Wien
- Her1896 Hertz, H. (1896). Miscellaneous papers (Macmillan. London)
- Hol64 Holland L. (1964). *The Properties of Glass Surfaces*, Chapman & Hall, London
- Ile79 Iler, R. (1979). *The Chemistry of Silica: Solubility, Polymerization, Colloid and Surface Properties, and Biochemistry*, Wiley, New York, NY
- Isr00 Israelachvili, J. (2000). *Intermolecular & Surface Forces*, 2<sup>nd</sup> Ed., Academic Press, San Diego, CA
- Ito81 Ito, S. and Tomozawa, M. (1981). J. Am. Ceram. Soc., **64**, C-160
- Izu79 T. Izumitani, (1979). *Treatise on Materials Science and Technology*, M. Tomozawa, R. Doremus, Editors, Academic Press, New York, NY, 115
- Izu82 Izumitani, T. (1982). Tech. Digest, Topical Meeting on Optical Fabrication and Technology, Optical Society of America, Paper TuB-A1
- Jac98 Jacson, R., Broadbent, E., Cacouris, T., Harrus, A., Biberger, M., Patton, E., and Walsh, T. (1998). Solid State Technology, **41**, 49
- Jai94a Jairath R., Farkas J., Huang C.K., Stell M., Tzeng S.-M. (1994). Solid State Technol. **37**, 71
- Jai94b Jairath R. Desai M., Stell M., Telles R., and Scherber-Brewer D. (1994). Mat. Res. Soc. Symp. Proc. **337**, 121
- Jen94 Jeng S.P., Havemann R.H., and Chang M.C. (1994). Mat. Res. Soc. Symp. Proc., **337**, 25
- Joh85 Johnson, K.L. (1985). *Contact Mechanics*, Cambridge University Press, Cambridge
- Kau00a Kaufman, V.B. and Wang, S. (2000). U.S. Patent 6,039,891

- Kau00b Kaufman, V.B. and Kistler, R.C., and Wang, S. (2000). U.S. Patent 6,126,853
- Kau91 Kaufman F.B., Thomson D.B., Broadie, R.E., Jaso M.A., Guthrie W.L., Pearson D.J., and Small M.B. (1991). *J. Electrochem. Soc.*, **138**, 3460
- Kir94 Kirk, N.B. and Wood, J.V. (1994). *British Ceramic Trans.*, **93** (1), 25
- Lan85 Lanford, W., Burman, C., and Doremus, R. (1985). In *Advances in Materials Characterization II*, Snyder R., Condrate, R., and Jonston, P., Editors, New York, NY
- Lan92a Landis, H., Burke, P., Cote, W., Hill, W., Hoffman, C., Kaanta, C., Koburger, C., Lange, W., Leach, M., and Luce, S. (1992). *Thin Solid Films*, **220**, 1
- Lan92b Landis, H., Burke, P., Cote, W., Hill, W., Hoffman, C., Kaanta, C., Koburger, C., Lange, W., and Luce, S. (1992). *Thin Solid Films*, **347**, 248.
- Law75 Lawn, B. and Wilshaw, R. (1975). *J. Mater. Sci.* **10**, 1049
- Lee02 Lee, S.-M., Choi, W., Craciun, V., Jung, S.-H. and Singh, R.K. (2002). *Mat. Res. Soc. Sym.* **1411**.
- Lee03 Lee, S.-M. (2003). "Characterization of Chemical Interactions during Chemical Mechanical Polishing (CMP) of Copper," Ph. D. Dissertation, University of Florida
- Li03 Li, Y. and Babu, S.V. (2003). *Semiconductor Fabtech –13<sup>th</sup> Edition*, 259
- Li94 Li, J., Seidel, T.E. and Mayer, J. W. (1994). *Mat. Res. Soc. Bull.*, **19** (8), 15
- Liu99 Liu, R., Pai, C.-S., and Martinez, E. (1999). *Solid-State Electronics*, **43**, 1003
- Mac74 Macmillan, N. H., Huntington. R. D., and Westood, A.R.C. (1974). *J. Mat. Sci.* **9**, 697
- Mah00 Mahajan, U. (2000). "Fundamental Studies on Silicon Dioxide Chemical Mechanical Polishing," Ph.D Dissertation, University of Florida, Gainesville, FL
- Mah99a Mahajan, U., Bielman, M., and Singh, R.K. (1999). *Electrochem. Solid State Lett.* **2**(1), 46
- Mah99b Mahajan U., Bielman, M., and Singh, R.K. (1999). *Electrochem. Solid-State Lett.*, **2**(2), 80
- Mah99c Mahajan, U., Bielman, M., and Singh, R.K. (1999). *Mater. Res. Soc. Proc.* **566**, 27

- McB86    McBrayer J.D., Swanson R.M. and Sigmon T.W. (1986). J. Electrochem. Soc., **133**, 1243
- Mey92    Meyer, E. (1992). Prog. Surf. Sci. **41**, 3
- Mic82    Michalske, T.A. and Freiman, S.W. (1982). J. of Am. Ceram. Soc., **66**(4), 284
- Mod96    *Modern Plastics Encyclopedia 96*(1996). McGraw Hill/Modern Plastics, New York, NY
- Mog92    Moghadam F. (1992). Proc. SRC Topical Research Conference on Chem-Mechanical Polishing for Planarization, SRC, Research Triangle Park, NC, vol. #P92008
- Moo65    Moore, G. E. (1965). Electronics, **38**, April
- Moo99    Moon Y. (1999). "Mechanical aspects of the material removal mechanism in chemical mechanical polishing (CMP)," Ph.D. Thesis, Mechanical Engineering Department, University of California, Berkeley, CA
- Mor87    Morii, Y., Yamuchi, K., and Endo, K. (1987) Precision Engineering, **9**, 123.
- Moy89    Moy, D., Schadt, C.K., Kaufman, F., Ray, A.K., Mazzeo, N., Baran, E., and Pearson, D.J. (1989). Proc. 6<sup>th</sup> VMIC, Santa Clara, CA, IEEE Cat. No. 91TH0359-0
- Mue99    Mueller, B. L., Streinz, C. C., and Grumbine, S. K. (1999). U.S. Patent 5,958,288
- Mur91    Murarka S.P. (1991). Mat. Res. Soc. Symp. Proc. **179**, 89
- Mur93    Murarka, S.P. (1993). *Metallization Theory and Practice for VLSI and ULSI*, Butterworth-Heinemann, Boston, MA
- Mye99    Myers, D. (1999). *Surface, Interfaces, and Colloids: Principles and Applications* 2<sup>nd</sup> Edition, p454, John Wiley & Sons, New York, NY
- Nev80    Nevot, L. and Croce, P. (1980). Revue Phys. Appl., **15**, 761
- Nog84    Nogami, M. and Tomozawa, M. (1984). Phys. Chem. Glasses, **25**, 82
- Obe98    Obeng, Y., K. Forsthoefel, M., Richardson, A., and Burton R. H. (1998). Electrochemical Society Proceedings Series, **98-7**, 151
- Oli02    Oliver, M. (2000). Mat. Res. Soc. Symp. Proc., **566**, 73
- Ols93    Olsen J. and Moghadam, F. (1993). *In Multilevel Metallization for Integrated Circuits*, S.R. Wilson, C.J. Tracy and J.L. Freeman, Editors, Noyes Publications, Park Ridge, NJ

- Oro55 Orowan E. (1955). Weld. Res. (London), Suppl., 157
- Par69 Park, G.A. (1965). Chem. Rev., **65**, 177
- Pou74 Pourbaix, M. (1974). *Atlas of Electrochemical Equilibria in Aqueous Solution*, NACE, Houston, TX
- Pre27 Preston, F. (1927). J. Soc. Glass Technol., **11**, 247
- Raj97 Rajan, K., Singh, R.K., Adler, J., Mahajan, U., Rabinovich, Y., and Moudgil, B.M. (1997). Thin Solid Films, **308-309**, 529
- Ram00 Ramarajan, S., Hariharaputhiran, M., Her, Y.-S., and Babu, S. V. (2000). Electrochem. Solid-State Lett. **3(5)**, 232
- Ren94 Renteln P. and Coniff J. (1994). Mat. Res. Soc. Symp. Proc. **337**, 105
- Ric71 Rice, R.W. (1971). In *Materials Science research, Vol. 5: Ceramics in Severe Environments* (W.W. Kriegel and H. Palmour III, eds.), Plenum, New York, 195
- Rod03 Rodel Corp [www.rodel.com](http://www.rodel.com), 451 Bellevue Road, Newark, DE 19713 (2003).
- Run94a Runnels, S.R. and Eyman L.M. (1994). J. Electrochem. Soc., **141(6)**, 1698
- Run94b Runnels, S.R. (1994). J. Electrochem. Soc., **141(7)**, 1900
- Rut95 Rutten, M. and Huynh, C. (1995). Presented at the SRC Topical Conference on CMP.
- Rya95 Ryan, J. G., Geffken, R. M., Poulin, N. R., and Paraszcak, J. R. (1995). IBM J. Res. Dev., **39(4)**, 371
- Sas92 Sasaki S. (1992). Bulletin of Mech. Eng. Lab. Japan, **No. 58**, 43
- Sch79 Schlichting, H. (1979). *Boundary Layer Theory*, McGraw-Hill, New York, NY
- Sci03 Science and Focus "Force and Motion"  
<http://www.learner.org/channel/workshops/force/workshop3/highlights.html>  
(2003).
- Sha00 Shan L., Levert J., Meade, L., Tichy, J., and Danyluk, S. (2000). J. Tribology, **122**, 539
- Shi98 Shi, F.G. and Zhao, B. (1998). Appl. Phys. **A67**, 249
- Sho00 Shon-Roy, L. (2000). Solid State Technol., **43 (6)**, 67

- Sin02a Singh, R. K., Lee, S.-M., Choi, K.-S., Basim, D. B., Choi, W., Chen, Z., and Moudgil, B. M. (2002). *Mat. Res. Soc. Bull.*, **27**, 752
- Sin02b Singh, R.K. and Bajaj, R. (2002). *Mat. Res. Soc. Bull.* **27(10)**, 743
- Siv92 Sivaram, S., M. Bath, H.M., Lee, E., Leggett, R., and Tolles, R. (1992). *Proc. SRC Topical Research Conference on Chem-Mechanical Polishing for Planarization*, SRC, Research Triangle Park, NC, 8
- Sta03 Starck, H.C. [www.bayer-echemicals.com](http://www.bayer-echemicals.com) (2003).
- Sta95 Stavreva, Z., Zeidler, D., Plotner M., and Drescher K. (1995). *App. Surf. Sci.*, **91**, 192
- Ste97 Steigerwald, J. M., Murarka, S. P., and Gutmann, R. J. (1997). *Chemical Mechanical Planarization of Microelectronic Materials*, John Wiley & Sons, New York
- Sti97 Stix G. (1997). *Sci. Am.*, **276**, 45
- Str03 Strasbaugh 6EC, <http://www.nnf.cornell.edu/equipment/CMP.html> (2003).
- Sze81 Sze, S. M. (1981). *Physics of Semiconductor Devices*, John Wiley Sons Inc., New York, NY
- Tho98 Thomas, T. (1998). *Rough Surfaces* 2<sup>nd</sup> Edition, Imperial College Press
- Tic99 Tichy, J., Levert, J.A., Shan, L. and Danyluk, S. (1999). *J. Electrochem. Soc.* **146 (4)**, 1523
- Tim51 Timoshenko, S. and Goodier, J.N. (1951). *Theory of Elasticity*, McGraw-Hill, New York, NY
- Tom94 Tomozawa, M., Yang, K., Li, H., and Murarka, S.P. (1994). *Mat. Res. Soc. Proc. Symp.*, **337**, 89
- Tro94 Trogolo, J. A. and Rajan K. (1994). *J. Mater. Sci.*, **29**, 4554
- Utt91 Uttecht R.R. and Geffken R.M. (1991). *Proc. 8<sup>th</sup> VMIC*, Santa Clara, CA, 20
- Vie01 Viet, N. H. (2001). *Ph.D. Dissertation*, Universiteit Twente, Netherlands
- Wan94 Wang, S. Q. (1994). *Mat. Res. Soc. Bull.*, **19 (8)**, 15
- Wes85 Weste, N., and Eshraghian, K. (1985). *Principles of CMOS Design*, Addison Wesley Pub. Co., MA
- Xie96 Xie, Y. and Bhushan, B. (1996). *Wear*, **200**, 281



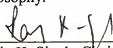
- Yu93 Yu, T.-K. Yu, C.C. and Orlowski M. (1993). IEEE IEDM **865** 35.4.1.
- Zha00 Zhao, Y., Maietta, D.M., and Chang, L. (2000). Trans. of the ASME, **122**, 86
- Zha01a Zhao, E., Xu, C.S., (2001). Semicond. Int., **24**, 145
- Zha01b Zhao, Y. and Chang, L. (2001). Wear, **9026**, 1
- Zha98 Zhang, F. and Busnaina, A.A. (1998). Electrochem. Solid-State Lett., **1** (4), 184
- Zha99a Zhang, F., Busnaina, A.A., and Ahmadi, G. (1999). J. Electrochem. Soc., **146** (7), 2665
- Zha99b Zhao, B. and Shi, F.G. (1999). Electrochem. Solid-State Lett., **2** (3), 145
- Zho02 Zhou, C., Shan, L., Hight, J.R., and Danyluk, S. Ng, S.H., and Paszkowski, A.J. (2002). J. Soc. Tri. Lub. Eng. Apr. 35

## BIOGRAPHICAL SKETCH

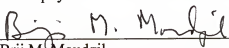
The author was born on August 25, 1970, in Chungju City, Chung-Chong-Buk-Do, South Korea. He entered Han Yang University, Seoul, Korea, in March 1989. In September 1990, he joined the Korean Armed Service and was discharged as a sergeant in February 1993. In August 1993, he has continued his study again and received the Bachelor of Science degree in metallurgical engineering in February 1996. In March of 1996, he enrolled in graduate school in the same department at Han Yang University and received the Master of Science degree in February 1998.

After graduating, he pursued his professional career as a researcher in the Korea Institute of Science and Technology (KIST), where he worked for one and a half years. While working with KIST, he felt the need for higher education in the United States. In fall 1999, he enrolled in the Ph.D. program in the Department of Materials Science and Engineering at the University of Florida. In May 2000, he joined Dr. Singh's research group where he focused on fundamental and applied study of chemical mechanical polishing. His particular emphasis is on slurry design, interfacial interaction, and tribology for silica CMP.

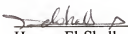
I certify that I have read this study and that in my opinion it conforms to acceptable standards of scholarly presentation and is fully adequate, in scope and quality, as a dissertation for the degree of Doctor of Philosophy.

  
\_\_\_\_\_  
Rajiv K. Singh, Chairman  
Professor of Materials Science and  
Engineering


I certify that I have read this study and that in my opinion it conforms to acceptable standards of scholarly presentation and is fully adequate, in scope and quality, as a dissertation for the degree of Doctor of Philosophy.

  
\_\_\_\_\_  
Brij M. Moudgil  
Professor of Materials Science and  
Engineering


I certify that I have read this study and that in my opinion it conforms to acceptable standards of scholarly presentation and is fully adequate, in scope and quality, as a dissertation for the degree of Doctor of Philosophy.

  
\_\_\_\_\_  
Hassan El-Shall  
Associate Professor of Materials Science  
and Engineering

I certify that I have read this study and that in my opinion it conforms to acceptable standards of scholarly presentation and is fully adequate, in scope and quality, as a dissertation for the degree of Doctor of Philosophy.

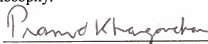
  
\_\_\_\_\_  
David P. Norton  
Professor of Materials Science and  
Engineering

I certify that I have read this study and that in my opinion it conforms to acceptable standards of scholarly presentation and is fully adequate, in scope and quality, as a dissertation for the degree of Doctor of Philosophy.

  
\_\_\_\_\_  
Chang-Won Park  
Professor of Chemical Engineering

This dissertation was submitted to the Graduate Faculty of the College of Engineering and to the Graduate School and was accepted as partial fulfillment of the requirements for the degree of Doctor of Philosophy.

December' 2003

A handwritten signature in dark ink, appearing to read "Pramod P. Khargonekar", written over a horizontal line.

Pramod P. Khargonekar  
Dean, College of Engineering

---

Winfred M. Phillips  
Dean, Graduate School